

Halvor Hølmkjær West

Test of a Francis turbine with new guide vanes

Master's thesis in Mechanical Engineering

Supervisor: Ole Gunnar Dahlhaug

Co-supervisor: Johannes Opedal Kverno, Igor Iliev

March 2022

Halvor Hølmkjær West

Test of a Francis turbine with new guide vanes

Master's thesis in Mechanical Engineering
Supervisor: Ole Gunnar Dahlhaug
Co-supervisor: Johannes Opedal Kverno, Igor Iliev
March 2022

Norwegian University of Science and Technology
Faculty of Engineering
Department of Energy and Process Engineering

Masteravtale/hovedoppgaveavtale

Sist oppdatert 11. november 2020

Fakultet	Fakultet for ingeniørvitenskap
Institutt	Institutt for energi- og prosesseteknikk
Studieprogram	MIPROD
Emnekode	TEP4925

Studenten	
Etternavn, fornavn	West, Halvor Hølmkjær
Fødselsdato	09.02.1994
E-postadresse ved NTNU	halvorhw@stud.ntnu.no

Tilknyttede ressurser	
Veileder	Ole Gunnar Dahlhaug
Eventuelle medveiledere	Igor Iliev, Johannes Opedal Kverno
Eventuelle medstudenter	

Oppgaven	
Oppstartsdato	27.09.2021
Leveringsfrist	21.02.2022
Oppgavens arbeidstittel	Test of a Francis turbine with new guide vanes
Problembeskrivelse	<p>Background The renewable energy system of the future need the capability to produce/store energy and generate power when needed. Today, this flexibility is mostly provided from fossil-fueled power plants while in the future, hydropower can provide the flexibility with high reliability. Today's hydropower technology has been developed to operate with a relatively stable loading over long periods of time. Norwegian hydropower plants are still operated like this, but as the future load variations become increasingly aggressive, the technology lifetime is reduced and maintenance costs are increased. In the Horizon 2020-project HydroFlex, the focus is to on increasing hydropower's flexibility. This includes variable speed operation of generators and turbines. Recently, researchers in the Waterpower Laboratory at the Norwegian University of Science and Technology (NTNU), designed their own high head Francis turbine and published both geometry and model performance data in order to provide other researchers with a relevant case to work with and to promote the Francis-99 workshops. This turbine is further modified to accommodate variable speed operation. The turbine has been designed by Igor Iliev and Johannes Kverno at NTNU and it will be produced and tested in the period from April 2021 to April 2022. In this project, the student will focus on model tests on this turbine in order to obtain the performance of</p>

	the turbine with new guide vanes. Objective Conduct a model test of a variable speed operated Francis turbine with new guide vanes
--	---

Risikovurdering og datahåndtering	
Skal det gjennomføres risikovurdering?	Nei
Dersom «ja», har det blitt gjennomført?	Nei
Skal det søkes om godkjenninger? (REK*, NSD**)	Nei
Skal det skrives en konfidensialitetsavtale i forbindelse med oppgaven?	Nei
Hvis «ja», har det blitt gjort?	Nei

* Regionale komiteer for medisinsk og helsefaglig forskningsetikk (<https://rekportalen.no>)

** Norsk senter for forskningsdata (<https://nsd.no/>)

Eventuelle emner som skal inngå i mastergraden

Retningslinjer - rettigheter og plikter

Formål

Avtale om veiledning av masteroppgaven/hovedoppgaven er en samarbeidsavtale mellom student, veileder og institutt. Avtalen regulerer veiledningsforholdet, omfang, art og ansvarsfordeling.

Studieprogrammet og arbeidet med oppgaven er regulert av Universitets- og høyskoleloven, NTNUs studieforskrift og gjeldende studieplan. Informasjon om emnet, som oppgaven inngår i, finner du i emnebeskrivelsen.

Veiledning

Studenten har ansvar for å

- Avtale veiledningstimer med veileder innenfor rammene master-/hovedoppgaveavtalen gir.
- Utarbeide framdriftsplan for arbeidet i samråd med veileder, inkludert veiledningsplan.
- Holde oversikt over antall brukte veiledningstimer sammen med veileder.
- Gi veileder nødvendig skriftlig materiale i rimelig tid før veiledning.
- Holde instituttet og veileder orientert om eventuelle forsinkelser.
- Inkludere eventuell(e) medstudent(er) i avtalen.

Veileder har ansvar for å

- Avklare forventninger om veiledningsforholdet.
- Sørgе for at det søkes om eventuelle nødvendige godkjenninger (etikk, personvern hensyn).
- Gi råd om formulering og avgrensning av tema og problemstilling, slik at arbeidet er gjennomførbart innenfor normert eller avtalt studietid.
- Drøfte og vurdere hypoteser og metoder.
- Gi råd vedrørende faglitteratur, kildemateriale, datagrunnlag, dokumentasjon og eventuelt ressursbehov.
- Drøfte framstillingsform (eksempelvis disposisjon og språklig form).
- Drøfte resultater og tolkninger.
- Holde seg orientert om progresjonen i studentens arbeid i henhold til avtalt tids- og arbeidsplan, og følge opp studenten ved behov.
- Sammen med studenten holde oversikt over antall brukte veiledningstimer.

Instituttet har ansvar for å

- Sørgе for at avtalen blir inngått.
- Finne og oppnevne veileder(e).
- Inngå avtale med annet institutt/ fakultet/institusjon dersom det er oppnevnt eksterne medveileder.
- I samarbeid med veileder holde oversikt over studentens framdrift, antall brukte veiledningstimer, og følge opp dersom studenten er forsinket i henhold til avtalen.
- Oppnevne ny veileder og sørgе for inngåelse av ny avtale dersom:
 - Veileder blir fraværende på grunn av eksempelvis forskningstermin, sykdom, eller reiser.
 - Student eller veileder ber om å få avslutte avtalen fordi en av partene ikke følger den.
 - Andre forhold gjør at partene finner det hensiktsmessig med ny veileder.
- Gi studenten beskjed når veiledningsforholdet opphører.
- Informere veileder(e) om ansvaret for å ivareta forskningsetiske forhold, personvern hensyn og veiledningsetiske forhold.
- Ønsker student, eller veileder, å bli løst fra avtalen må det søkes til instituttet. Instituttet må i et slikt tilfelle oppnevne ny veileder.

Avtaleskjemaet skal godkjennes når retningslinjene er gjennomgått.

Godkjent av

Halvor Hølmkjær West
Student

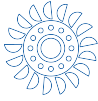
01.10.2021
Digitalt godkjent

Ole Gunnar Dahlhaug
Veileder

01.10.2021
Digitalt godkjent

Anita Yttersian
Institutt

06.10.2021
Digitalt godkjent



Abstract

The world has through the Paris Agreement of 2015 and the later updated Glasgow Agreement in 2021 agreed on out-phasing coal power. So in addition to an increased demand for variable power in the future, there is a need to increase the capacity of renewable energy sources. Solar and wind power are considered the two key unharvested energy sources. However, the challenge with these two energy sources is that they are dependent on the weather, and are not able to provide power on-demand. Hydro power is on the hand capable doing exactly that, and is therefore considered as a viable renewable energy source that can fully complement the solar and wind power. Though this means that hydro power needs to be installed in places where conditions are sub-optimal, and operations are more variable. Such variable operation deteriorates the various elements of a hydro power turbine, and consequently reduce the lifetime. The international collaborative project HydroFlex, supported by EU, has as its purpose to develop tools and research solutions for operating hydro power plants at sub-optimal places. The Waterpower Laboratory at NTNU is one of the collaborators of the project, and is responsible for the physical tests and the validation of the numerical simulations.

In this masters thesis a model test of the new guide vanes has been conducted according to the IEC60193 standard. The new guide vanes are designed by PhD candidates Filip Stojkovski and Marija Lazarevikj, who has tried to design guide vanes that perform better for variable operation of Francis turbines. Prior numerical simulations had shown promising results.

The Waterpower Laboratory at NTNU has been through an extensive refurbishment, where generator and valves have been replaced, and a new control program has been developed. After the refurbishment a reference model test were made to

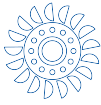
control for any effect it may have had on the results. The test revealed no noticeable changes apart from the new logging system showed a too high uncertainty. This was solved by increasing the sampling time.

The new guide vanes has a design fault as they were 0.77 mm too high. An attempt to solve this was made by expanding the lock ring using an old band saw blade.

The model test of the new guide vanes shows a 2 % reduction in efficiency at best operating point from 92.5 % to 90.7 % when compared to the old ones. The new guide vanes has a different opening pattern, which means that they have to open more, to allow for the same amount of discharge. The increased opening angle affects the velocity triangle, and thereby reduce the velocity at the inlet as given by Eulers turbine equation. Additionally, the changed angle may give rise to disturbances and create flow separations on the pressure sides of the turbine blades. Combined these may be explain the 2 % reduction in efficiency.

Two of the guide vanes has been instrumented with strain gauges to measure the torque on their shaft. These shows that the maximum torque point is at the lowest flow rate, and is reduced as the discharge increases. The torque never changes direction and has therefore no zero points. Consequently, in a case of a servo failure, the guide vanes will seek to a full opening angle, as this is the point with least torque.

The model test of the new guide vanes was also conducted according to the IEC60193 standard. Results show that these new guide vanes leads to worse efficiency compared to the old ones. However, the results are highly uncertain, mainly due to low sampling rate of the new system installed after the refurbishment of the laboratory. Nonetheless, the results can be used to validate the numerical simulations and further develop design tools for guide vanes.



Sammendrag

Verden har gjennom Parisavtalen i 2015 og senere den oppdaterte Glasgowavtalen i 2021 blitt enig om å fase ut kullkraft. I tillegg til et større forbruk med store variasjoner, er det et behov for å bygge ut fornybare energikilder. Sol og vindkraft er i dag sett på som en av de viktigste utnyttede kildene. Utfordringen for disse fornybare energikildene er at de kun kan produsere strøm når det henholdsvis er sol og vind. Vannkraft er sett på som en fornybare kilde som kan komplettere energiproduksjonen og i teorien produsere for å dekke behovet. Det betyr at vannkraft må brukes mer på ugunstige driftspunkter og det vil være mer start og stopp. Dette reduserer levetiden til aggregatene. Det internasjonale samarbeidsprosjektet HydroFlex, støttet av EU har som mål å utvikle verktøy og undersøke løsninger for mer ugunstig drift av vannkraft. Vannkraftlaboratoriet ved NTNU er en samarbeidspartner som står for blant annet de fysiske testene og validering av de numeriske beregningene som er gjort.

I denne masteroppgaven har det blitt gjennomført en modell test i henhold til standarden IEC60193 for nye ledeskovler designet av PhD kandidatene Filip Stojkovski og Marija Lazarevkj. Nevnte ledeskovler er laget for å validere de numeriske beregningene og videreutvikle et verktøy for design av ledeskovler for større variabel drift av francis turbiner.

Vannkraftlaboratoriet ved NTNU har gjennomgått en større oppgradering med bytte ut generator, ventiler og samtidig designet nytt kontrollprogram. Etter oppgraderingen ble gjennomført en referanse modelltest skulle gjennomføres for å sjekke at riggen oppførte seg som forventet/før oppusingen. Testen viste at riggen oppførte seg normalt, men det nye målesystemet hadde en for høy usikkerhet. Dette ble løst ved å øke måletiden.

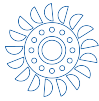
De nye ledeskovlene har blitt designet feil. Dette ble løst ved å bygge opp låseringen med et gammelt sagblad.

Modelltesten av de nye ledeskovlene viser en reduksjon i virkningsgrad på beste virkningsgrads punkt fra 92.5% med gamle ledeskovler til 90.7% med nye. De nye

ledeskovlene har endret åpningsmønster slik at ledeskovlene må åpnes mer for å slippe like mye vann inn i turbinen. Dette diskuteres som mulig årsak til virkningsgradreduksjonen, da endret vinkel kan endre hastighetstrekantene og dermed redusere hastighetskomponenten i innløp beskrevet i Eulers turbinligning. Den endrede vinkelen kan også skape ujevn strøm og separasjon på trykksiden av turbinbladene.

To av ledeskovlene har vært instrumentert med strekkklapper på ledeskovlakslingene for å måle moment. Disse viser at det er høyeste momentet er ved lavest massestrøm, og synker når vannmengden øker. Momentet snur aldri vei og har dermed ingen nullpunkt. Dette vil ved en driftsstans i servoen som kontrollerer ladeapparatet resultere i at ladeapparatet vil søke der det er lavest moment, som er ved full åpning.

Modelltesten har blitt gjennomført etter IEC60193 og resultatet viser ledeskovlene ikke leverer like godt som referanseledeskovlene. Det er høy usikkerhet som skyldes lav prøvetakningshastighet. Resultatene vil kunne brukes til å validere numeriske bergeninger og videreutvikling av designverktøyet for ledeskovler.



Acknowledgments

Even though a master thesis like this is a solo project. It is in fact a team work. I am thankful for all of you that I can call as my team. The Laboratory technicians, Joar, Halvor and Trygve. Thank you for always finding solutions. I can not say this enough, you are magicians, and it is always fun to go down to the Laboratory to ask for something. Actually, all of the employees of the Waterpower Laboratory and its associates is fun and meaningful to work with and around. I really love working at the Waterpower laboratory and an extra year here, has not been the worst thing to happen.

To my supervisor, Ole Gunnar, and co supervisors, Igor and Johannes: Thank you for including me, discussing with me and correcting me. I always learn something new when I talk with you, and there has been a pleasure with all your knowledge you have tried to transfer. The Waterpower Laboratory is unique because this kind of cooperation. Johannes, I really like to work with you, and you have made my stay at Waterpower Laboratory a lot easier with at all time having time for discussion if the topic is important or not at all important. I really hope you are enjoying the rest of your PhD.

The team of co students from both years I have been sitting here at the loft has been really helpful. I am grateful for all the breaks, table tennis matches, excursions and hydro power relevant discussions. There is no doubt that I enjoy spending time at NTNUI Roing, and Im sure that my three years in Trondheim had not been this fun and rewarding if it was not for the rowing club. Thank you for being hard task that are easy to use as procrastinating.

The most important part of my team is off course the family and friends that always gives my energy. You have been a key inspiration to this sometimes impossible task. I have really needed all your support and most of your criticism. Thanks for all the nice phone calls and dinners. Thank you all for all your help, but especially thank you Kajwan. What you have done for me is incomprehensible, and I will always be thankful for that!

Most of the Phd and master thesis that i have read, there is a common factor for all of them, they end the acknowledge with thanking their wife/husband, partner, or boyfriend/girlfriend. You are not one of those things to me, but Erling. Thank you.

Contents

Abstract	vii
Sammendrag	ix
Acknowledgments	xi
Contents	xiii
List of tables	xviii
List of figures	xx
Nomenclature	xxi
1 Introduction	1
1.1 Introduction	1
1.2 Objective	3
1.3 Prior and ongoing work	4
2 Theory	5
2.1 Hydro power theory	5

2.2	Guide Vanes	8
2.3	Measurements	12
2.4	Phenomena	14
2.5	Calibration and uncertainty	15
3	Methods	21
3.1	Francis rig - Configurations	23
3.2	Francis rig - Components	24
3.3	Francis rig - Instrumentation	27
3.4	Calibration	30
3.5	Measurement procedure	32
4	Calibration and uncertainty	35
4.1	Calibration	35
4.2	Uncertainty analysis of the calibration	35
4.3	Uncertainty analysis of the results	37
4.4	Work in the laboratory	37
5	Results	39
5.1	Refurbishment of the lab	39
5.2	Preliminary model test of F99 with old guide vanes	39
5.3	Repeatability	40
5.4	F99 with new guide vanes	41
6	Discussion	49
6.1	Old guide vanes	49
6.2	New guide vanes	49

Contents	xv
7 Conclusions	55
7.1 Further work	56
References	57
A Appendix A	61
A.1 Calibration constants	61
A.2 Results	62
A.3 Calibration reports	65
B Appendix B	113
C Appendix C	119
C.1 Calibration report from Langleite[1]	119

List of Tables

2.1 Geometrical parameters of guide vanes shown in Figure 2.2 [2].	10
2.2 Calibration errors from the component in a instrument [3].	18
2.3 Component error in a measurement [3].	18
3.1 Components of the Waterpower Laboratory [4] , The AC generator was installed on rig fall 2021	24
3.2 Collected parameters and sensor types in the LabVIEW program, Where the transducer measuring torque and rotational speed was installed on rig fall 21	27
4.1 Systematic uncertainty of the flow meter	36
4.2 Random uncertainty of the flow meter	36
5.1 Generator torque uncertainty with different sets of guide vanes.	40
5.2 Data on reference points for the F99 with old guide vanes.	41
5.3 Uncertainty of guide vane torque measurements	42
5.4 Data on reference points for the F99 with new guide vanes	43
5.5 Uncertainty of efficiency measurement	45
A.1 Calibration constants	61

A.2 Calibration constants wheigning tank 62

List of Figures

2.1	Guide vane torque factor versus guide vane angle measured [5] . . .	10
2.2	Illustration of geometrical parameters of guide vanes provided by Stojkovski et al. [2].	11
2.3	Illustration of new guide vane	12
2.4	Velocity field at runner inlet [6, 7].	14
2.5	Illustrations of velocity triangles [8].	15
3.1	Graphical overview of a part of the Waterpower Laboratory’s piping system.	22
3.2	Schematic overview of the Waterpower Laboratory as seen in the SCADA in the control room.	22
3.3	The Francis turbine rig at Waterpower Laboratory and placement of sensors used in efficiency measure [9]	29
3.4	Placement of three pressure transducers in the vane less space between the runner and the turbine [10].	29
3.5	Illustration of the connection between a instrumented guide vane and the Wheatstone bridge inside a DAQ module.	30
3.6	Guide vane torque calibration device.	32
5.1	Reference points distribution for the F99 turbine with old guide vanes.	40

5.2	Measured torque on guide vane shaft plotted against guide vane opening angle.	42
5.3	Reference points distribution for the F99 turbine with new guide vane	44
5.4	Comparing efficiency and flow of old and new guide vanes.	44
5.5	Hill diagram for F99 turbine with old guide vanes.	46
5.6	Hill diagram for F99 turbine with new guide vanes.	47
6.1	Illustration showing the velocity triangle change between a guide vane and a runner blade.	52

Nomenclature

Abbreviation

AC	Alternating Current
BEP	Best Efficiency Point
CFD	Computational Fluid Dynamics
cRIO	compact reconfigurable IO Modules
DAQ	Data acquisition
DC	Direct Current
DFT	Discrete Fourier Transform
F99	Francis turbine
F100	Francis turbine
F101	Francis turbine
FDB	Flow Design Bureau
Fr	Froude number
GVA	Guide Vane Angle [°]
GV	Guide Vane
GVT	Guide Vane Torque
IEC	Internation Electrotechnical Commision

NACA	National Advisory Committee for Aeronautics
n_{ED}	Speed factor factor
NTNU	Norwegian University of Science and Technology
NVE	Noregs vassdrags- og energidirektorat
PIV	Particle image velocimetry
PP	Pressure pulsations
Q_{ED}	Discharge factor
Re	Reynolds number
RSI	Rotor Stator interaction
SCADA	Supervisory Control And Data Acquisition
SSO	Synchronous Speed Operation
VKL	Waterpower Laboratory/Vannkraftlaboratoriet
VSO	Variable speed operations

Latin symbols

a	Coefficient
b	Coefficient
c	Absolute velocity [$\text{m} \cdot \text{s}^{-1}$]
D_1	Inlet diameter of the runner [m]
D_2	Outlet diameter of the runner[m]
E	Energy [$\text{J} \cdot \text{kg}^{-1}$]
e_i	Error
f	frequency [Hz]
f_i	Relative uncertainty
g	Gravitational Coefficient [m s^{-2}]
H	Head [m]

n	Rotational speed [rpm]
P	Power [W]
p	pressure [kPa]
Q	Discharge / Flow rate [$\text{m}^3 \cdot \text{s}^{-1}$]
S_Y	Standard deviation
T	Torque [Nm]
u	Peripheral velocity [$\text{m} \cdot \text{s}^{-1}$]

Greek symbols

α	angle [$^\circ$]
β_2	Outlet surface angle [$^\circ$]
β	Surface angle [$^\circ$]
η	efficiency [%]
ω	angular velocity [$\text{rad} \cdot \text{s}^{-1}$]
ρ	density [$\text{kg} \cdot \text{m}^{-3}$]
τ	Torque [Nm]

Chapter 1

Introduction

1.1 Introduction

The Paris agreement in 2016 and the updated Glasgow meeting fall of 2021 is the beginning of the end of coal and fossil energy production. Over 190 countries have agreed to the 2 degrees Celsius goal, later revised to a 1.5 degrees Celsius goal. The main human contribution to the global warming is the fossil-fuel based energy production [11]. In order to phase out carbon based energy sources, the different renewable energy sources are to be operated in a optimal way. Non-dispatchable sources, such as solar and wind, needs to be combined with dispatchable sources in order to fulfil the energy demand [12]. Hydro power is a key potential dispatchable energy source, especially when it comes to Norways energy production [13].

Hydro power was initially developed in the mid 18th century by the derivation of *Euler's pump and turbine* equations, named after the famous mathematician Leonhard Euler. These equations are fundamental for the operation of pumps and turbines, and consequently the development of modern hydro power technologies [14]. James Francis invented the first modern hydro power turbine, later known as the Francis turbine, in 1849. It is of today the most common turbine design [15]. He was furthermore recognised as the creator of the scientific method for testing hydraulic machinery. Francis calculated his original turbine design to run at an efficiency of 79.31%, and demonstrated through testing the efficiency to be 79.37%. [15]. In 1870 professor Fink further developed the Francis turbine and introduced guide vanes turning on a pivot [16]. This made it possible to control the discharge of the turbine.

The Norwegian Water Resources and Energy Directorate (NVE) states in their *2019 rapport on the changes in power production from 2019 to 2040* that the hydro power

capacity can increase with 6 % from 219 to 232 TWh. Wind power is on the other hand expected to increase by 205 % from 53 to 161 TWh, while solar power is to increase by 20 TWh [17]. This significant increase in non-dispatchable renewable energy sources results in an increasing demand for adjustable energy sources to complement. Hydro power offers itself as such a variable energy source. However, to fully complement solar and wind sources at their peak production, the hydro power turbines needs to be able to run at less efficient operation points and on off design.

The desire for better efficiency of hydro power plants has only grown ever since Francis began testing turbines. Especially in recent years, more powerful computers have accelerated the development through simulations and testing. These improved tools have enabled researchers to take turbines to a new level through marginal improvements.

As the computational power and the simulation tools have been better the last 20 years. The possibility to simulate hydro power turbines better. the EU program HydroFlex has taken the new operation scheme into account and uses a multi national team to evolve the hydro power for the future. The goal for HydroFlex is to use CFD combined with experimental work at the Waterpower Laboratory at NTNU. With the iterative process of designing and simulating in CFD, validate the results with experimental work in the laboratory and further adjusting the simulations and tools for better designs of hydro power turbines is the goal of the program.

Since James Francis initially introduced hydraulic machinery testing in the late 19th century, the tests have been standardized. The IEC60193 *hydraulic turbines, storage pumps and pump-turbines model acceptance tests* are used to control and quality assure the model tests of hydraulic turbines [5]. The Waterpower Laboratory at NTNU in Trondheim was refurbished in 2006 to match the IEC60193 with regards to high head Francis turbines. The rig was built for model testing the hydro power plant at Tokke in Norway. It has since been used to test multiple high head Francis turbines, and various phenomena such as fatigue failure and vibrations have been simulated [1, 18, 7].

There has been made significant and successful research on the Francis turbine, which now can reach a peak performance of 96 % (industrial peak according to word of mouth). The research and development of the turbine is not solely focused on improving maximum efficiency, but also a higher efficiency across a wider area

of operating points. The Francis turbine normally has a pointy hill diagram, but researchers such as NTNU's Igor Iliev attempts to improve the efficiency of the turbine running at off-design. The purpose of this is to make it possible to operate the runner at variable speeds without losing too much efficiency, while others are focusing on getting a better understanding of the expected lifetime and fatigue failures. Furthermore, researchers are also utilizing CFD design tools for cheaper and faster development of improved turbines. All this research is in its essence trying to ensure that hydro power becomes a viable and significant technological solution to climate change.

Scientific research on this theme is often done in collaboration with corporations, which unfortunately means the the published material often is confidential, mainly so that the companies can keep their trade secrets and competitive advantage. The theory and method of the research undertaken is described thoroughly, but results are mostly normalized and design blueprints almost impossible to find due to industry secrets. This can leave independent researchers with the feeling of undertaking research, which most likely have been done before. On the specific topic of Guide Vanes the literature is scarce, even though there exists multiple theories on the shape of the ideal guide vane. Nonetheless the literature rarely describes whether their guide vanes are hour glass shaped, have a classic NACA profile, or is twisted.

One of the goals for projects in the Waterpower Laboratory is to publish open access research and share results that contributes to better hydro power in the future.

1.2 Objective

The main objective of this master's thesis is to perform a model test of the Francis runner made for the Tokke test in 2006 when combined with new guide vanes. The model test will be done according to the IEC 60193 standard (*Hydraulic turbines, storage pumps and pump-turbines - Model acceptance tests*), and be done in the Waterpower Laboratory at NTNU.

In the summer of 2021 the laboratory was refurbished, and therefore the control program, the generator, and valves were upgraded. To ensure repeatability and comparability of the tests before and after the changes, model tests with the F99 turbine with the old guide vanes will be made first. The model test done with the new guide vanes will be done with two guide vanes instrumented with strain gauges to control for the torque on the shaft of the guide vanes. The results will then be used to validate future CFD simulations.

1.3 Prior and ongoing work

The HydroFlex project aims towards scientific and technological breakthroughs to enable hydro power to operate with very high flexibility in order to utilize the full power and storage capability. The project will create the environmental, social and technical basis for successful future industrial developments by performing well-focused research and innovation activities on the key bottlenecks of hydro power units that restrict their operating range and thus limit their flexibility.

[19]

As quoted above the HydroFlex project focuses on various aspects of hydro power. Igor Iliev focused his PhD research on the variable speed operation of the Francis turbine, and developed multiple turbine designs to operate the turbine at different speeds and operation points. The ability to operate the runner at different rotational speeds were made possible with the use of a frequency converter. The overall goal was to be able to operate the turbine at less stress and thereby extend its lifetime. Gro Langleite performed a model test of one of the turbines designed by Iliev et al [1], while West performed a model test of the second runner, also made by Iliev. In these model tests it was shown, as suggested/discussed/predicted/hypothesised by Iliev [10], that it is possible to improve efficiency of the turbine when operating with variable speeds. West furthermore demonstrated lower pressure pulsations while operating at variable speeds instead of operating with a constant and static runner speed as it is normally done [20]. Johannes Kverno will also use the guide vanes used in this model test for his ongoing PhD work. His objective is to investigate the Francis turbine with an increased use of start-stop operations, high ramping rates and rapid load changes using the F101 turbine, which was tested by West in the spring of 2021. His experimental results will, as this model test, be used to validate the numerical analysis undertaken in the HydroFlex project, which is to be completed in May 2022. The papers by Stojkovski et al. "*Constraints of Parametrically Defined Guide Vanes for a High-Head Francis Turbine*" [2] and "*Parametric design tool for development of a radial guide vane cascade for a variable speed Francis turbine*" [21] are fundamental for this project. The theoretical work published in the papers above on the numerical analysis and development of a design tool to develop guide vane cascades requires experimental validation. This is partly done by the research undertaken for this thesis. The goal is to develop a way to obtain a quality "flow feeding" of a variable speed high head Francis turbine [2].

Chapter 2

Theory

2.1 Hydro power theory

2.1.1 Energy conversion

Hydro power is essentially about converting potential energy, stored in water at high altitudes, to energy that human society can utilize. This is done in multiple steps. First, the potential energy of water is converted to kinetic energy (or hydraulic energy) as it falls along rivers and streams pulled by gravity. Then the hydraulic energy in the falling water is converted to mechanical energy using a turbine, which is finally converted to electrical energy by a generator. In IEC60193:2019, the head, H , is defined as

$$H = \frac{\Delta p}{\rho \cdot g} + \frac{v_1^2 - v_2^2}{2 \cdot g} + (z_1 - z_2), \quad [\text{m}] \quad (2.1)$$

where Δp and $z_1 - z_2$ are the pressure and elevation differences between the inlet and outlet, respectively; v_1 and v_2 are the respective inlet and outlet velocities; ρ is the water density, and g is the gravity constant.

Hydraulic power, P_h , is then given by

$$P_h = E \cdot \rho \cdot Q \cdot \eta_h \cdot \eta_m = H \cdot g \cdot \rho \cdot Q \cdot \eta_h \cdot \eta_m, \quad [\text{W}] \quad (2.2)$$

where H is the head given by Equation 2.1, E is the hydraulic energy of the water, Q is the flow rate of the system, and η_m and η_h are the efficiencies described in the next section.

2.1.2 Efficiencies

The share of hydraulic energy converted to mechanical energy by the turbine is known as the total efficiency, η , and is given by

$$\eta = \frac{P}{P_h} = \eta_h \cdot \eta_m, \quad [\%] \quad (2.3)$$

where P is the total power and P_h is the hydraulic power. The total hydraulic efficiency can also be decomposed into two factors, the hydraulic efficiency, η_h , and the mechanical efficiency, η_m . These can be expressed in terms of the power variables as

$$\eta_h = \frac{P_m}{P_h}, \quad [\%] \quad (2.4)$$

and

$$\eta_m = \frac{P}{P_m}, \quad [\%] \quad (2.5)$$

where P_m is the mechanical power given as function of the angular speed, ω , and the torque, T of the rotating shaft attached to the turbine:

$$P_m = T \cdot \omega \quad [\text{W}] \quad (2.6)$$

2.1.3 Speed number

The speed number is used as a way to classify turbines [22], such that turbines with the same speed number has a similar characteristics and geometry. The speed number is a dimensionless variable and is given by

$$\Omega = \underline{\omega} \cdot \sqrt{\underline{Q}}, \quad [] \quad (2.7)$$

where

$$\underline{\omega} = \frac{\omega}{\sqrt{2 \cdot g \cdot H}}, \quad [-] \quad (2.8)$$

and

$$\underline{Q} = \frac{Q}{\sqrt{2 \cdot g \cdot H}^3}. \quad [-] \quad (2.9)$$

The speed number of the Tokke (F99) turbine is $\Omega = 0.274$ [23].

2.1.4 Hill diagram

The key characteristics of a hydro power turbine can be presented with a Hill diagram. The Hill diagram is a map of the hydraulic efficiency of the turbine at different operation points, where the rotational speed of the runner and the discharge

is known. To compare the functionality of a turbine to another, the rotational speed and discharge can respectively be expressed in a dimensionless version as n_{ED} plotted on the X axis and Q_{ED} plotted on the y axis.

$$n_{ED} = \frac{n \cdot D_2}{\sqrt{g \cdot H_n}}, \quad [-] \quad (2.10)$$

$$Q_{ED} = \frac{Q}{D_2^2 \cdot \sqrt{g \cdot H_n}}, \quad [-] \quad (2.11)$$

where D_2 is the outlet diameter of the turbine [5].

In the Hill diagram, the contour lines are the efficiencies calculated by

$$\eta_h = \frac{\omega \cdot (\tau_f + \tau_g)}{H \cdot g \cdot \rho \cdot Q}, \quad [-] \quad (2.12)$$

where τ_f and τ_g are the torques of friction and the generator. The nominator is an expression for the mechanical power, while the denominator is an expression for the hydraulic power, in agreement with Equation 2.4.

The contour lines of the Hill diagram are interpolated between the measured operation points. This obviously raises the dilemma of how frequent measurements should be taken to properly demonstrate the correct behaviour of the turbine, while minimising the collection of unnecessary data. Lines showing the different guide vane angles are normally added to the diagram for comparison. Once the parameters are given, the Hill diagram provides insight to how a turbine operates at different operation point, and how it is affected by changing discharge amount, guide vane opening angle, or rotational speed.

2.1.5 Turbine

The design philosophy of the turbine depends on numerous factors. The most important ones being the amount of head and discharge flow the turbine is going to handle. The rule of thumb is that the Pelton turbine handles high head and low flow, high head Francis handles medium head and flow, low head Francis handles low head and medium flow, while the Kaplan turbine handles low head and high flow. The above order of turbines is also roughly the order of use in the Nordic countries (Norway, Sweden, and Finland) when going from the west of Norway (little flow, high head) to the far east of Finland (low head, high flow). In this project, model tests are made for a high head Francis turbine designed for the power plant in Tokke, which is located in the middle of Norway. The Francis turbine is the worlds most used turbine design[15], the model tests done in this work will be relevant for a great deal of hydro power projects.

2.1.6 Runner

The turbine used in this project is a high head Francis with a low specific speed number. It is named F99, and was developed at NTNU for the Tokke powerplant in 2005 [23].

2.2 Guide Vanes

The guide vanes are the moving part outside the turbine runner that controls the flow of the turbine. The guide vanes are even distributed around the turbine. Every guide vane is connected to each other and moves together and equal. The main task of the guide vanes is to control the discharge and make the flow more uniform as it reaches the runner.

2.2.1 Wicket gate

Wicket gate is an umbrella term for the complete set of guide vanes in a turbine. Antonsen describes the term in his master thesis as *"There are some overlapping names on the wicket gate. The expression Wicket gate is often used on the whole set of guide vanes, while one or more guide vanes are simply called guide vane or guide vanes"* [24]. When operating the turbine, the wicket gate provides the the only means to control the flow in to the turbine. A closing wicket gate reducing the guide vane angle and vice versa when it is opening. Hence there is no flow in the turbine when the wicket gate is closed. The discharge is dependent on the opening angle of the guide vanes combined with the rotational speed of the turbine. For most of the Francis turbines operated in the industry, the rotational speed is fixed, which means that the only way to regulate the flow rate is by adjusting the wicket gate.

2.2.2 Design of guide vanes

Guide vanes are mainly designed based on empirical observations, and hence no exact design philosophy exist. The HydroFlex program has tried to develop such a philosophy where numerical analysis is used to guide the design process. As discussed in the paper by Skopje [2] there are multiple geometrical parameters, constrained to turbine design, that needs to be considered in the development of the guide vane cascade. The number of guide vanes, $z_{GuideVanes}$, is restricted by the number of runner blades, $z_{RunnerBlades}$, through

$$\frac{z_{GuideVanes}}{z_{runnerblades}} \neq Integer. \quad (2.13)$$

Hence a wrong number of guide vanes could break the above inequality and thereby

increase the risk of pressure pulsations in the turbine. The number of guide vanes then also restricts the length and the overlap of the guide vanes.

If the wicket gate is closed, there should be no clearance between the guide vanes such that there is no flow going through. The angle of the guide vanes relative to when the wicket gate is closed is known as the opening angle. Hence the zero point of the opening angle is when the wicket is closed, and will be determined by the thickness of the guide vane blades. Consequently, the behaviour of the guide vanes will also be determined by the thickness of them.

The max opening angle, α_{max} , is given by

$$\alpha_{max} = 4 \cdot (-4 \cdot \Omega^2 + 13 \cdot \Omega + 1), \quad [^\circ] \quad (2.14)$$

where Ω is the speed number given by Equation 2.7. This formula are empirical[25].

A critical feature when designing guide vanes is the position of zero torque on the guide vane shaft. If a fault in the system affects the servo controlling the wicket gate, the guide vanes may turn freely, and will therefore seek the point with minimal torque. If the zero torque point is close to a maximum or minimum opening angle, a servo fault will cause a rapid closing or opening of the wicket gate. This cause an extended pressure pulsation in the form of what is known as a water hammer. Normally a power plant is designed to withstand a water hammer of 120% of maximum pressure [26]. The ideal design of a zero torque point is between 40 and 70 % of BEP.

The IEC60193 standard describes examples of turbines that has two zero torque point, see Figure 2.1. For such turbines, a servo failure, could cause the wicket gate to move to either zero torque point, which are difficult to prepare safety measures for.

An example of geometrical parameters for guide vanes are given by Stojkovski et al. (2021), shown in Table 2.1. They used a NACA foil design when developing the new design tool used to design guide vanes.

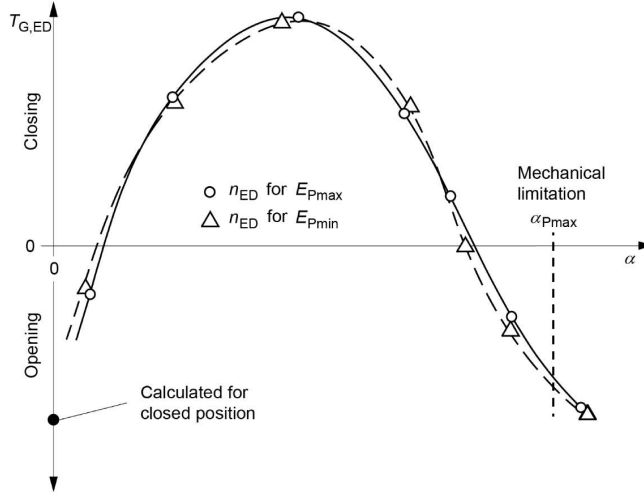


Figure 2.1: Guide vane torque factor versus guide vane angle measured [5]

Table 2.1: Geometrical parameters of guide vanes shown in Figure 2.2 [2].

Symbol	Unit	Description
R_i	[m]	Cascade inlet design radius
R_o	[m]	Cascade outlet design radius
R_x	[m]	Cascade Axis circumference radius
B_{gv}	[m]	Cascade Height
R_1	[m]	Runner blade inlet radius
φ	[deg]	Blade chord wrap angle
A	[-]	Starting point for chord placement
B	[-]	Strating point for the end of chord
B'	[-]	Rotated point B about the blade chord wrap angle
L	[m]	Blade chord lenght
t	[m]	Cascade pitch measured at axis circumference
t_o	[m]	Cascade pitchmeasured at blades outlet
L/t	[-]	Cascade density at axis circumference
α_i	[deg]	Cascade inlet flow angle
α_o	[deg]	Cascade outlet flow angle
δ	[deg]	Blade chord angle encloded with outlet radius
a_o	[m]	Blades opening
a_o/L	[-]	Relative Blade opening

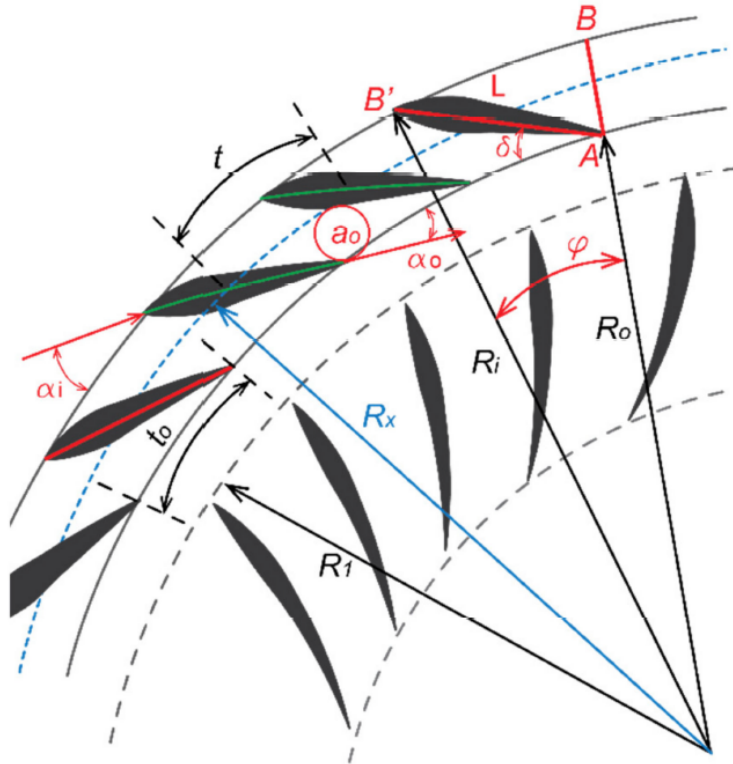


Figure 2.2: Illustration of geometrical parameters of guide vanes provided by Stojkovski et al. [2].

The nomenclature chosen for describing the different elements of the guide vanes is found in Figure 2.3. It has been done make it simpler to reference the elements of the guide vanes.

- A. Guide vane blade
- B. Shaft collar
- C. Guide vane shaft
- H. Height of guide vane blade

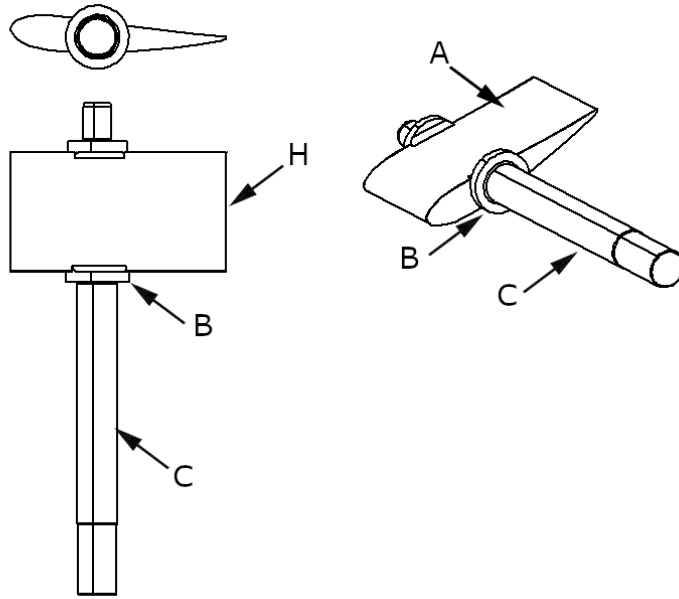


Figure 2.3: Illustration of new guide vane

2.2.3 Validation

The development of hydro power turbines in the last decade is driven by CFD simulations. However, these simulations need to be experimentally validated through tests. The model test presented in this work is such a test, and can be used to adjust the simulation parameters and thereby improve the simulation [27].

2.3 Measurements

2.3.1 Data acquisition

To collect data from all the sensors a data acquisition (DAQ) tool is used. The sensors convert parameters such as length, pressure, speed, etc. to electric signals. Then the DAQ tool converts the electric signals to digital signals, which are then logged as data using a logging program. The DAQ can be connected to a CompactRIO(cRIO), which is a controller chassis with a re-configurable input/output modules. This provides a way to control and monitor transducers. It has an ethernet connection and can push signals out to external logging computers [28].

The sampling rate and its resolution determines how much storage the data takes up. However, too low a sampling rate increases the likelihood of missing a key recording, which may then lead to a misinterpretation of the signal as an alias signal [29].

Nyquist's sampling theorem describes how the sampling rate should be twice as high as the highest expected frequency. However, according to the PhD work of Carl Bergan [30], it should be 10 times higher than the expected frequency. This means the model tests requires significantly more digital storage for data and computational power to process and analyse the results if one wants to adhere to the latter.

2.3.2 Strain gauge

A strain gauge is a simple sensor consisting of a thin copper thread. The strain gauge is mounted on a surface and when the surface changes length, the copper thread follows. The change in length makes it possible to measure the copper threads change in resistance, Ω [ohm], as the resistance of the copper thread is directly dependent on its length [31].

Wheatstone bridge

Since the change in resistance is small compared to the change in strain, one needs to to amplify the change in resistance. The circuit of the strain gauge resistor is mounted in what is called a Wheatstone bridge. This is a simple method to amplify the signal. This is taken care of in the data acquisition units.

2.3.3 Flow meter

In the Waterpower Laboratory, a Khrono flow meter is used to measure the discharge. The flow meter uses Faraday's law of induction applied to conductive liquids. The theory simply states that when a conductive liquid, such as water, moves through a magnetic field, a electric voltage is induced in the conductor. The induced voltage is proportional to the fluid's velocity. So if the velocity and the cross section area of the pipe is known, the flow rate can be determined. It is important to calibrate the flow meter which is done by the weighing tank in the laboratory [32, 4].

2.3.4 Torque sensor

Torque measurements are needed for both the torque on the generator-turbine shaft and the guide vane shaft. The former can be measured in two ways, either directly by using a HBM torque sensor mounted on the shaft, or indirectly from measurements of the generator. However, as the generator measurements has its own energy

losses, uncertainty will be propagated when using the indirect method. The generator at the Waterpower Laboratory has an efficiency of 95%, so that will have an severe impact on the uncertainties in the torque calculations. The guide vane shaft torque is on the other had measured with strain gauges mounted in a rosette setup. The measurements returns a torsion strain that can be used to calculate the torque.

2.4 Phenomena

Various phenomena can occur in the waterway and in the turbine. This section provides an overview of the phenomena relevant for this thesis and that can be measured by pressure sensors.

Rotor-stator interaction

Rotor-stator interaction (RSI) is occurs in the turbine. The phenomenon is caused by a pressure field that is being built up in front of the rotating part of the turbine. So when the blades of the turbine passes the guide vane blade, the pressure will fluctuate and pulsations will occur. as shown in Figure 2.4 it is the phenomen of the flow field distorton of the fuide wane combined wit the flow field distorton of the runner that combined makes the RSI.

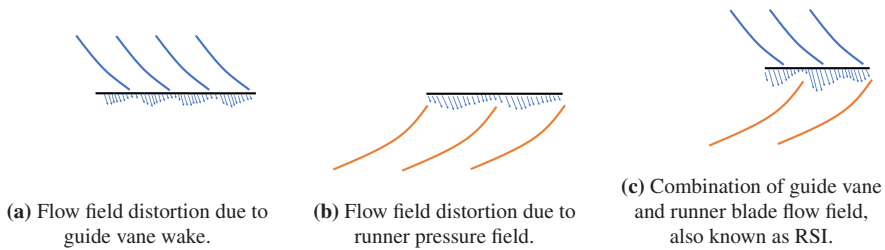


Figure 2.4: Velocity field at runner inlet [6, 7].

Velocity triangles

Euler's turbine equation is defined as

$$\eta = \frac{u_1 \cdot c_{\Theta 1} - u_2 \cdot c_{\Theta 2}}{g \cdot H_n} \cdot 100, \quad [\%] \quad (2.15)$$

where u_1 and u_2 are the rotational speed of the blade at the inlet and outlet, respectively, while $c_{\Theta 1}$ and $c_{\Theta 2}$ are the absolute velocities at inlet and outlet. Clearly, the best efficiency is achieved when the difference in the nominator are greatest. Thus

the best efficiency point is when $c_{\theta 2}$ is zero, and no swirl occurs in the draft tube [14, 33]. Figure 2.5 shows how the guide vane angle opening, which is directly correlated to α_1 , is determined by the velocities used in Equation 2.15.

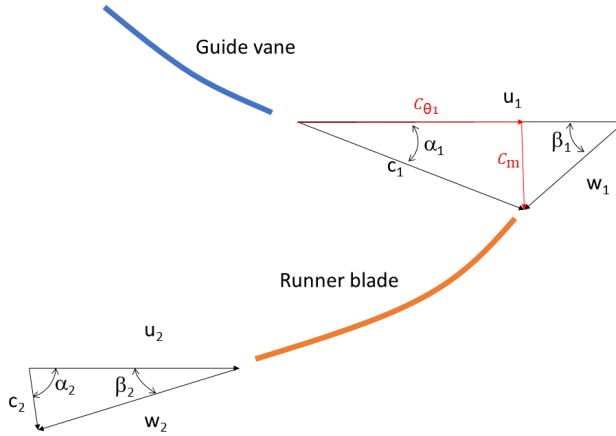


Figure 2.5: Illustrations of velocity triangles [8].

2.4.1 Water hammer

Water hammer is a phenomena that occurs when there is sudden changes in the hydro power system. Joukowsky defines the instantaneous pressure change, ΔH , as

$$\Delta H = \frac{a \cdot \Delta V}{g}, \quad [\text{m}] \quad (2.16)$$

where a is the speed of sound (~ 1450 [m/s] in water), and ΔV is the change in fluid velocity. However, the above equation only works for the instantaneous case, where the closing time T_c is less than $\frac{2 \cdot L}{a}$, where L is the distance to the closest water mirror.

2.5 Calibration and uncertainty

When something is measured it is important to know the validity of the measurement. *"There will always be some deviation between the actual value of the measured and the measurement system output. This deviation must simply be small enough that the output can be used for its intended purpose"* [31]. This deviation

is quantified by calibrating the measurement system and performing uncertainty analysis. In general terms, the error is defined as

$$\text{Error} = \text{Measured value} - \text{True value.} \quad (2.17)$$

According to the IEC60193 standard, a model test of a turbine must be done with a certain accuracy. Limit values are given for how large the uncertainty and errors should be. Measurement instruments used in the model test must be calibrated.

2.5.1 Calibration

There are seven physical variables known as the primary standards. These variables are *mass, time, length, temperature, electric current, amount of a substance and light intensity*. All other variables can be derived from these seven variables, e.g., velocity is derived as length divided by time. Calibration of sensors done using only these seven variables is called a the primary standard [31]. Calibration using derived parameters is called secondary standard, and one must be able to trace these either back to the primary standard or to another secondary standard.

An example of a calibration of a primary and secondary standard is the weighing tank and flow meter. First, the weighing tank is calibrated using the fixed water supply and a known dead weight of 5 tons. The dead weight is calibrated by the Justervesen(Norwegian Metrology Service), and can be traced back to the international standardised mass. The weight of the weighing tanks is therefore a primary standard calibration. Then the calibration of the flow meter can be made, as it relies on the calibration of the calibration of the weighing tank, and is therefore by a definition a secondary calibration. It is important to calibrate the sensors in its full measurement range, as errors are usually greatest at the extreme points of the range. If a sensor is damaged, mishandled, moved, or just systematically displays deviations of significant magnitude, it should be recalibrated. Uncertainties greater than the accepted limits also qualifies the sensor for a recalibration [5].

Every sensor and measurement system in the Waterpower Laboratory is calibrated by the manufacturer, who guarantees the measurements to lie within a specified error range. An in-house calibration can further reduce this range and thereby improve the accuracy of the measurements.

2.5.2 Uncertainty

Spurious errors

Spurious errors are errors arising from human mistakes or due to a failure in the measurement system. These occur often, but should be detectable as the the results often are clear outliers that can confidently be rejected. Outliers can further be

classified as measurements being more than two or three standard deviations from the expected value, and should also be discarded. The statistical method used for rejecting outliers in this project is a modified Thompson τ test [3, 31].

Random errors

If a measurement is repeated multiple times, but the output of the sensor deviates, the deviation is called a random error. This type of error is directly impacting the repeatability of the experiment, and it is therefore essential that they are properly quantified. It is normally assumed that random errors follow a normal distribution, and its distribution is therefore defined by its mean and standard deviation. However, for smaller sample sizes, Student's t-distribution is assumed instead. The standard deviation of the sample is given by

$$S_X = \sqrt{\frac{1}{n-1} \sum_{n=1}^{\infty} (x_i - \bar{X})^2}, \quad [-] \quad (2.18)$$

where x is an measurement, \bar{X} is the sample mean, and n is the number of measurements in the sample. The random error is given as

$$e_y = \pm \frac{t_{\alpha/2} \cdot S_X}{\sqrt{n}} \quad (2.19)$$

where $t_{\alpha/2}$ is the student t value. Hence increasing the number of measurements reduces the impact of random errors.

Systematic errors

Measurements, repeated with the same sensor, that are constantly either too high or low to the expected value, are classified as systematic errors. These errors can be minimised through calibration, albeit there will always be a difference between the true and measured value. The main sources for systematic errors are *Hysteresis*, *Linearity*, *Accuracy*, *zero offset* and *Drift*.

By taking into account the previously mentioned errors and adjusting for these, the calibration will be improved and thereby reduce the systematic errors

2.5.3 Total uncertainty

The total uncertainty is the combination of systematic and random errors, and can be determined using the *root square sum method* (RSS). It is given by

$$f_{TotalUncertainty} = \pm \sqrt{f_{systematic}^2 + f_{random}^2} \cdot 100, \quad [\%] \quad (2.20)$$

The RSS method is also used to determine the total uncertainty of calibration and measurement. The calibration errors one needs to take into account for the uncertainty analysis are listed in Table 2.2.

Table 2.2: Calibration errors from the component in a instrument [3].

Error	Description
$\pm f_{Xa}$	Systematic error of the primary calibration method
$\pm f_{Xb}$	Random error of the primary calibration method
$\pm f_{Xc}$	Systematic error(repeatably) of the secondary instrument
$\pm f_{Xd}$	Random error of the secondary instrument
$\pm f_{Xe}$	Physical phenomena and external influences
$\pm f_{Xf}$	Error in physical properties

The total uncertainty of the calibration errors are then calculated as [1].

$$f_{X_{cal}} = \pm \sqrt{\sum (f_{X_i})^2} \cdot 100, \quad [\%] \quad (2.21)$$

where i loops over the types listed in Table 2.2.

Similarly, the total uncertainty of the measurement errors in each measurement component is calculated using the RSS method on the error types listed in Table 2.3.

Table 2.3: Component error in a measurement [3].

Error	Description
$\pm f_{X_{cal}}$	Systematic error in calibration
$\pm f_{Xh}$	Additional systematic error in the instrument
$\pm f_{Xj}$	Error in physical properties
$\pm f_{X_{ks}}$	Systematic errors due to physical phenomena and external influences
$\pm f_{X_{kr}}$	Random errors due to physical phenomena and external influences
$\pm f_{Xl}$	Random error in repeatably of secondary instrument

and as before, the total uncertainty in the measurements are given by

$$f_{X_{total}} = \pm \sqrt{\sum (f_{X_n})^2} \cdot 100 \quad [\%] \quad (2.22)$$

where n loops over the types listed in Table 2.3.

Chapter 3

Methods

■ The chapter is written both by Gaute Elde Vefring and Halvor West as they collaborated on the laboratory work.

The Waterpower Laboratory has two reservoirs, one in the basement and one in the attic. Between these there is a piping system, a Francis test rig, a Pelton test rig, a cascade rig, two pressure tanks, and two pumps. The Francis rig holds an international standard for model testing according to IEC60193 [18, 5]. Figure 3.1 provides an overview of the laboratory with the Francis rig in focus.

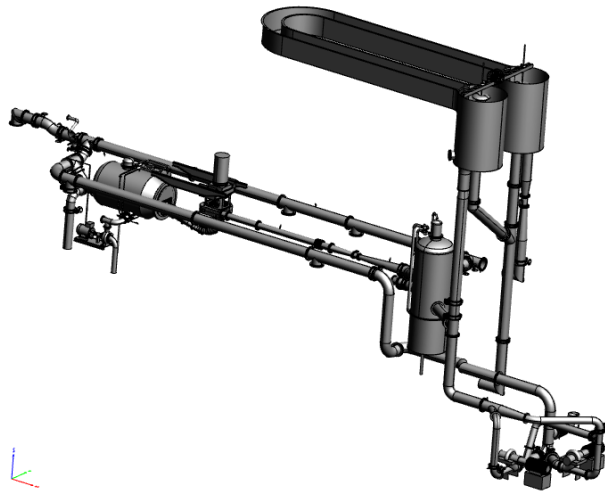


Figure 3.1: Graphical overview of a part of the Waterpower Laboratory's piping system.

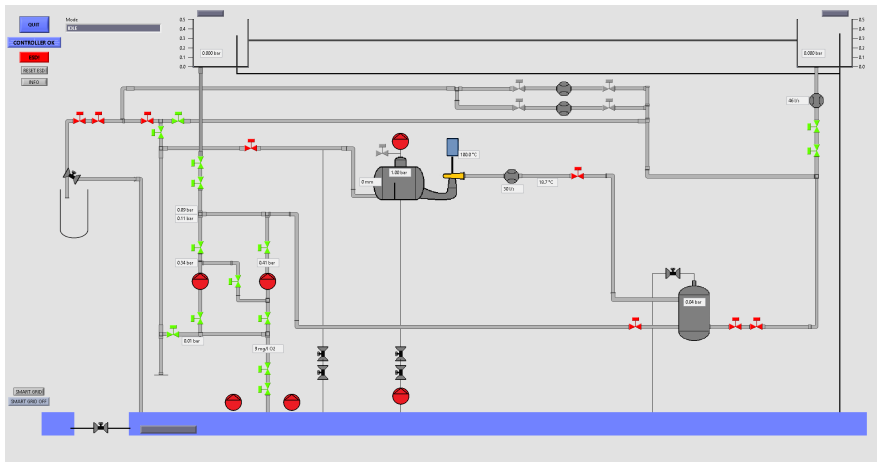


Figure 3.2: Schematic overview of the Waterpower Laboratory as seen in the SCADA in the control room.

3.1 Francis rig - Configurations

The Francis rig in the Waterpower Laboratory can be run with different configurations. These can be categorised as either *Open*, *Semi-closed* or *Closed* depending on the sequence the free surface pools, pumps, and turbine are placed relative to each other. The *Closed* loop can operate with the biggest head, while the *Open* loop is the easiest to operate.

3.1.1 Open loop

Open loop configuration uses the upper reservoir to build head. The head is determined by the difference in elevation between the free surface of the upper reservoir and the water level of the draft tube tank. The head does not change with a discharge change, making this configuration easy to operate. This is made possible by setting the discharge from the pumps greater than the one thru the turbine and utilizing the fact that excess water from the upper reservoir is transported directly to the basement sump.

3.1.2 Semi-closed loop

In a Semi-closed configuration the water goes directly from the pumps in the basement to the pressure tank. The pressure can be controlled to be higher than the elevation difference between the water level in the pressure tank and the draft tube tank. From the draft tube tank, the water goes to the sump, which is a free surface pool.

3.1.3 Closed Loop

A Closed loop is the configuration that provides control of the pressure in both the pressure tank and the draft tube tank. The water goes from the pumps into the pressure tank and then to the turbine. From the draft tube and draft tube tank, the water goes directly to the pump. In this way, it is possible to create a higher pressure difference and operate at a higher head for the turbine. The Closed loop is also the desired configuration when measuring the cavitation characteristics of the turbine because it allows for the creation of under pressure in the draft tube tank. Furthermore, the Closed loop gives the opportunity to control more of the system, for example the amount of oxygen dissolved in the water.

3.1.4 Operating the rig

All different configurations is operated from the control room. An Interactive Graphical SCADA System is used to control which configuration to run by showing which valves are open in the system. The user interface can be seen in Fig-

ure 3.2. The SCADA can control the valves and set the desired rotational speed of the pumps and the generator.

All sensors used in the measurement system are recorded with a professionally developed LabVIEW program which makes it possible to monitor outputs from all the sensors in real time. Hence the SCADA simplifies the operation of the rig.

3.2 Francis rig - Components

This subchapter is in large part based on information from the reference runner report of F99 [23], with some modifications. Table 3.1 shows the components which make up the Francis test loop along with key information. Some of the components will also be presented more thoroughly later on. For a figurative outlook of the rig see Figure 3.1 and Figure 3.2

Table 3.1: Components of the Waterpower Laboratory [4] , The AC generator was installed on rig fall 2021

Component	Key information
Upper reservoir	$V = 75m^3$ $z = 16.25m$ above deck
Lower reservoir	$V = 450m^3$ $z = 4.775m$ below deck
Pump motor	Manufacturer: ABB $P = 315kW$,
Pumps	Manufacturer: KSB RDLO $Q_{max} = 1m^3s^{-1}$ at 2 bar $\Delta p_{max} = 10$ bar at $0.5m^3s^{-1}$
High pressure tank	$V = 18m^3$ at 10 bar at $50^\circ C$
Spiral casing and Stay vanes	14 Stay vanes
Wicked gates	28 Guide vanes
Runner	$D_1 = 0.62m$ $D_2 = 0.349m$ F99: 15 full blades and 15 splitter blades F101: 17 full blades
AC Generator*	Manufacturer: ABB 8 poles $P = 400kW$ $\eta = 96\%$
Draft tube tank	$V = 7m^3$

3.2.1 Pumps

There are two identical pumps in the basement that can be operated in series, in parallel, or individually. Each pump is driven by a 315 kW motor and a frequency transformer, that enables variable speed operation of the pumps. This provides a flexible driving force for the rig, which can produce an extensive range of flow rates and heads.

3.2.2 Runner

Francis 99

The Francis 99 (F99) runner is a model replica (geometrically similar) of the prototype installed at the Tokke power plant around 2006. The prototype data are:

- $H = 377m$
- $Q = 31m^3/s$
- $n = 375rpm$
- $n_s = 0,27$

Hence the prototype runner can be categorized as a high head Francis. F99 is made in a 1:5.1 scale to the prototype and has 15 full blades and 15 splitter blades. The inlet and outlet diameter are $D_1 = 0.63m$ and $D_2 = 0.349m$, respectively. The runner has been utilized for multiple research projects at Waterpower Laboratory over the years, making it suitable as a reference study for the refurbished rig.

3.2.3 Generator

The new ABB generator is an AC generator in contrast to the old Siemens generator, a DC generator with an ACDC converter. AC generators are the standard in the hydro power industry. The generator requires a frequency converter to operate the turbine at different rotational speeds. The new generator is coupled to the Smart Grid Laboratory at NTNU, making it possible to further research the generator digitalization of the power grid, grid behavior and cyber security connected to the power system. The change from DC to AC generator is due to the development of better control of AC generators.

- Model: ABB M3MP 400LKC8 [34]
- Power: 400 [kW]

- Frequency: 50 hz
- Efficiency: $\eta_{generator} = 0.96$
- Torque: $\tau_{generator} = 5134Nm$

In the context of efficiency test of the turbine, the generator itself is not being tested. Instead the efficiency is tested by measuring the torque and speed of the turbine-generator shaft. The generator is used to fix the speed of the turbine at the different operating conditions.

3.3 Francis rig - Instrumentation

Table 3.2 gives a brief overview of sensors used on the Francis rig, while Figure 3.3 gives an overview of the placements of the sensors used for the efficiency measurements.

Table 3.2: Collected parameters and sensor types in the LabVIEW program, Where the transducer measuring torque and rotational speed was installed on rig fall 21

Measurand	Sensor	Output	Sampling frequency
Generator torque	HBM T12HP *	V	5 kHz
Rotational speed	HBM T12HP *	V	5 kHz
Friction torque	HBM Hottinger Z6FC3	V	5 kHz
Guide vane angle	Pepperl+Fuchs Multiturn absolute encoder	V	~10 Hz
Inlet pressure	Kulite HKM375 7bara	V	5 kHz
Differential pressure	Fuji electric FKCW 36V	A	5 kHz
Vaneless space pressure	Kulite XTE190 3.5bara	V	5 kHz
Draft tube pressure	Kulite HKM375 1.7bara	V	5 kHz
Dissolved oxygen	YSI FDO 700 IQ	V	5 kHz
Temperature	Siemens pt100	V	5 kHz
Atmospheric pressure	Vaisala barometer PTB 220	A	~4 Hz
Discharge	Krohne Altoflux IFS 4000	V	~10 Hz
Guide Vane Torque	HBM Series Y 1-XY41-3/350	V	5 kHz

3.3.1 Flow meter

The flow meter has the function of measuring the flow rate of water entering the turbine. It is installed between the pressure tank and the turbine, approximately 9 meters upstream of the turbine inlet. It is of the electromagnetic flow meter type utilizing Faraday's law of induction, where the water functions as a conductor moving in a magnetic field to measure the flow rate [23, 32]. It is manufactured by Krohne.

3.3.2 Pressure sensor

Pressure is measured at multiply points on the stationary part of the rig: turbine inlet, differential pressure over the turbine, three locations in the vaneless space

between guide vanes and runner, and at two locations in the draft tube. These sensors are calibrated frequently. For the absolute pressure measurements, the height difference between the measurement point and the sensor location has to be considered. However, for the differential pressure measurement this effect cancels out. All sensors are manufactured by the same producer, Kulite. However, due to the variation in pressure, the sensors have different requirements depending on their installed location. Additionally, the atmospheric pressure is measured using a digital barometer located in the control room.

Vaneless space sensor

Three pressure transducers are mounted downstream of one guide vane and upstream of the runner. In this the behaviour of the flow right after the guide vanes can be measured. This shows the influence of the guide vane on the flow. See Figure 3.4 for an example of the placement of the vaneless space pressure transducers.

3.3.3 Temperature

The temperature of the water is measured downstream of the high pressure tank, using a temperature probe with an internal amplifier/signal converter. The sensor is of the Siemens Pt100 type.

3.3.4 Generator torque and rotational speed

Along with the newly installed generator, a new measurement system for the generator torque and rotational speed was installed in the laboratory. This is a non-contact digital transducer from the manufacturer HBM [35].

3.3.5 Guide vane shaft torque

Two of the NACA guide vanes are instrumented with strain gauges to measure torque on the shaft, as seen in Figure 3.5. The strain gauges are of the type HBM Series Y 1-XY41-3/350, and are connected to a DAQ module with an in-built Wheatstone bridge.

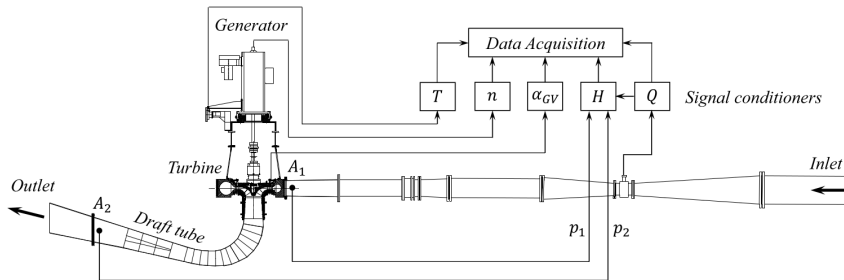


Figure 3.3: The Francis turbine rig at Waterpower Laboratory and placement of sensors used in efficiency measure [9]

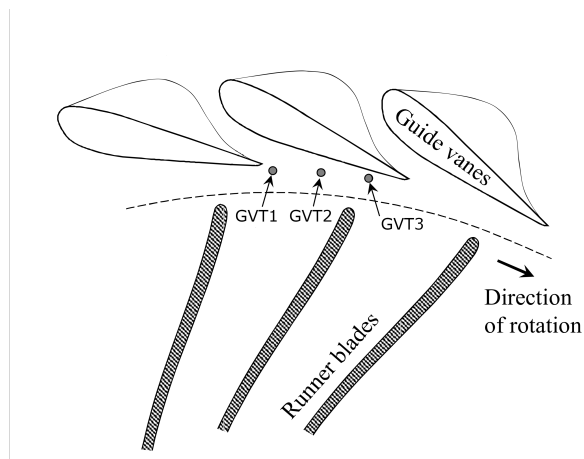


Figure 3.4: Placement of three pressure transducers in the vane less space between the runner and the turbine [10].

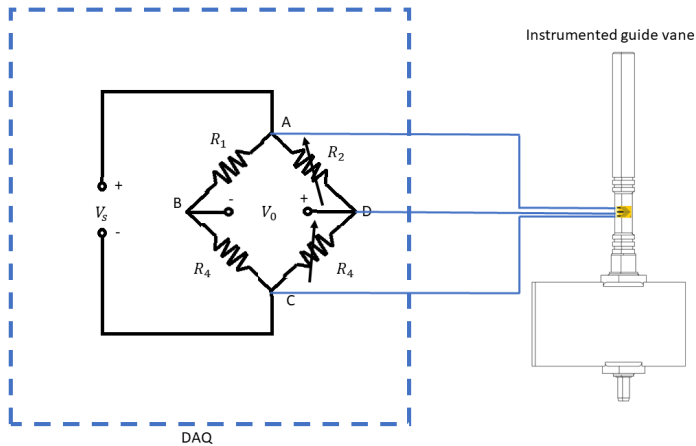


Figure 3.5: Illustration of the connection between an instrumented guide vane and the Wheatstone bridge inside a DAQ module.

3.3.6 DAQ & cRIO

The sensors and transducer signals are connected to DAQ and cRIO for logging. The DAQ chassis is sampling the signal with a 5 KHz frequency. For the sensors connected to the cRIO the signals are then transmitted to the logging program, which transmits the signals at 1 Hz frequency. The reason why some of the sensors are connected to the cRIO instead of a DAQ, is that this provided the opportunity to share the data with research partners of the laboratory, such as the SmartGridLab and SINTEF [36].

3.4 Calibration

As a part of the preparations made for the model test, some of the sensors have been calibrated in accordance with the Waterpower Laboratory procedures. Below follows a brief presentation of the calibrations done throughout this semester. All sensors should be calibrated evenly according to the IEC60193. There are some sensors such as water temperature and rotational speed that is not calibrated, because of refurbishments in the lab. This kind of sensors does not need to be calibrated that often when they are not moved or tampered with. The Torque transducer should have been calibrated but because of the lack of equipment and procedures, the manufactures calibration is used.

3.4.1 Pressure

The pressure sensors were calibrated in two steps. First, the draft tube sensors were calibrated using the low pressure dead weight testers with air as the working fluid. Second, the differential and inlet pressure sensors were calibrated using the high pressure dead weight testers with water as the working fluid. In both cases, weights of known accuracy are put on a piston of known area, which is pumped up so that it is floating and spun, so no static friction acts between piston and cylinder. This increases the pressure of the working fluid which is connected to the pressure sensors. In this way it is possible with highly precision to decide what pressure is applied to the pressure sensor and then know what the pressure sensor measures. These calibrations were done in accordance with the Waterpower Laboratory procedures.

The pressure as the weights are loaded onto the piston is calculated from:

$$p = \frac{m \cdot g}{A}, \quad [\text{kPa}] \quad (3.1)$$

where g is the gravity constant and A the area of the piston are known, and m , the mass of the dead weights are the varying parameter. The pressure transducer gives an output signal in Volts that varies linearly with load, hence the calibration equation can be determined using the following linear interpolation:

$$p = a[\text{measured value}] + b \quad [\text{kPa}] \quad (3.2)$$

3.4.2 Guide vane torque

The torque acting on the guide vane shaft is measured with two rosette strain gauges and a Wheatstone bridge as described in subsection 2.3.2. The calibration is done with an in-house designed rig, see Figure 3.6. The guide vane is mounted with an arm. In order to avoid bending the shaft, the calibrated weights are applied on both sides simultaneously. The length of the arm and the weight of the hanging fixtures are known.

As the weights are applied, the torque on the shaft will increase according to

$$T_G = m_1 \cdot l_1 g + m_2 \cdot l_2 g, \quad [\text{Nm}] \quad (3.3)$$

where m_1 and m_2 are the masses added (varying parameter), l_1 and l_2 the arm lengths (known) and g the gravitational acceleration (known).

The strain gauge gives an output signal varying linearly with applied load. Hence the calibration equation is given by

$$T_G = a[\text{measured value}] + b, \quad [\text{Nm}] \quad (3.4)$$

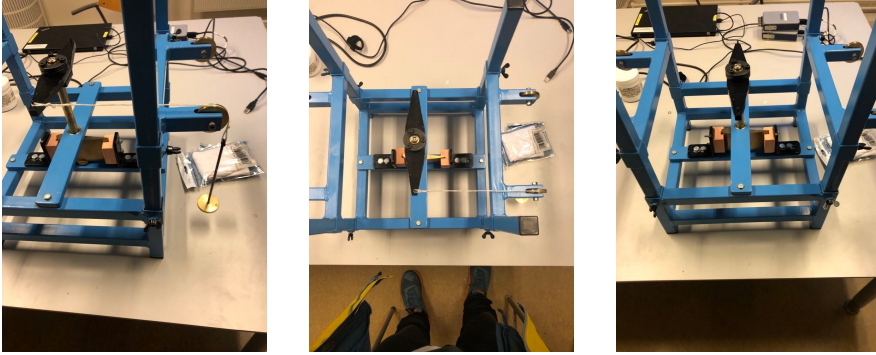


Figure 3.6: Guide vane torque calibration device.

3.5 Measurement procedure

As previously mentioned, the laboratory has been refurbished this summer/fall, where the valves, actuator and generator has been changed, as well as the SCADA. To test the new components, a reference study of the F-99 runner will be conducted and compared to the results from the master thesis of G.K.Støren [18].

After this, the model tests that are part of the HydroFlex project can be conducted. A new set of calibrations will have to be done between each test. Each model test will be conducted to the procedure described in the following subsection.

3.5.1 Procedure

To check the repeatability and drift of the rig, a fixed point should be measured every morning after startup routine and every evening before closing routine. This is called the reference point and is a way to compare the rig with itself when the tests are done over several days.

1. Choose a reference point. In this project the best efficiency point was chosen as it was already known. Measure the reference point before any new series of measurements. These reference points will be used in the repeatability check.
2. Set Guide vane angle to the desired value.
3. Use the generator to increase shaft speed, so the runner speed is $n_{ED} = 0.1$. Wait for the system to stabilize and then start measuring.

-
4. Decrease the runner speed such $\Delta n_{ED} = 0.05$. Wait for the system to stabilize and measure the new point.
 5. Repeat until torque on generator equals zero.

Steps 2-5 are repeated for every guide vane angle. For guide vane angles with odd numbers the starting point should be $n_{ED} = 0.105$ to make the grid "tighter".

The runaway curve is measured as a stand-alone series. Due to friction in the generator and thrust block, the runaway curve is measured when the generator is driven as a motor to compensate for the frictional losses.

Chapter 4

Calibration and uncertainty

4.1 Calibration

All calibration constants are provided in Appendix A.

4.1.1 Calibration of differential pressure sensor

First calibration of the sensor was rejected, hence a recalibration was needed.

4.2 Uncertainty analysis of the calibration

The uncertainty analysis of calibration is thoroughly done by G. Langleite [1, 37] and is attached in appendix. Most calibration work in the Waterpower Laboratory was done by Storli in 2006 [4] and Bjørn Winther Solemslie in 2011 [3]. Langleites formalised the procedures to make it more transparent and clear in 2020 as part of her work.

The total uncertainty is calculated using the RSS method described in subsection 2.5.3.

Flow meter

The systematic uncertainties of the flow meter, as calculated by Storli, are provided in Table 4.1.

Table 4.1: Systematic uncertainty of the flow meter

Uncertainty	Magnitude
$f_{Q\Delta W}$	$\pm 0.05043\%$
$f_{Q\Delta t}$	$\sim 0\%$
$f_{Q_{divider}}$	$\pm 0.072611\%$
$f_{Q\rho}$	0.01%

The resulting total systematic uncertainty of the flow meter is then

$$f_{Q_a} = \sqrt{(f_{Q\Delta W})^2 + (f_{Q\Delta t})^2 + (f_{Q_{divider}})^2 + (f_{Q\rho})^2} = \pm 0.08897\%. \quad (4.1)$$

The random uncertainty of the flow meter, as calculated by Storli, are provided in Table 4.2

Table 4.2: Random uncertainty of the flow meter

Uncertainty	Magnitude
$f_{Q\Delta W}$	$\pm 0.00072\%$
$f_{Q_{divider}}$	$\pm 0.050339\%$
$f_{Q\rho}$	$\sim 0\%$

The resulting total random uncertainty of the flow meter is then

$$f_{Q_b} = \sqrt{(f_{Q\Delta W})^2 + (f_{Q_{divider}})^2} = \pm 0.0503\% \quad (4.2)$$

The regression error combines the random and systematic error, and is found in the calibration report. For the extreme points, the regression error is greater than for ordinary operation points. The regression error is presented for the BEP where the flow is around 214 liter per second. The regression uncertainty is $f_{Q_{reg}} = \pm 0.0723\%$ and the calibration uncertainty of the flow calibration is given by

$$f_{Q_{cal}} = \sqrt{f_{Q_a}^2 + f_{Q_b}^2 + f_{Q_{reg}}^2} = \pm 0.1278\%. \quad (4.3)$$

4.3 Uncertainty analysis of the results

Torque transducer

The errors in the calibration are not determined for the new torque transducer, but the calibration certificate gives a value of $\pm 0.015\%$ [35].

4.3.1 Flow meter

After the refurbishment the signal from the flow meter is now logged directly as a current signal in the cRIO, instead of the old method of converting to a voltage signal and logging with a DAQ.

$$Q = a \cdot V_{measured} + b \quad [\text{m}^3/\text{s}] \quad (4.4)$$

4.4 Work in the laboratory

After the preliminary tests of the system with the old guide vane and F99 runner, a session of work in the laboratory has been done: Together with Trygve Opland a oil leakage has been fixed, the old guide vane has been disassembled, and a new guide vane has been mounted. It is a careful process where small clearances down to < 0.05 mm are measured and adjusted. A problem occurred due to the new guide vane being drawn wrong with a height difference of 0.77 mm. This means the guide vanes had no room for movement and was jammed between the upper and lower ring.

Chapter 5

Results

5.1 Refurbishment of the lab

The laboratory has been refurbished multiple times in the last year. Equipment that have been replaced includes the torque transducer, generator, valves, logging program, and SCADA. All these replacements makes errors more likely to occur and consequently results more unreliable. It was therefore crucial to check the refurbished rig for any technical issues and ensure that outputs made sense. As a result, multiple leakages, missing signals, and other smaller non-optimal issues were fixed, all due to the refurbishment. Once this was done, the preliminary model test of the F99 rig was conducted.

5.2 Preliminary model test of F99 with old guide vanes

After the refurbishment the test of the rig setup was done following the model test procedure (see subsection 3.5.1). The test included measurements for the entire operation area of the turbine. The new cRIO and an updated version of the FDB logging program was used to log in the FDB program at a rate of 1 Hz. This low sampling rate gave rise to a high uncertainty, which is discussed in subsection 2.3.1. 61 measurements of the torque delivered to the generator was collected. The data has a mean of 657.87 Nm and a standard deviation 11.5 Nm, resulting in a random error of 2.9 Nm and an uncertainty of 0.45 % at 95 % confidence level, when assuming a Student t-distribution. The random error and uncertainty of the efficiency is found to be 0.47 and 0.503 %. The IEC60193 recommends a maximum random uncertainty of 0.10 %. As a solution to the high uncertainty, the sampling time was doubled from 60 to 120 seconds. Table 5.1 shows both the generator torque for old guide vanes with 60 sec sampling time and the new guide vanes where the sampling is doubled.

Table 5.1: Generator torque uncertainty with different sets of guide vanes.

Guide vanes	Mean \bar{Y}	Standard deviation S_y	Random error e_y	Uncertainty f_y
Old	657.87 Nm	11.46 Nm	2.93 Nm	0.45 %
New	595.39 Nm	9.96 Nm	1.79 Nm	0.301 %

5.3 Repeatability

Figure 5.1 and Table 5.2 shows that the distribution of the measurements are all close to the mean. Again, assuming a Student t-distribution, a mean and standard deviation of 92.4% and 0.1579% is achieved at a 95% confidence level. The diagram Figure 5.1 shows the reference points measured for the test series of F99 with old guide vanes. Maximum and minimum lines are plotted along the mean and standard deviation. The Table 5.2 shows the movement of reference by including the data for the n_{ED} and Q_{ED} .

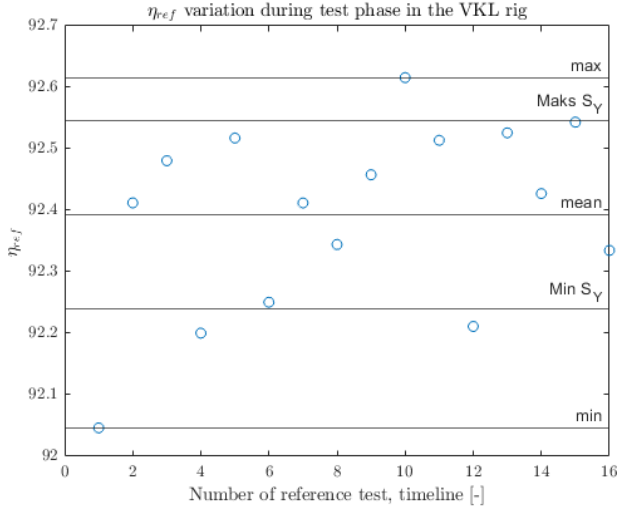
**Figure 5.1:** Reference points distribution for the F99 turbine with old guide vanes.

Table 5.2: Data on reference points for the F99 with old guide vanes.

Index	Name	η [%]	Q_{ED}	n_{ED}
1	"dag3_ref_kveld"	92.05	0.1544	0.1812
2	"dag4_ref_kveld"	92.41	0.1537	0.1814
3	"dag3_ref_morgen"	92.48	0.1544	0.1796
4	"dag4_ref_morgen"	92.20	0.1528	0.1813
5	"dag4_GV03"	92.52	0.1539	0.1814
6	"dag4_GV04"	92.25	0.1539	0.1814
7	"dag1_GV05"	92.41	0.1538	0.1809
8	"dag3_GV06"	92.34	0.1548	0.1806
9	"dag1_GV07"	92.46	0.1535	0.1812
10	"dag2_GV08"	92.62	0.1537	0.1811
11	"dag2_GV09"	92.51	0.1536	0.1812
12	"dag3_GV10"	92.21	0.1547	0.1807
13	"dag2_GV11"	92.53	0.1538	0.1810
14	"dag4_GV12"	92.43	0.1539	0.1814
13	"dag3_GV13"	92.54	0.1543	0.1796
14	"dag4_GV14"	92.34	0.1529	0.1812

5.4 F99 with new guide vanes

A misunderstanding meant that the new guide vanes were designed with a blade height 0.77 mm higher than the original ones. However, the height of the inlet of the turbine was still higher than the new blades, so by expanding the lock ring and the turbine shaft, the new guide could be fitted. Guide vanes could then move, and the flow did not meet an edge in the turbine inlet.

5.4.1 Guide vane shaft torque

The torque on the guide vane shaft decreases as the guide vane angle increases. Figure 5.2 shows that there no zero points, but as the flow increases due to an increasing opening angle of the wicket gate, the torque is decreasing. The two instrumented guide vanes is called GVT1 and GVT2. GVT1 is upstream of GVT2.

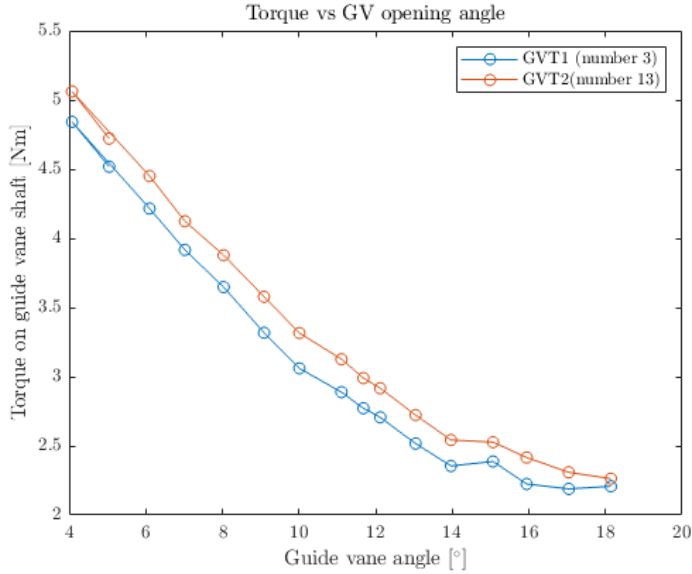


Figure 5.2: Measured torque on guide vane shaft plotted against guide vane opening angle.

5.4.2 Uncertainty of torque measurements

The uncertainties provided in Table 5.3. Errors were low for both sets of instrumented guide vanes, but lower for the GVT1.

Table 5.3: Uncertainty of guide vane torque measurements

Guide vanes	Mean \bar{Y}	Standard deviation S_y	Random error e_y	Uncertainty f_y
GVT1	2.706 Nm	0.0114 Nm	2.8937e-05 Nm	0.001 %
GVT2	2.916 Nm	0.0846 Nm	2.1415e-04 Nm	0.007 %

5.4.3 Distribution of reference measurements

The reference points of the model test (F99 with new guide vanes) has a standard deviation of 0.1667, an error of 0.0615, and a uncertainty of 0.0682, at a 95

% confidence interval. The mean of the measurements is 90.11 % efficiency. In Figure 5.3 the standard deviation, mean, and extreme points are plotted for each reference measurement, while Table 5.4 provides n_{ED} and Q_{ED} values for all the measurements.

Table 5.4: Data on reference points for the F99 with new guide vanes

Index	Name	η [%]	Q_{ED}	n_{ED}
1	"F99_newGV5"	90.17	0.1391	0.1778
2	"F99_newGV6"	90.21	0.1395	0.1781
3	"F99_newGV7"	90.24	0.1396	0.1779
4	"F99_newGV8"	90.45	0.1394	0.1780
5	"F99_newGV9"	90.13	0.1397	0.1778
6	"F99_newGV11"	89.75	0.1392	0.1778
7	"F99_newGV12"	89.90	0.1391	0.1779
8	"F99_newGV13"	90.22	0.1391	0.1779
9	"F99_newGV14"	90.19	0.1392	0.1778
10	"F99_newGV15"	89.98	0.1395	0.1780
11	"F99_newGV16"	90.12	0.1392	0.1779
12	"F99_newGV185"	89.99	0.1394	0.1780
13	"F99_newGV_dag1_ref_kveld"	89.92	0.1395	0.1779
14	"F99_newGV_dag3_ref_kveld"	90.16	0.1391	0.1778
15	"F99_newGV_dag4_ref_kveld"	90.24	0.1398	0.1781
16	"F99_newGV_dag5_ref_kveld"	89.86	0.1409	0.1745
17	"F99_newGV_dag1_ref_morgen"	90.02	0.1398	0.1780
18	"F99_newGV_dag2_ref_morgen"	90.38	0.1394	0.1779
19	"F99_newGV_dag3_ref_morgen"	90.15	0.1397	0.1778
20	"F99_newGV_dag4_ref_morgen"	89.96	0.1392	0.1778
21	"F99_newGV_dag5_ref_morgen"	90.11	0.1396	0.1779
22	"F99_newGV_dag4_ref_midday"	90.25	0.1396	0.1781

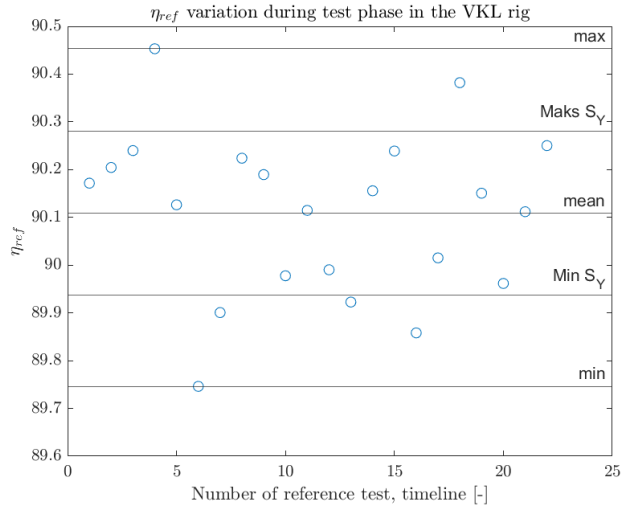


Figure 5.3: Reference points distribution for the F99 turbine with new guide vane

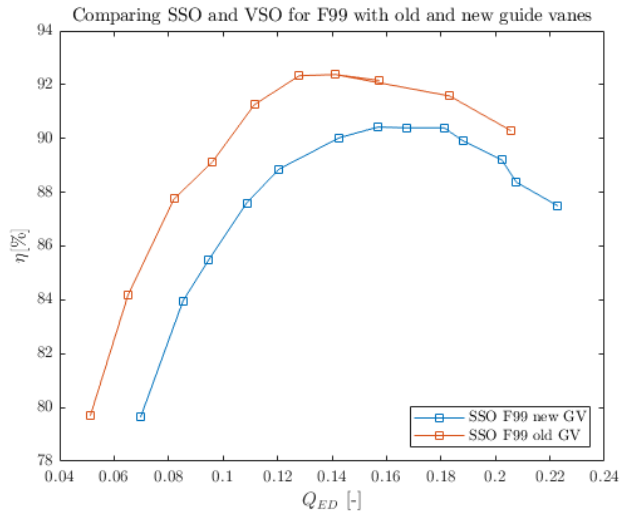


Figure 5.4: Comparing efficiency and flow of old and new guide vanes.

5.4.4 Efficiency comparison

Figure 5.4 clearly shows that the new guide vanes have a significant lower efficiency across the whole operation range. The highest efficiency point for the old guide vanes is 92.5 %, while for the new guide vanes it is 90.6 %. Note that the new guide vanes has been tested for a higher range of flow rates.

5.4.5 Uncertainty of efficiency measurements

Table 5.5 shows that a doubling of sampling time to 120 seconds reduces the uncertainty to 0.25 %, which is higher than desired according to IEC60193.

Table 5.5: Uncertainty of efficiency measurement

Guide vanes	Mean \bar{Y}	Standard deviation S_y	Random error e_y	Uncertainty f_y
Old	92.5%	4.05	0.466	0.503%
New	90.6 %	2.87	0.234	0.258%

5.4.6 Hill diagram

Hill diagrams have been made in for both model tests in cooperation with Gaute Elde Vefring. Vefring has developed the program used for interpolating measurements, which enables the plotting of the hill diagram. The "horizontal" lines shows the guide vanes opening angle. The small dots are measurement points, while the contour lines are interpolated efficiencies.

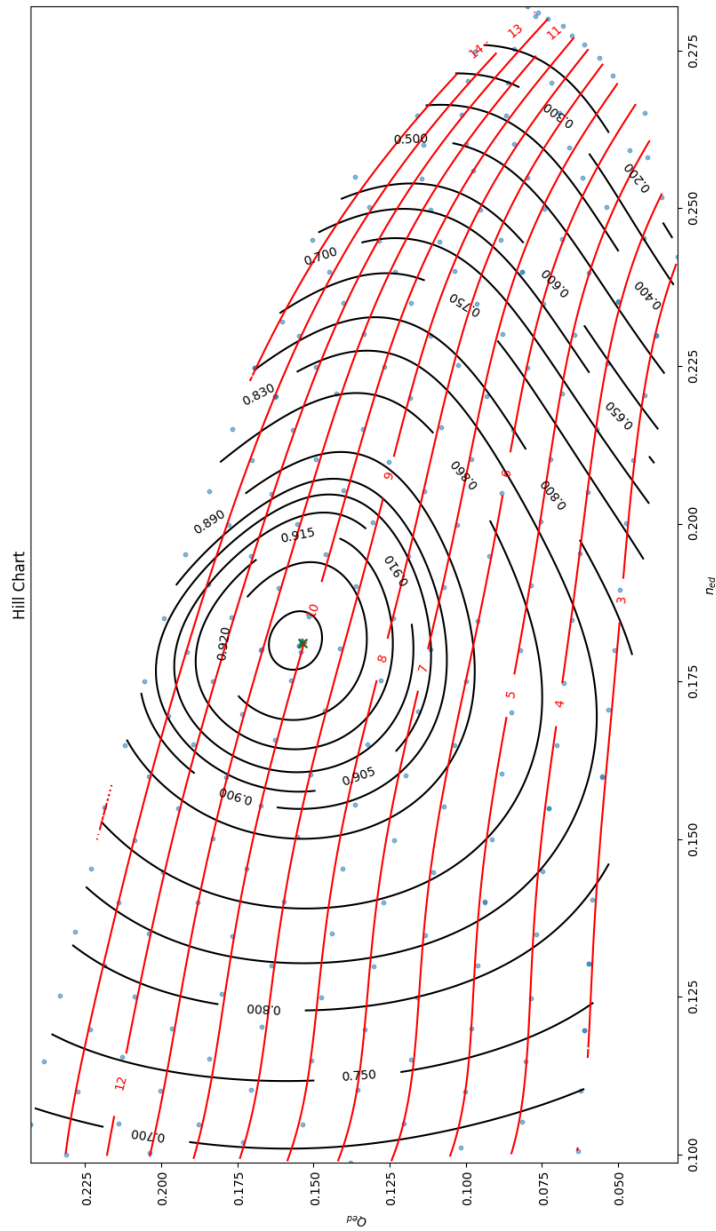


Figure 5.5: Hill diagram for F99 turbine with old guide vanes.

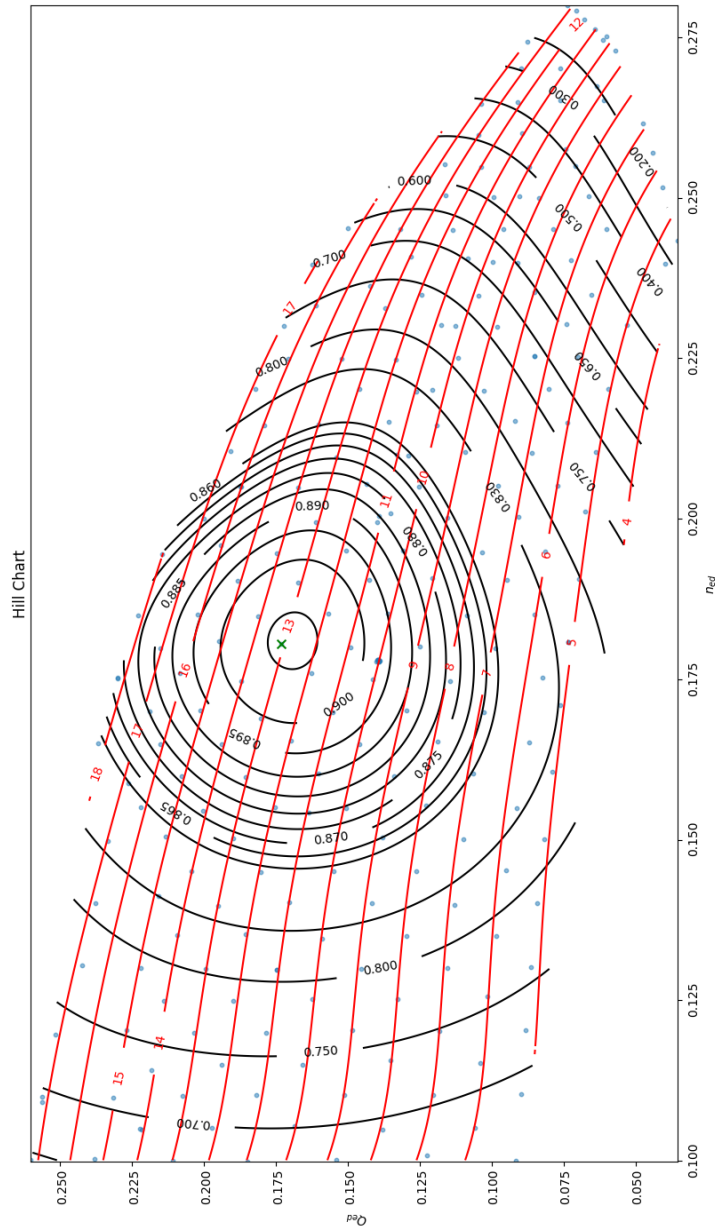


Figure 5.6: Hill diagram for F99 turbine with new guide vanes.

Chapter 6

Discussion

6.1 Old guide vanes

The test of the F99 turbine with old guide vanes revealed no significant impact on the efficiencies post refurbishment. However, it was observed that operating the rig with the new generator is more stable, compared to the old setup. This was due to an improved control of the rotational speed of the rig.

6.2 New guide vanes

6.2.1 Observations

As mentioned in the results, the new guide vanes are 0.77 higher than the old guide vanes. The expansion of the lock ring was done using a band saw blade with the desired thickness. This is discussed further in subsection 6.2.2.

In addition to the height difference, the new guide vanes differs from the old ones on a range of points. The pivot point of the guide vanes are moved such that the blades are further away from the turbine. It is expected to reduce the Rotor-Stator interaction (RSI) between the runner blades and guide vanes. The effect of this was measured, but due to time constraints, the data has not been processed and analysed. Furthermore, the movement of the pivot point gives the "tail" a longer radius and makes it move longer. This is expected to increase the torque on the shaft of the guide vanes at off design points.

6.2.2 Height difference solution

The solution to the design mistake was to shim down the lower ring with 0.8 mm made from a old band saw blade. However, the solution caused the turbine opening not match the guide vanes opening, which consequently would induce non-uniform

flow. This was again solved by shimming down 0.4 mm. The final solution was not ideal, but acceptable for the model test. In an ideal world, the guide vanes should have been redesigned to match the original drawing, such that opening turbine is significantly greater than the height of the guide vanes.

6.2.3 Post processing

The first series of tests with the F99 and old guide vanes, the quality of the measured data was poor. This was due to the new system, which logged the torque via the cRIO, had the logging rate going from 5 KHz to 1 Hz. Consequently, the results had a higher uncertainty. The new logging program also increased the logging channels from 75 to 263. As explained in subsection 2.3.1 on *Data acquisition*, a high sampling rate requires higher computational power. Despite the low sampling rate, logging files were too large in size (>750 MB). Before the refurbishment file sizes were around 600 MB, while they now were approximately 1.5 GB. This meant that even the powerful CFD computers at the Waterpower Laboratory was unable to process the data in MATLAB. The solutions for this was to split up the test series into four pieces. However, this increased the risk of losing data, which ended up happening.

6.2.4 Guide vane angle movement relative to discharge

The discharge is clearly dependent on the guide vane opening angle. At a constant pump and runner rotational runner speeds, and the same guide vane opening, the discharge was lower for the new guide vanes compared to the old. A five degree opening of the new guide vane corresponds roughly to a seven/eight degree opening for the old one. This meant that the mechanical stop had to be moved, such that the max guide vane angle opening was extended from 14 to 18 degrees. Consequently, the reference point is not the best efficiency point for the turbine. The guide vane opening angle is measured relative to the closing point. Hence the blade thickness will have an influence on this. To investigate whether this was the reason for the reduced discharge, the cross section area between guide vanes was measured at both zero and ten degrees opening angle. However, no difference were found compared to the old guide vanes, and is therefore not a reason for the reduced discharge.

6.2.5 Low efficiency

The SSO curve for both the new and old guide vanes has been plotted in Figure 5.4 to illustrate the decrease in efficiency when using the new guide vanes. The new design is clearly not improving the efficiency. However, all tests are done with ~ 12 meters of head, instead of the recommended 30 meters head that ensures a sufficiently high Reynolds number [5]. It is expected that the overall efficiency of

the new guide vanes will increase, though unlikely it will catch up with the old ones. The efficiency at BEP of F99 with the old guide vanes at 30 meters head 93.5 %. The complete SSO curve for the new guide vanes can be assumed to have the same form as the SSO curve for the reference guide vane in Figure 5.4, as the turbine is identical and is the main component for generating the energy.

The new guide vanes were meant to be an upgraded version of the old guide vanes, but with the same constraints on shaft diameter, shaft length etc. Figure 2.3 shows how the shaft collar height and diameter is the same for the new and old ones. The latter however has two supporting wedges that covers the clearance, whilst the former does not have one. This clearance that is present in the new guide vanes, may be disturbing the flow, and thereby reduce the efficiency.

Taking into account the historical efforts made in the field to increase hydro power turbines efficiency by just 2 %, a 2 % loss is significant.

6.2.6 Low efficiency due to movement of discharge

Another reason for the decreased efficiency could be due to the movement of guide vane angles. An increased guide vane angle will increase the α angle in Figure 6.1. Then $c_{\Theta}1$ will decrease, as c_m is constant, and consequently the efficiency will decrease as explained by Euler's turbine equation Equation 2.15. As described in subsection 2.4, the new guide vanes needed an 2 degree increase in opening angle to produce the same discharge.

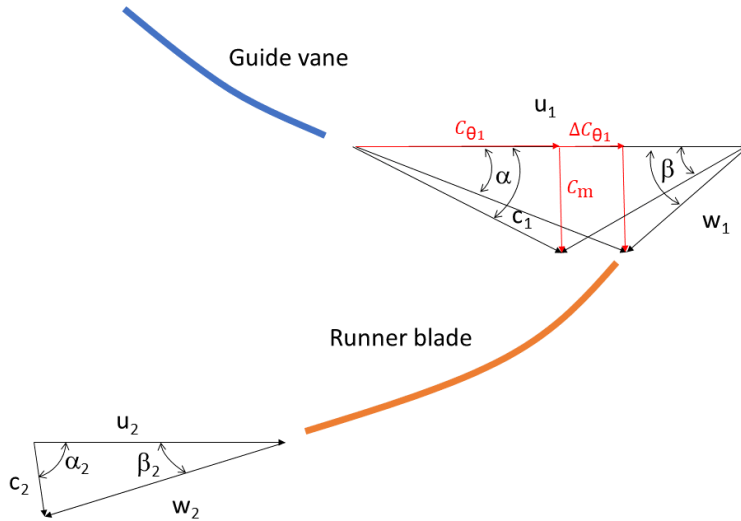


Figure 6.1: Illustration showing the velocity triangle change between a guide vane and a runner blade.

At a given operation point, rotational speed, u_1 , and discharge, $c_{\theta 1}$, are constant, but α may change. The latter will consequently make w_1 and β_1 change as well. This impacts the inlet angle and the flow relative velocity, β and W , which will become suboptimal for the turbine. Thus the optimal efficiency point, where there is a perfect flow, does not align with the efficiency point, at which the velocity triangle matches the turbine design. Euler's turbine equation Equation 2.15 states that the efficiency will drop as c_{θ} decreases. This is exactly what happens when α increases. However, it is not clear if the drop in efficiency is mainly caused by change of c_{θ} or the suboptimal relative velocity direction, w_1 . The latter can cause flow separation at the pressure side of the leading edge of the runner blade. Flow separation is a secondary flow that dissipates heat, and therefore decreases efficiency. This happens when the β angle decreases and the relative velocity, W , changes direction.

6.2.7 Instrumented guide vane vibration

The two guide vanes that were instrumented with strain gauges behaved strangely compared to regular ones. The logged measurements had a lot of noise, and upon

inspection it was clear that they vibrated noticeably. However, the vibration was only noted without further investigation. A reason for the vibration could be the ball bearings, which allows the guide vanes to move freely. The instrumented guide vanes are lathed down to increase the interaction with the strain gauges. This makes the guide vanes weaker and may have induced more vibration. The uncertainty analysis of the guide vanes also shows that guide vane vibration is proportional to its uncertainty.

6.2.8 Guide vane shaft torque

The main reason for measuring the torque on the guide vane shaft is in case a failure occurs. This is called a servo failure and explained in subsection 2.2.2. A promising result of the tested guide vanes is that the form of the curve (see Figure 5.2) and its uncertainty (see Table 5.3). These shows only a single zero point, which means that in case of a failure, it will always be known, how the guide vanes will move. This makes it easier to operate in case of a failure and thereby mitigate the impacts. Additionally, that the two sets of guide vanes have a similar curve in Figure 5.2 indicates a good result. However, the differences between the two curves could be due to a pressure loss in the spiral casing, a poor calibration, or different mounting. The change in torque around the spiral casing, which is seen in case, is also reported by [38].

6.2.9 Uncertainty

The uncertainty of sensors sampled using the cRIO is unacceptably high. This high uncertainty is due to the low sampling rate (1 Hz) of these sensors. An attempt to improve it was done by doubling the sampling time from 60 to 120 seconds, however this did not have the desired effect. In the spring of 2021, a sampling rate of 5 KHz was used, so the doubling of the sampling time still provides relatively little information. A consequence of this increased sampling time was larger data files for post processing, which caused significant challenges, without any real impact on results. The reason why the sampling rate in 2021 was 5 KHz, is that those sensors were connected directly in a DAQ tool and into the logging program instead of the cRIO.

The effect of both the sampling time and rate on the uncertainty is also evident for the combined efficiency, η , shown in Table 5.5. For the new guide vanes, the uncertainty drops down to the half of the uncertainty of the old guide vanes, when the number of log points doubles. Nevertheless, the uncertainty is still significantly higher than the recommended value provided by IEC60193.

Another consequence of increasing the sampling time with one minute, is an increased overall test time. As 260 measurements are taken a minute, the one minute

increase, causes the the total time to increase by 4 hours. On the other hand, measurements are usually taken five minutes apart from one another, just in case there is a human error and the test conductor starts the measurement before the rig has stabilized. Despite that increasing sample time will make measurements more stable, it is not a viable strategy due to the significant addition of time.

Regardless of the high uncertainty due to the low sampling rate, the results clearly show that the guide vanes are not performing better than the old ones. A 2 % decrease in efficiency is however too large to counter weight the hypothetical benefits of the new guide vanes, such as an increased lifetime of the turbine.

6.2.10 Final thoughts

The experimental laboratory work and physical tests done as a part of this thesis has been subject to substantial delays and issues. The root cause for these has been the refurbishment of the laboratory in 2021. The refurbishment was highly needed, and have brought a lot of improvements to the laboratory. The generator has made it considerably easier to operate the rig, while the in-house developed SCADA has made it possible to update and modify the software easier. However, there has been numerous delays, leakages, and issues with the execution of this model test. It has been time consuming, stressful, and has to a high degree affected the amount of post processing and analysis that could be done within the time frame of the thesis. Several last minute changes has also meant a lot of work had to be redone. So even though it is possible to conduct a model test using the Francis rig, there is still a need for continuing the crucial work with upgrading the laboratory.

Chapter 7

Conclusions

In this work new guide vanes for the F99[23] Francis turbine has been tested. Initially a model test of the turbine with the old guide vanes was conducted to control for any changes made during the refurbishment in the Francis rig at Waterpower Laboratory in 2021. All tests was done according to IEC60193 and showed no significant difference in performance before and after the upgrade. Then a similar model test was made with a new set of guide vanes. These were built to validate the numerical analysis done by Stojkovski et al. [39, 2] as a part of the multinational HydroFlex project[40].The model test was executed despite a design fault in new guide vanes, which meant they were 0.77 mm to high. The fault is unlikely to have affected the model test itself, but did delay the process. The new guide vanes performed poorly compared to the existing guide vanes. Its efficiency was almost 2 % lower than the old guide vanes for all measured points, for best efficiency point from 92.5% to 90.7%. Additionally, the guide vanes did not let enough discharge through to the turbine. This mean that the new guide vanes needed to be opened an additional 2 degrees to achieve the desired flow rate for the best efficiency point. The analysis of the results indicates that the change of direction of the velocity at the inlet will change the velocity triangles and could be the reason for the 2 % efficiency loss.

Two of the guide vanes were instrumented with strain gauges as prescribed by the IEC60193. This was done to measure the torque on the guide vane shaft, and locate any potential zero points of the opening angle. The test revealed that no such points exist, and in case of a servo failure, the guide vanes will open fully.

The first set of measurements showed unacceptable high uncertainty due to random errors. An analysis revealed that this was most because of the low sampling rate of the components logged using the cRIO as a data acquisition. An attempt to make a quick solution was made by doubling the sampling time to 120 seconds. Even

though this resulted in a lower uncertainty, it was still too high compared to our expectations. This is a clear weakness of the new setup and affected the quality of the model test performed. Nevertheless, the random error on the guide vane torque measurements was acceptable.

The purpose of this model test was to validate the result of numerical simulation models which is a part of the HydroFlex program. It is therefore natural to place this work as a small chapter in the development of the design tools used to discover improved guide vane designs. In this test, it was clear that the guide vane design has an important impact on the efficiency and the characteristics of the turbine. Hence further development of guide vanes could play a vital part in the development of increased flexibility of hydro power turbines for the future.

7.1 Further work

The refurbishment of the Waterpower Laboratory has improved the quality of the laboratory, however some work still remains to be done. First, the new torque transducer needs to be calibrated in-house. Secondly, the sampling rate of the logging system needs to be increased significantly. Currently, the transducers that are logged using the cRIO have too high an uncertainty. This needs to be thoroughly investigated, such that the random error and uncertainty can be reduced.

The model test has been focused on the guide vane shaft torque and efficiency. However, there are still more data to be analysed. Especially the pressure in both the draft tube and the vane less space between guide vanes and the turbine runner should be analysed further. This may give important insight into the behaviour of the guide vane. Furthermore, a PIV test of the area between guide vanes and turbine runner inlet could provide a better understanding of the changed velocity triangles, and thereby validate whether this is the cause for the reduced efficiency.

The upgrade of the Francis turbine rig at the Waterpower Laboratory at NTNU has been a success, but there is still some work to do. The arguments and decisions made with the upgrades are good, but there is a feeling that some of the systems used earlier is rejected just because they are old, not because of malfunction. This is eg. the logging system. With the new logging system with cRIO and in house software development. The opportunities are endless, but the Waterpower Laboratory Francis rig is made to do model test of hydraulic machinery, and this is the basis that needs to function before fancy upgrades can be prioritised.

References

- [1] Langleite, G. M. K., 2020, “Test of a Francis turbine with variable speed operation,” Ph.D. thesis.
- [2] Stojkovski, F., Lazarevikj, M., Markov, Z., Iliev, I., and Dahlhaug, O. G., 2021, “Constraints of Parametrically Defined Guide Vanes for a High-Head Francis Turbine,” *Energies*, **14**(9), p. 2667.
- [3] Solemslie, B. W., 2010, *Compendium in Instrumentation, Calibration & Uncertainty Analysis*.
- [4] Storli, P. T., 2006, “Modelltest av Francis turbin i Vannkraftlaboratoriet ved NTNU,” Ph.D. thesis, Norwegian University of Science and Technology.
- [5] International Standard, 2019, “Hydraulic turbines, storage pumps and pump-turbines -Model acceptance tests IEC60193,” Tech. Rep. NEK IEC 60193:2019, Norsk Elektronisk Komite.
- [6] Sannes, D., 2018, “Variable Speed Turbines,” Ph.D. thesis, Norwegian University of Science and Technology.
- [7] Agnalt, E., 2019, *Rotor-Stator Interaction in Low-Specific Speed Francis Turbines*, NTNU, Accepted: 2019-09-02T12:53:29Z ISSN: 1503-8181.
- [8] Kverno, J. O., 2019, “EP4811 Turbines,” .
- [9] Iliev, I., Tengs, E. O., Trivedi, C., and Dahlhaug, O. G., 2020, “Optimization of Francis Turbines for Variable Speed Operation Using Surrogate Modeling Approach,” *Journal of Fluids Engineering*, **142**(10).
- [10] Iliev, I., Trivedi, C., and Dahlhaug, O. G., 2019, “Variable-speed operation of Francis turbines: A review of the perspectives and challenges,” *Renewable and Sustainable Energy Reviews*, **103**, pp. 109–121.

-
- [11] “the Paris Agreement - UNFCCC,” accessed 2021-07-08, <https://unfccc.int/process-and-meetings/the-paris-agreement/the-paris-agreement>
- [12] Nakićenović, N. and on Climate Change, I. P., eds., 2000, *Special report on emissions scenarios: a special report of Working Group III of the Intergovernmental Panel on Climate Change*, Cambridge University Press, Cambridge ; New York, OCLC: ocm44652561.
- [13] Statnett, 2021, “verdien av regulerbar vannkraft statnett mars 2021,” Tech. Rep. Dok. 20/00565, accessed 2021-07-08, <https://www.statnett.no/contentassets/b82dcf206acc4762b2abcc3182e5bc52/verdien-av-regulerbar-vannkraft-statnett-mars-2021.pdf>
- [14] Brekke, H., 2003, *Pumper & Turbiner*.
- [15] Lewis, B. J., Cimbala, J. M., and Wouden, A. M., 2014, “Major historical developments in the design of water wheels and Francis hydroturbines,” *IOP Conference Series: Earth and Environmental Science*, **22**(1), p. 012020.
- [16] Kjølle, A., 2001, *HYDROPOWER IN NORWAY - Mechanical Equipment*, Trondheim.
- [17] Østenby, A. M., Veie, C. A., Sidelnikova, M., Skau, S., Koestler, V. J., and Aksnes, N. Y., 2019, “KRAFTPRODUKSJON I NORDEN TIL 2040.pdf,” Tech. rep., Norges vassdrags- og energidirektorat, accessed 2021-11-01, https://publikasjoner.nve.no/rapport/2019/rapport2019_43.pdf
- [18] Støren, G. K., 2021, “Signature investigation of typical faults on a Francis turbine[Master thesis],” Ph.D. thesis, Norwegian University of Science and Technology.
- [19] hydroadmin, “Objectives,” accessed 2021-11-25, <https://www.h2020hydroflex.eu/about/objectives/>
- [20] West, H. H., 2021, “Test of a Francis turbine with variabel speed operation,” Ph.D. thesis, Norwegian University of Science and Technology.
- [21] Stojkovski, F., Markov, Z., and Kostikj, Z., 2020, *DESIGN OF RADIAL BLADE CASCADES USING PARAMETRIZATION AND CORRELATION OF GEOMETRY AND FLOW PARAMETERS*.
- [22] Haugan, K., 2007, “Trykkpulsasjoner i Francisturbiner,” **180**, Accepted: 2014-12-19T11:44:42Z Publisher: Institutt for energi- og prosesssteknikk.

-
- [23] Dahlhaug, O. G., Ramdal, J., and Brandåstrø, B. A., 2007, “Tokke model test,” .
- [24] Antonsen, , 2007, “Unsteady flow in wicket gate and runner with focus on static and dynamic load on runner,” Ph.D. thesis, Norwegian University of Science and Technology.
- [25] Dahlhaug, O. G., 2021, “Guide vanes in Francis turbines,” .
- [26] Brekke, H., 2001, “HYDRAULIC TURBINES Design, Erection and Operation,” , p. 324.
- [27] 1998, *Guide: Guide for the Verification and Validation of Computational Fluid Dynamics Simulations (AIAA G-077-1998(2002))*, American Institute of Aeronautics and Astronautics, Inc., Washington, DC, _eprint: <https://arc.aiaa.org/doi/pdf/10.2514/4.472855>.
- [28] “CompactRIO Systems,” accessed 2022-02-25, <https://www.ni.com/en-no/shop/compactrio.html>
- [29] Kverno, J. O., 2018, “Pressure Pulsations and Thermodynamic Efficiency Measurements at Smeland Power Plant,” Ph.D. thesis, Norwegian University of Science and Technology.
- [30] Bergan, C. W., 2019, *Dynamic Loads on Francis Turbines: An Experimental Study*, NTNU, Accepted: 2019-05-06T12:19:18Z ISSN: 1503-8181.
- [31] Wheeler, A. J., Ganji, A. R., Krishnan, V. V., and Ganji, A. R., 2010, *Introduction to engineering experimentation*, 3rd ed., Pearson, Boston, Mass. Munich.
- [32] Kjølle, A., 2003, *Hydraulisk Måleteknikk*.
- [33] Solemslie, B. W., 2021, “Hydraulic turbines - Francis turbines,” .
- [34] “3GBP401830-BXG | ABB,” accessed 2022-03-03, <http://new.abb.com/products/3GBP401830-BXG/3gbp401830-bxg>
- [35] 2020, “T12HP Torque Transducer: High Precision Over Entire Range,” accessed 2021-11-18, <https://www.hbm.com/en/6384/t12hp-torque-transducer-with-maximum-precision/>
- [36] “Nasjonalt Smart Grid Laboratorium,” accessed 2022-02-25, <https://www.sintef.no/alle-laboratorier/smartgrid/>

- [37] Langleite, G. M. K., 2019, “Test of a Francis turbine with variable speed operation - project work,” Ph.D. thesis.
- [38] Schweiger, F. and Gregori, J., 1989, “Rapport I.7 Turbine guide vanes torque estimation,” *Journées de l’hydraulique*, **20**(1), pp. 1–6, Publisher: Persée - Portail des revues scientifiques en SHS.
- [39] Stojkovski, F., Lazarevikj, M., and Markov, Z., 2021, “Parametric Design Tool for Development of a Radial Guide Vane Cascade for a Variable Speed Francis Turbine,” *IOP Conference Series: Earth and Environmental Science*, **774**(1), p. 012112, Publisher: IOP Publishing.
- [40] “HydroFlex,” accessed 2021-12-05, <https://www.h2020hydroflex.eu/>

Appendices

Appendix A

A.1 Calibration constants

Table A.1: Calibration constants

Device	Sensor Type	c0	c1
Flow meter		-0,129132384	0,031811302
GVT1	Strain gages	5,66252644	-15219,22662
GVT2	Strain gages	-7,95801729	-15664,58369
Differential Pressuresensor	diffPressure	-99,602006	50,043148
Inlet Pressure	Pressure	-124,680889	62,55607
Draft tube pressuresensor DT2	Pressure	-5,593137	22,447604
Draft tube Pressuresensor DT3	Pressure	-7,043156	22,829246
GVL1	Pressure	2,273456	35,008972
GVL2	Pressure	18,881082	34,810727
GVL3	Pressure	-2,887937	35,009554
Friction torque		0,2213537	2,83554799

Table A.2: Calibration constants weighing tank

Constants	Value
a1=	1,67544490569354 E-23
a2=	-2,63298757430449 E-18
a3=	2,58036911982524 E-13
a4=	-1,15804747645975 E-08
a5=	0,999003362940342

A.2 Results

GVA	nED	qed	Eta	gvt1	gvt2	gvl1	GVL2	GVL3	dt2	DT3
10,0	0,1776	0,1394	89,95	3,28	3,54	168,09	176,52	159,97	97,72	96,92
10,0	0,1778	0,1393	90,02	3,28	3,53	168,30	176,73	160,17	97,99	97,19
5,0	0,1801	0,0738	81,07	4,52	4,72	164,41	171,39	155,42	102,64	101,92
4,1	0,1799	0,0620	77,17	4,84	5,06	162,86	169,76	154,20	102,47	101,73
6,1	0,1802	0,0874	84,23	4,22	4,45	166,46	173,69	157,49	102,54	101,77
7,0	0,1800	0,0998	85,18	3,92	4,12	165,99	173,93	157,86	102,13	101,34
8,0	0,1799	0,1129	88,26	3,65	3,88	166,74	175,28	159,14	101,46	100,61
9,1	0,1802	0,1266	88,90	3,32	3,58	167,40	176,07	159,82	100,54	99,70
10,0	0,1803	0,1378	90,13	3,06	3,32	166,99	175,57	159,23	99,09	98,25
11,1	0,1796	0,1521	90,57	2,89	3,13	167,07	175,59	158,97	96,54	95,74
11,7	0,1790	0,1584	89,85	2,77	2,99	166,79	175,41	158,85	95,53	94,73
12,1	0,1803	0,1633	90,65	2,71	2,92	167,31	175,97	159,43	95,29	94,47
13,0	0,1784	0,1740	89,73	2,52	2,72	166,89	175,69	159,38	94,89	94,07
14,0	0,1803	0,1842	90,46	2,35	2,54	166,42	175,20	159,17	93,89	93,06
15,1	0,1798	0,1958	89,78	2,39	2,53	169,15	177,53	161,46	91,41	90,54
15,9	0,1807	0,2043	89,31	2,22	2,42	169,73	178,00	162,15	91,15	90,26
17,0	0,1800	0,2151	87,93	2,19	2,31	170,20	178,65	162,82	91,29	90,40
18,1	0,1796	0,2249	87,53	2,21	2,26	171,76	180,68	164,81	91,14	90,20

New GV

VSO					SSO						
j	GVA	Eta	i	n_ED	Q_ED	j	GVA	Eta	i	n_ED	Q_ED
1	5,044648	81,62917	9	0,171004	0,076137	1	4,956758	79,63861	12	0,190655	0,069716
2	6,055391	83,96716	10	0,185111	0,085319	2	6,055391	83,96716	10	0,185111	0,085319
3	6,978242	86,49981	9	0,169921	0,102749	3	6,934297	85,47967	11	0,190499	0,094677
4	7,988984	88,15508	9	0,174658	0,114531	4	7,857148	87,60818	10	0,184956	0,108708
5	8,955781	89,2868	10	0,180106	0,124852	5	9,043672	88,86409	11	0,190719	0,120569
6	10,88937	90,45086	11	0,179947	0,149031	6	10,80148	90,03017	12	0,190499	0,142716
7	11,76828	90,42459	10	0,185178	0,156826	7	11,76828	90,42459	10	0,185178	0,156826
8	12,99875	90,69363	10	0,180507	0,173263	8	12,99875	90,39651	11	0,190004	0,167396
9	13,96555	90,39497	10	0,184771	0,181137	9	13,96555	90,39497	10	0,184771	0,181137
10	15,02023	89,90813	10	0,180936	0,194691	10	15,02023	89,89931	11	0,190344	0,188288
11	16,03098	89,20654	10	0,185003	0,202283	11	16,03098	89,20654	10	0,185003	0,202283
12	10,05441	90,1255	17	0,177713	0,139995	12	17,04172	88,37356	11	0,190183	0,20767
13	18,36008	87,49305	11	0,184983	0,222888	13	18,36008	87,49305	11	0,184983	0,222888

Old GV

VSO					SSO						
j	GVA	Eta	i	n_ED	Q_ED	j	GVA	Eta	i	n_ED	Q_ED
1	2,988711	81,39741	9	0,159979	0,055156	1	2,988711	79,69888	12	0,180003	0,051287
2	3,999453	85,31927	9	0,16483	0,070238	2	3,999453	84,19663	11	0,184723	0,065186
3	5,010195	88,29775	10	0,170155	0,085045	3	5,010195	87,75004	11	0,179928	0,08197
4	5,976992	89,675	8	0,164812	0,103742	4	5,976992	89,13137	10	0,18465	0,096102
5	6,943789	91,26059	10	0,180043	0,111524	5	6,943789	91,26059	10	0,180043	0,111524
6	7,910586	92,33387	9	0,175115	0,127975	6	7,910586	92,33387	9	0,175115	0,127975
7	9,053164	92,48657	9	0,170372	0,146392	7	9,053164	92,3769	10	0,180167	0,141232
8	9,976016	92,15785	9	0,175166	0,157331	8	9,976016	92,15785	9	0,175166	0,157331
9	11,0307	92,3379	10	0,180121	0,167085	9	11,0307	90,22955	9	0,179963	0,167199
10	11,9975	91,70569	10	0,185105	0,176958	10	11,9975	91,57885	9	0,175047	0,183176
11	14,01898	90,55897	10	0,185016	0,199205	11	14,01898	90,28917	9	0,175018	0,205682

A.3 Calibration reports

CALIBRATION REPORT

CALIBRATION PROPERTIES

Calibrated by: Halvor West and Gaute E. Vefring
Type/Producer: HBM XY41
SN: find later
Range: find later
Unit: Nm

CALIBRATION SOURCE PROPERTIES

Type/Producer: Calibrated Weights
SN: -
Uncertainty [%]: -

POLY FIT EQUATION:

$Y = + 5.66252644E+0X^0 - 15.21922662E+3X^1$

CALIBRATION SUMMARY:

Max Uncertainty : Inf [%]
Max Uncertainty : 0.020315 [Nm]
RSQ : 0.999985
Calibration points : 50

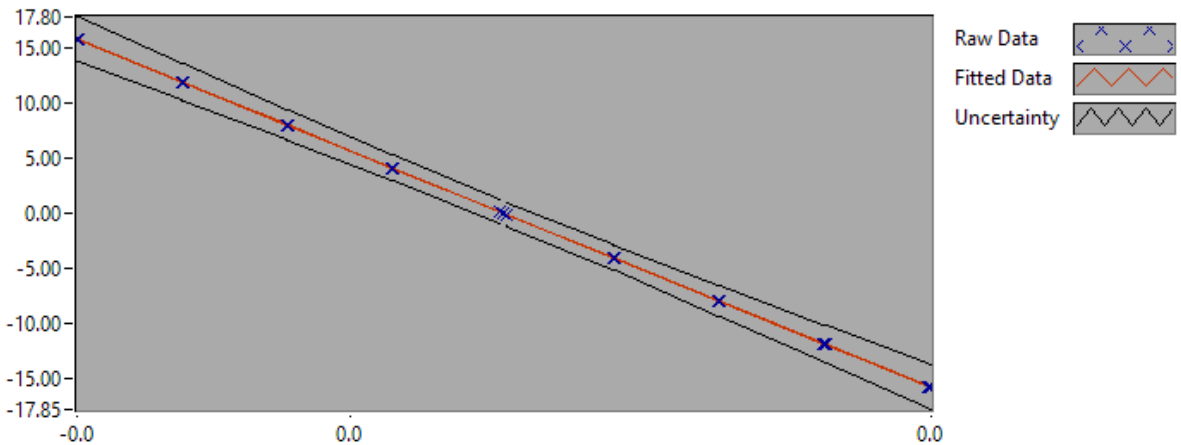


Figure 1 : Calibration chart (The uncertainty band is multiplied by 100)

Halvor West and Gaute E. Vefring

CALIBRATION VALUES

<u>Value [Nm]</u>	<u>Voltage [V]</u>	<u>Best Poly Fit [Nm]</u>	<u>Deviation [Nm]</u>	<u>Uncertainty [%]</u>	<u>Uncertainty [Nm]</u>
<u>-15.785763</u>	<u>0.001409</u>	<u>-15.780716</u>	<u>-0.005047</u>	<u>0.128514</u>	<u>-0.020287</u>
<u>-11.871897</u>	<u>0.001155</u>	<u>-11.920552</u>	<u>0.048655</u>	<u>0.141832</u>	<u>-0.016838</u>
<u>-7.958031</u>	<u>0.000899</u>	<u>-8.027135</u>	<u>0.069104</u>	<u>0.173501</u>	<u>-0.013807</u>
<u>-4.044165</u>	<u>0.000642</u>	<u>-4.101732</u>	<u>0.057567</u>	<u>0.286141</u>	<u>-0.011572</u>
<u>-0.130299</u>	<u>0.000381</u>	<u>-0.133082</u>	<u>0.002783</u>	<u>8.185138</u>	<u>-0.010665</u>
<u>0.000000</u>	<u>0.000372</u>	<u>0.002421</u>	<u>-0.002421</u>	<u>Inf</u>	<u>NaN</u>
<u>0.130299</u>	<u>0.000363</u>	<u>0.132752</u>	<u>-0.002453</u>	<u>8.185146</u>	<u>0.010665</u>
<u>4.044165</u>	<u>0.000105</u>	<u>4.068984</u>	<u>-0.024819</u>	<u>0.285677</u>	<u>0.011553</u>
<u>7.958031</u>	<u>-0.000151</u>	<u>7.959373</u>	<u>-0.001341</u>	<u>0.172985</u>	<u>0.013766</u>
<u>11.871897</u>	<u>-0.000407</u>	<u>11.851062</u>	<u>0.020835</u>	<u>0.141405</u>	<u>0.016787</u>
<u>15.785763</u>	<u>-0.000661</u>	<u>15.724931</u>	<u>0.060833</u>	<u>0.128160</u>	<u>0.020231</u>
<u>15.785763</u>	<u>-0.000661</u>	<u>15.724061</u>	<u>0.061703</u>	<u>0.128161</u>	<u>0.020231</u>
<u>11.871897</u>	<u>-0.000409</u>	<u>11.890120</u>	<u>-0.018223</u>	<u>0.141620</u>	<u>0.016813</u>
<u>7.958031</u>	<u>-0.000154</u>	<u>8.005962</u>	<u>-0.047931</u>	<u>0.173379</u>	<u>0.013798</u>
<u>4.044165</u>	<u>0.000103</u>	<u>4.095883</u>	<u>-0.051718</u>	<u>0.285995</u>	<u>0.011566</u>
<u>0.130299</u>	<u>0.000362</u>	<u>0.146562</u>	<u>-0.016263</u>	<u>8.185335</u>	<u>0.010665</u>
<u>0.000000</u>	<u>0.000371</u>	<u>0.013809</u>	<u>-0.013809</u>	<u>Inf</u>	<u>NaN</u>
<u>-0.130299</u>	<u>0.000380</u>	<u>-0.117974</u>	<u>-0.012325</u>	<u>8.184969</u>	<u>-0.010665</u>
<u>-4.044165</u>	<u>0.000639</u>	<u>-4.058659</u>	<u>0.014494</u>	<u>0.285664</u>	<u>-0.011553</u>
<u>-7.958031</u>	<u>0.000895</u>	<u>-7.964628</u>	<u>0.006597</u>	<u>0.172971</u>	<u>-0.013765</u>
<u>-11.871897</u>	<u>0.001150</u>	<u>-11.834738</u>	<u>-0.037159</u>	<u>0.141290</u>	<u>-0.016774</u>
<u>-15.785763</u>	<u>0.001404</u>	<u>-15.710851</u>	<u>-0.074912</u>	<u>0.128066</u>	<u>-0.020216</u>
<u>-15.785763</u>	<u>0.001404</u>	<u>-15.710945</u>	<u>-0.074818</u>	<u>0.128066</u>	<u>-0.020216</u>
<u>0.000000</u>	<u>0.000371</u>	<u>0.009280</u>	<u>-0.009280</u>	<u>Inf</u>	<u>NaN</u>
<u>15.785763</u>	<u>-0.000664</u>	<u>15.768878</u>	<u>0.016886</u>	<u>0.128428</u>	<u>0.020273</u>
<u>15.785763</u>	<u>-0.000664</u>	<u>15.761442</u>	<u>0.024321</u>	<u>0.128428</u>	<u>0.020273</u>
<u>0.000000</u>	<u>0.000372</u>	<u>0.008043</u>	<u>-0.008043</u>	<u>Inf</u>	<u>NaN</u>
<u>-15.785763</u>	<u>0.001411</u>	<u>-15.815997</u>	<u>0.030233</u>	<u>0.128693</u>	<u>-0.020315</u>
<u>-15.785763</u>	<u>0.001411</u>	<u>-15.810238</u>	<u>0.024475</u>	<u>0.128693</u>	<u>-0.020315</u>
<u>-11.871897</u>	<u>0.001156</u>	<u>-11.936039</u>	<u>0.064142</u>	<u>0.141940</u>	<u>-0.016851</u>
<u>-7.958031</u>	<u>0.000899</u>	<u>-8.023118</u>	<u>0.065087</u>	<u>0.173501</u>	<u>-0.013807</u>
<u>-4.044165</u>	<u>0.000641</u>	<u>-4.087982</u>	<u>0.043817</u>	<u>0.285982</u>	<u>-0.011566</u>
<u>-0.130299</u>	<u>0.000381</u>	<u>-0.133946</u>	<u>0.003647</u>	<u>8.185138</u>	<u>-0.010665</u>
<u>0.000000</u>	<u>0.000372</u>	<u>0.000699</u>	<u>-0.000699</u>	<u>Inf</u>	<u>NaN</u>
<u>0.130299</u>	<u>0.000363</u>	<u>0.134746</u>	<u>-0.004447</u>	<u>8.185146</u>	<u>0.010665</u>
<u>4.044165</u>	<u>0.000103</u>	<u>4.087571</u>	<u>-0.043406</u>	<u>0.285995</u>	<u>0.011566</u>
<u>7.958031</u>	<u>-0.000153</u>	<u>7.989707</u>	<u>-0.031675</u>	<u>0.173246</u>	<u>0.013787</u>
<u>11.871897</u>	<u>-0.000408</u>	<u>11.873628</u>	<u>-0.001731</u>	<u>0.141513</u>	<u>0.016800</u>
<u>15.785763</u>	<u>-0.000663</u>	<u>15.754433</u>	<u>0.031331</u>	<u>0.128339</u>	<u>0.020259</u>
<u>15.785763</u>	<u>-0.000663</u>	<u>15.752466</u>	<u>0.033297</u>	<u>0.128339</u>	<u>0.020259</u>
<u>11.871897</u>	<u>-0.000411</u>	<u>11.912757</u>	<u>-0.040860</u>	<u>0.141838</u>	<u>0.016839</u>
<u>7.958031</u>	<u>-0.000156</u>	<u>8.032973</u>	<u>-0.074941</u>	<u>0.173647</u>	<u>0.013819</u>

<u>4.044165</u>	<u>0.000102</u>	<u>4.114497</u>	<u>-0.070332</u>	<u>0.286154</u>	<u>0.011573</u>
<u>0.130299</u>	<u>0.000362</u>	<u>0.148695</u>	<u>-0.018396</u>	<u>8.185335</u>	<u>0.010665</u>
<u>0.000000</u>	<u>0.000371</u>	<u>0.012692</u>	<u>-0.012692</u>	<u>Inf</u>	<u>NaN</u>
<u>-0.130299</u>	<u>0.000380</u>	<u>-0.118873</u>	<u>-0.011426</u>	<u>8.184969</u>	<u>-0.010665</u>
<u>-4.044165</u>	<u>0.000639</u>	<u>-4.063368</u>	<u>0.019203</u>	<u>0.285664</u>	<u>-0.011553</u>
<u>-7.958031</u>	<u>0.000896</u>	<u>-7.971469</u>	<u>0.013438</u>	<u>0.173103</u>	<u>-0.013776</u>
<u>-11.871897</u>	<u>0.001153</u>	<u>-11.877966</u>	<u>0.006069</u>	<u>0.141615</u>	<u>-0.016812</u>
<u>-15.785763</u>	<u>0.001409</u>	<u>-15.778416</u>	<u>-0.007347</u>	<u>0.128514</u>	<u>-0.020287</u>

COMMENTS:

Calibrated at 5 Vex

The uncertainty is calculated with 95% confidence. The uncertainty includes the randomness in the calibrated instrument during the calibration, systematic uncertainty in the instrument or property which the instrument under calibration is compared with (dead weight manometer, calibrated weights etc.), and due to regression analysis to fit the calibration points to a linear calibration equation. The calculated uncertainty can be used as the total systematic uncertainty of the calibrated instrument with the given calibration equation.

CALIBRATION REPORT

CALIBRATION PROPERTIES

Calibrated by: Halvor West and Gaute E. Vefring
Type/Producer: HBM XY41
SN: find later
Range: find later
Unit: Nm

CALIBRATION SOURCE PROPERTIES

Type/Producer: Calibrated Weights
SN: -
Uncertainty [%]: -

POLY FIT EQUATION:

$Y = -7.95801729E+0X^0 - 15.66458369E+3X^1$

CALIBRATION SUMMARY:

Max Uncertainty : Inf [%]
Max Uncertainty : 0.014052 [Nm]
RSQ : 0.999993
Calibration points : 50

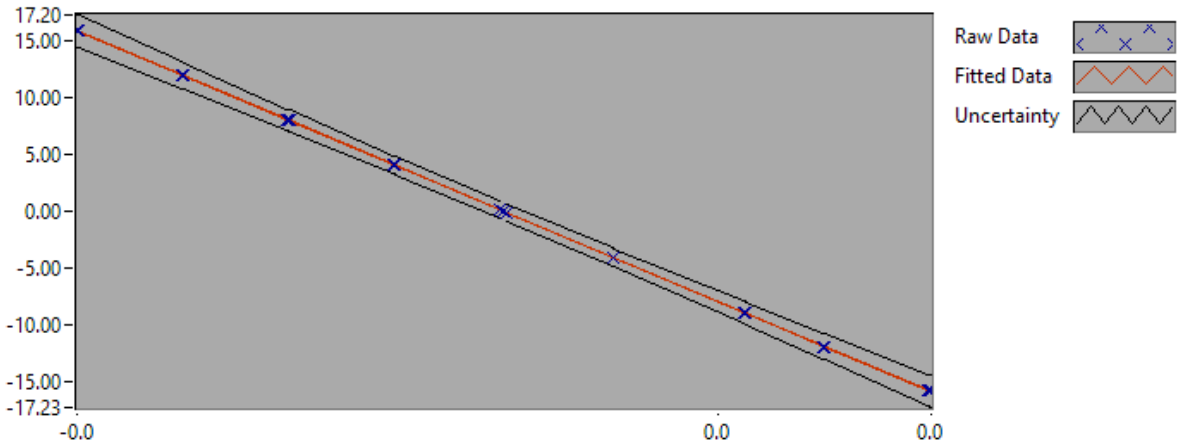


Figure 1 : Calibration chart (The uncertainty band is multiplied by 100)

Halvor West and Gaute E. Vefring

CALIBRATION VALUES

Value [Nm]	Voltage [V]	Best Poly. Fit [Nm]	Deviation [Nm]	Uncertainty [%]	Uncertainty [Nm]
<u>-15.785763</u>	<u>0.000498</u>	<u>-15.761239</u>	<u>-0.024524</u>	<u>0.088218</u>	<u>-0.013926</u>
<u>-11.871897</u>	<u>0.000251</u>	<u>-11.892509</u>	<u>0.020612</u>	<u>0.097386</u>	<u>-0.011562</u>
<u>-8.910291</u>	<u>0.000063</u>	<u>-8.940590</u>	<u>0.030299</u>	<u>0.111912</u>	<u>-0.009972</u>
<u>-4.044165</u>	<u>-0.000248</u>	<u>-4.073533</u>	<u>0.029368</u>	<u>0.197275</u>	<u>-0.007978</u>
<u>-0.130299</u>	<u>-0.000500</u>	<u>-0.126759</u>	<u>-0.003540</u>	<u>5.670970</u>	<u>-0.007389</u>
<u>0.000000</u>	<u>-0.000508</u>	<u>0.003370</u>	<u>-0.003370</u>	<u>Inf</u>	<u>NaN</u>
<u>0.130299</u>	<u>-0.000517</u>	<u>0.134533</u>	<u>-0.004234</u>	<u>5.672285</u>	<u>0.007391</u>
<u>4.044165</u>	<u>-0.000765</u>	<u>4.032425</u>	<u>0.011740</u>	<u>0.198015</u>	<u>0.008008</u>
<u>7.958031</u>	<u>-0.001015</u>	<u>7.934611</u>	<u>0.023420</u>	<u>0.119879</u>	<u>0.009540</u>
<u>11.871897</u>	<u>-0.001264</u>	<u>11.844427</u>	<u>0.027470</u>	<u>0.097890</u>	<u>0.011621</u>
<u>15.785763</u>	<u>-0.001513</u>	<u>15.742644</u>	<u>0.043120</u>	<u>0.088763</u>	<u>0.014012</u>
<u>15.785763</u>	<u>-0.001513</u>	<u>15.745694</u>	<u>0.040070</u>	<u>0.088763</u>	<u>0.014012</u>
<u>11.871897</u>	<u>-0.001267</u>	<u>11.888290</u>	<u>-0.016393</u>	<u>0.098120</u>	<u>0.011649</u>
<u>7.958031</u>	<u>-0.001018</u>	<u>7.993626</u>	<u>-0.035595</u>	<u>0.120161</u>	<u>0.009562</u>
<u>4.044165</u>	<u>-0.000768</u>	<u>4.078004</u>	<u>-0.033839</u>	<u>0.198354</u>	<u>0.008022</u>
<u>0.130299</u>	<u>-0.000517</u>	<u>0.140363</u>	<u>-0.010064</u>	<u>5.672285</u>	<u>0.007391</u>
<u>0.000000</u>	<u>-0.000509</u>	<u>0.007666</u>	<u>-0.007666</u>	<u>Inf</u>	<u>NaN</u>
<u>-0.130299</u>	<u>-0.000500</u>	<u>-0.123059</u>	<u>-0.007240</u>	<u>5.670970</u>	<u>-0.007389</u>
<u>-4.044165</u>	<u>-0.000251</u>	<u>-4.028794</u>	<u>-0.015371</u>	<u>0.196941</u>	<u>-0.007965</u>
<u>-8.910291</u>	<u>0.000059</u>	<u>-8.877797</u>	<u>-0.032494</u>	<u>0.111533</u>	<u>-0.009938</u>
<u>-11.871897</u>	<u>0.000247</u>	<u>-11.827128</u>	<u>-0.044769</u>	<u>0.097083</u>	<u>-0.011526</u>
<u>-15.785763</u>	<u>0.000497</u>	<u>-15.737051</u>	<u>-0.048712</u>	<u>0.088149</u>	<u>-0.013915</u>
<u>-15.785763</u>	<u>0.000497</u>	<u>-15.741817</u>	<u>-0.043947</u>	<u>0.088149</u>	<u>-0.013915</u>
<u>0.000000</u>	<u>-0.000509</u>	<u>0.011226</u>	<u>-0.011226</u>	<u>Inf</u>	<u>NaN</u>
<u>15.785763</u>	<u>-0.001517</u>	<u>15.797681</u>	<u>-0.011918</u>	<u>0.089018</u>	<u>0.014052</u>
<u>15.785763</u>	<u>-0.001516</u>	<u>15.794717</u>	<u>-0.008954</u>	<u>0.088954</u>	<u>0.014042</u>
<u>0.000000</u>	<u>-0.000508</u>	<u>0.006534</u>	<u>-0.006534</u>	<u>Inf</u>	<u>NaN</u>
<u>-15.785763</u>	<u>0.000500</u>	<u>-15.783771</u>	<u>-0.001992</u>	<u>0.088342</u>	<u>-0.013945</u>
<u>-15.785763</u>	<u>0.000500</u>	<u>-15.784422</u>	<u>-0.001342</u>	<u>0.088347</u>	<u>-0.013946</u>
<u>-11.871897</u>	<u>0.000253</u>	<u>-11.918548</u>	<u>0.046651</u>	<u>0.097539</u>	<u>-0.011580</u>
<u>-8.910291</u>	<u>0.000064</u>	<u>-8.959157</u>	<u>0.048866</u>	<u>0.111924</u>	<u>-0.009973</u>
<u>-4.044165</u>	<u>-0.000248</u>	<u>-4.080597</u>	<u>0.036432</u>	<u>0.197270</u>	<u>-0.007978</u>
<u>-0.130299</u>	<u>-0.000500</u>	<u>-0.126080</u>	<u>-0.004219</u>	<u>5.670970</u>	<u>-0.007389</u>
<u>0.000000</u>	<u>-0.000508</u>	<u>0.005951</u>	<u>-0.005951</u>	<u>Inf</u>	<u>NaN</u>
<u>0.130299</u>	<u>-0.000517</u>	<u>0.135041</u>	<u>-0.004742</u>	<u>5.672285</u>	<u>0.007391</u>
<u>4.044165</u>	<u>-0.000766</u>	<u>4.034453</u>	<u>0.009712</u>	<u>0.198128</u>	<u>0.008013</u>
<u>7.958031</u>	<u>-0.001015</u>	<u>7.938307</u>	<u>0.019724</u>	<u>0.119879</u>	<u>0.009540</u>
<u>11.871897</u>	<u>-0.001265</u>	<u>11.854101</u>	<u>0.017796</u>	<u>0.097967</u>	<u>0.011631</u>
<u>15.785763</u>	<u>-0.001515</u>	<u>15.777561</u>	<u>0.008202</u>	<u>0.088890</u>	<u>0.014032</u>
<u>15.785763</u>	<u>-0.001516</u>	<u>15.786140</u>	<u>-0.000377</u>	<u>0.088954</u>	<u>0.014042</u>
<u>11.871897</u>	<u>-0.001268</u>	<u>11.907289</u>	<u>-0.035392</u>	<u>0.098197</u>	<u>0.011658</u>
<u>7.958031</u>	<u>-0.001019</u>	<u>8.006759</u>	<u>-0.048728</u>	<u>0.120255</u>	<u>0.009570</u>

<u>4.044165</u>	<u>-0.000768</u>	<u>4.079344</u>	<u>-0.035179</u>	<u>0.198354</u>	<u>0.008022</u>
<u>0.130299</u>	<u>-0.000517</u>	<u>0.139111</u>	<u>-0.008812</u>	<u>5.672285</u>	<u>0.007391</u>
<u>0.000000</u>	<u>-0.000509</u>	<u>0.007679</u>	<u>-0.007679</u>	<u>Inf</u>	<u>NaN</u>
<u>-0.130299</u>	<u>-0.000500</u>	<u>-0.121941</u>	<u>-0.008358</u>	<u>5.670970</u>	<u>-0.007389</u>
<u>-4.044165</u>	<u>-0.000250</u>	<u>-4.047245</u>	<u>0.003080</u>	<u>0.197052</u>	<u>-0.007969</u>
<u>-8.910291</u>	<u>0.000063</u>	<u>-8.943377</u>	<u>0.033086</u>	<u>0.111804</u>	<u>-0.009962</u>
<u>-11.871897</u>	<u>0.000252</u>	<u>-11.906627</u>	<u>0.034730</u>	<u>0.097465</u>	<u>-0.011571</u>
<u>-15.785763</u>	<u>0.000503</u>	<u>-15.834543</u>	<u>0.048779</u>	<u>0.088532</u>	<u>-0.013975</u>

COMMENTS:

Calibrated at 5 Vex

The uncertainty is calculated with 95% confidence. The uncertainty includes the randomness in the calibrated instrument during the calibration, systematic uncertainty in the instrument or property which the instrument under calibration is compared with (dead weight manometer, calibrated weights etc.), and due to regression analysis to fit the calibration points to a linear calibration equation. The calculated uncertainty can be used as the total systematic uncertainty of the calibrated instrument with the given calibration equation.

CALIBRATION REPORT

CALIBRATION PROPERTIES

Calibrated by: Hvistendahl, Vefring og West

Type/Producer: Kulite XTE-190

SN: 8317-1-201

Range: 0-3.5bar a kPa

Unit: kPa

CALIBRATION SOURCE PROPERTIES

Type/Producer: DW tester P3223-1

SN: 66256

Uncertainty [%]: 0,010000

POLY FIT EQUATION:

$Y = 35,008972 * X + 2,273456$

CALIBRATION SUMMARY:

Max Uncertainty : 0,939422 [%]

Max Uncertainty : 0,931906 [kPa]

RSQ : 0,999846

Calibration points : 27

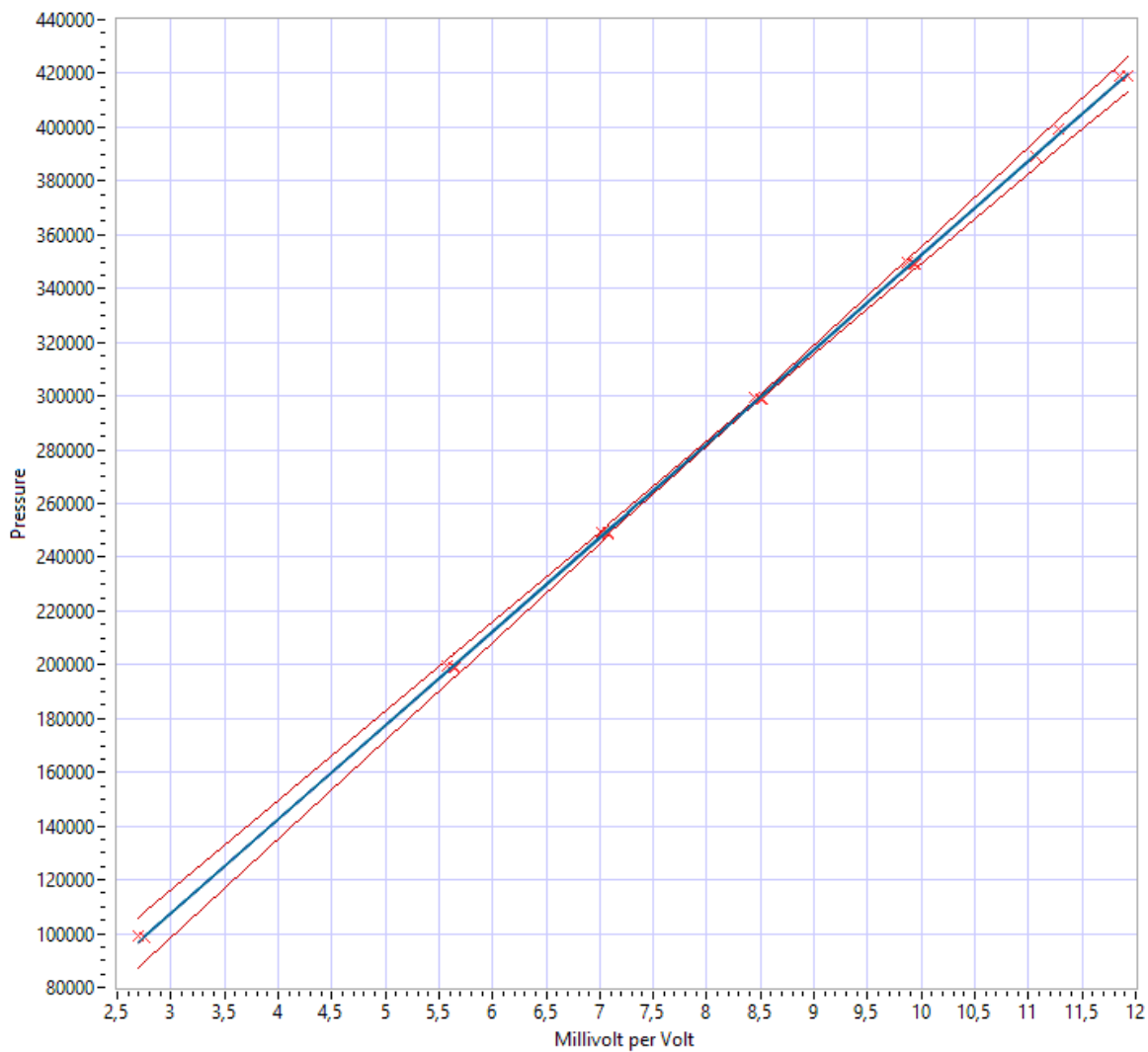


Figure 1 : Calibration chart (The uncertainty band is multiplied by 10)

CALIBRATION VALUES

<u>Value [kPa]</u>	<u>Voltage [V]</u>	<u>Best linear fit [kPa]</u>	<u>Deviation [kPa]</u>	<u>Total uncertainty [%]</u>	<u>Total uncertainty [kPa]</u>
<u>99,20000</u>	<u>2,694453</u>	<u>96,603503</u>	<u>2,596497</u>	<u>0,939422</u>	<u>0,931906</u>
<u>199,349073</u>	<u>5,578402</u>	<u>197,567583</u>	<u>1,781489</u>	<u>0,221129</u>	<u>0,440819</u>
<u>249,423609</u>	<u>7,011969</u>	<u>247,755289</u>	<u>1,668319</u>	<u>0,079236</u>	<u>0,197633</u>
<u>299,498145</u>	<u>8,443481</u>	<u>297,871045</u>	<u>1,627100</u>	<u>0,018997</u>	<u>0,056895</u>
<u>349,572681</u>	<u>9,867606</u>	<u>347,728204</u>	<u>1,844477</u>	<u>0,083806</u>	<u>0,292964</u>
<u>399,254285</u>	<u>11,284638</u>	<u>397,337028</u>	<u>1,917257</u>	<u>0,133720</u>	<u>0,533883</u>
<u>419,284096</u>	<u>11,850094</u>	<u>417,133051</u>	<u>2,151045</u>	<u>0,150295</u>	<u>0,630162</u>
<u>419,284096</u>	<u>11,849450</u>	<u>417,110523</u>	<u>2,173573</u>	<u>0,150269</u>	<u>0,630053</u>
<u>389,239380</u>	<u>11,075530</u>	<u>390,016389</u>	<u>-0,777009</u>	<u>0,128012</u>	<u>0,498272</u>
<u>349,179758</u>	<u>9,939672</u>	<u>350,251168</u>	<u>-1,071410</u>	<u>0,087396</u>	<u>0,305168</u>
<u>299,105231</u>	<u>8,512961</u>	<u>300,303478</u>	<u>-1,198247</u>	<u>0,022557</u>	<u>0,067469</u>
<u>249,030704</u>	<u>7,081849</u>	<u>250,201722</u>	<u>-1,171018</u>	<u>0,074616</u>	<u>0,185816</u>
<u>198,856177</u>	<u>5,645669</u>	<u>199,922517</u>	<u>-1,066340</u>	<u>0,215908</u>	<u>0,429347</u>
<u>98,707122</u>	<u>2,759567</u>	<u>98,883045</u>	<u>-0,175923</u>	<u>0,932886</u>	<u>0,920825</u>
<u>98,707122</u>	<u>2,759157</u>	<u>98,868708</u>	<u>-0,161586</u>	<u>0,932957</u>	<u>0,920895</u>
<u>198,856177</u>	<u>5,640739</u>	<u>199,749915</u>	<u>-0,893739</u>	<u>0,216319</u>	<u>0,430164</u>
<u>248,930704</u>	<u>7,077449</u>	<u>250,047666</u>	<u>-1,116963</u>	<u>0,074944</u>	<u>0,186559</u>
<u>299,005231</u>	<u>8,508070</u>	<u>300,132239</u>	<u>-1,127009</u>	<u>0,022276</u>	<u>0,066606</u>
<u>349,079758</u>	<u>9,935599</u>	<u>350,108565</u>	<u>-1,028807</u>	<u>0,087244</u>	<u>0,304552</u>
<u>389,139380</u>	<u>11,072229</u>	<u>389,900794</u>	<u>-0,761415</u>	<u>0,127907</u>	<u>0,497736</u>
<u>419,184096</u>	<u>11,921601</u>	<u>419,636451</u>	<u>-0,452356</u>	<u>0,153240</u>	<u>0,642358</u>
<u>419,184096</u>	<u>11,922684</u>	<u>419,674357</u>	<u>-0,490261</u>	<u>0,153281</u>	<u>0,642530</u>
<u>389,139380</u>	<u>11,073189</u>	<u>389,934423</u>	<u>-0,795043</u>	<u>0,127949</u>	<u>0,497901</u>
<u>349,079758</u>	<u>9,937473</u>	<u>350,174178</u>	<u>-1,094420</u>	<u>0,087323</u>	<u>0,304827</u>
<u>299,005231</u>	<u>8,511930</u>	<u>300,267363</u>	<u>-1,262132</u>	<u>0,022470</u>	<u>0,067186</u>
<u>198,856177</u>	<u>5,643184</u>	<u>199,835517</u>	<u>-0,979341</u>	<u>0,216109</u>	<u>0,429746</u>
<u>98,707122</u>	<u>2,758447</u>	<u>98,843861</u>	<u>-0,136739</u>	<u>0,933079</u>	<u>0,921016</u>

COMMENTS:

Raw data was stored in the path C:\Users\logger6\Documents\Vefring og West calibration 2022-01-26 1113.tdms

Calibrated using the new and improved VKL calibration program made by J-Dawg

The uncertainty is calculated with 95% confidence. The uncertainty includes the randomness in the calibrated instrument during the calibration, systematic uncertainty in the instrument or property which the instrument under calibration is compared with (dead weight manometer, calibrated weights etc.), and due to regression analysis to fit the calibration points to a linear calibration equation. The calculated uncertainty can be used as the total systematic uncertainty of the calibrated instrument with the given calibration equation.

CALIBRATION REPORT

CALIBRATION PROPERTIES

Calibrated by: Hvistendahl, Vefring og West

Type/Producer: Kulite XTL190

SN: 8317-1-202

Range: 0-3.5 bar a kPa

Unit: kPa

CALIBRATION SOURCE PROPERTIES

Type/Producer: DW tester P3223-1

SN: 66256

Uncertainty [%]: 0,010000

POLY FIT EQUATION:

$Y = 34,810727 * X + 18,881082$

CALIBRATION SUMMARY:

Max Uncertainty : 1,133740 [%]

Max Uncertainty : 1,119082 [kPa]

RSQ : 0,999767

Calibration points : 28

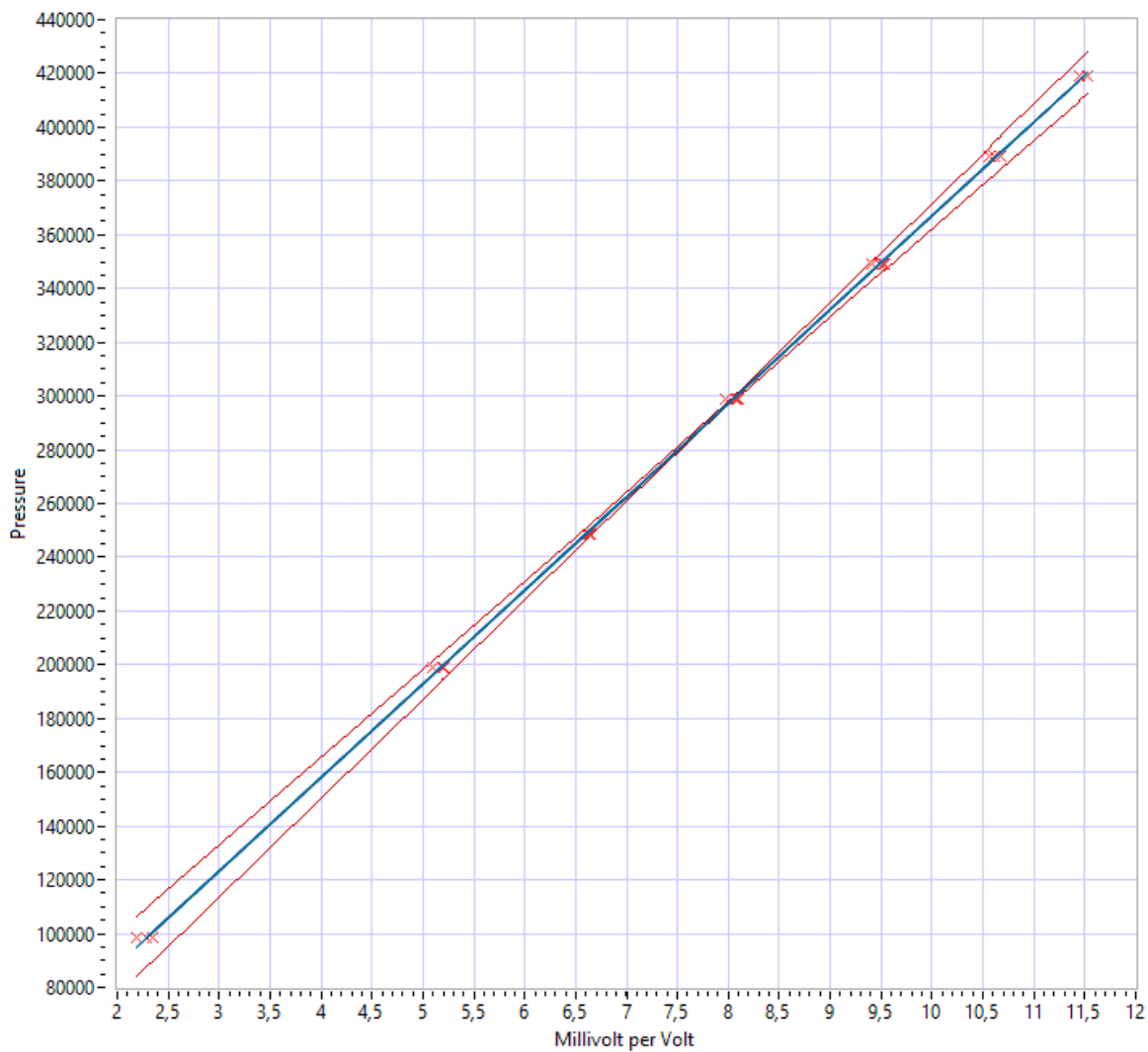


Figure 1 : Calibration chart (The uncertainty band is multiplied by 10)

CALIBRATION VALUES

<u>Value [kPa]</u>	<u>Voltage [V]</u>	<u>Best linear fit [kPa]</u>	<u>Deviation [kPa]</u>	<u>Total uncertainty [%]</u>	<u>Total uncertainty [kPa]</u>
<u>98,707122</u>	<u>2,193532</u>	<u>95,239514</u>	<u>3,467608</u>	<u>1,133740</u>	<u>1,119082</u>
<u>198,856177</u>	<u>5,093595</u>	<u>196,192840</u>	<u>2,663337</u>	<u>0,265354</u>	<u>0,527673</u>
<u>299,005231</u>	<u>7,970413</u>	<u>296,336937</u>	<u>2,668294</u>	<u>0,022555</u>	<u>0,067442</u>
<u>349,079758</u>	<u>9,410102</u>	<u>346,453561</u>	<u>2,626197</u>	<u>0,101824</u>	<u>0,355448</u>
<u>389,139380</u>	<u>10,560244</u>	<u>386,490859</u>	<u>2,648520</u>	<u>0,151533</u>	<u>0,589676</u>
<u>419,184096</u>	<u>11,442368</u>	<u>417,198215</u>	<u>1,985881</u>	<u>0,183578</u>	<u>0,769529</u>
<u>419,184096</u>	<u>11,452263</u>	<u>417,542670</u>	<u>1,641426</u>	<u>0,184058</u>	<u>0,771543</u>
<u>389,139380</u>	<u>10,611914</u>	<u>388,289536</u>	<u>0,849844</u>	<u>0,154237</u>	<u>0,600196</u>
<u>349,079758</u>	<u>9,481333</u>	<u>348,933173</u>	<u>0,146585</u>	<u>0,105967</u>	<u>0,369911</u>
<u>299,005231</u>	<u>8,058786</u>	<u>299,413275</u>	<u>-0,408044</u>	<u>0,028045</u>	<u>0,083855</u>
<u>248,930704</u>	<u>6,626049</u>	<u>249,538675</u>	<u>-0,607971</u>	<u>0,086810</u>	<u>0,216098</u>
<u>248,930704</u>	<u>6,628917</u>	<u>249,638513</u>	<u>-0,707810</u>	<u>0,086577</u>	<u>0,215516</u>
<u>198,856177</u>	<u>5,189483</u>	<u>199,530773</u>	<u>-0,674596</u>	<u>0,255513</u>	<u>0,508103</u>
<u>98,707122</u>	<u>2,289812</u>	<u>98,591118</u>	<u>0,116004</u>	<u>1,113837</u>	<u>1,099436</u>
<u>98,707122</u>	<u>2,289061</u>	<u>98,564966</u>	<u>0,142157</u>	<u>1,113992</u>	<u>1,099589</u>
<u>198,856177</u>	<u>5,191483</u>	<u>199,600384</u>	<u>-0,744207</u>	<u>0,255308</u>	<u>0,507695</u>
<u>248,930704</u>	<u>6,638340</u>	<u>249,966528</u>	<u>-1,035825</u>	<u>0,085811</u>	<u>0,213610</u>
<u>299,005231</u>	<u>8,081748</u>	<u>300,212615</u>	<u>-1,207385</u>	<u>0,029436</u>	<u>0,088016</u>
<u>349,079758</u>	<u>9,520510</u>	<u>350,296937</u>	<u>-1,217179</u>	<u>0,108233</u>	<u>0,377820</u>
<u>389,139380</u>	<u>10,668533</u>	<u>390,260485</u>	<u>-1,121105</u>	<u>0,157191</u>	<u>0,611692</u>
<u>419,184096</u>	<u>11,529182</u>	<u>420,220296</u>	<u>-1,036201</u>	<u>0,187791</u>	<u>0,787190</u>
<u>419,184096</u>	<u>11,530358</u>	<u>420,261216</u>	<u>-1,077121</u>	<u>0,187848</u>	<u>0,787429</u>
<u>389,139380</u>	<u>10,677038</u>	<u>390,556531</u>	<u>-1,417152</u>	<u>0,157636</u>	<u>0,613424</u>
<u>349,079758</u>	<u>9,531772</u>	<u>350,689003</u>	<u>-1,609245</u>	<u>0,108888</u>	<u>0,380108</u>
<u>299,005231</u>	<u>8,093861</u>	<u>300,634272</u>	<u>-1,629042</u>	<u>0,030213</u>	<u>0,090338</u>
<u>248,930704</u>	<u>6,650002</u>	<u>250,372494</u>	<u>-1,441791</u>	<u>0,084828</u>	<u>0,211164</u>
<u>198,856177</u>	<u>5,204172</u>	<u>200,042096</u>	<u>-1,185919</u>	<u>0,253996</u>	<u>0,505086</u>
<u>98,707122</u>	<u>2,345866</u>	<u>100,542384</u>	<u>-1,835261</u>	<u>1,102238</u>	<u>1,087988</u>

COMMENTS:

Raw data was stored in the path C:\Users\logger6\Documents\Vefring og West calibration 2022-01-26 1113.tdms

Calibrated using the new and improved VKL calibration program made by J-Dawg

The uncertainty is calculated with 95% confidence. The uncertainty includes the randomness in the calibrated instrument during the calibration, systematic uncertainty in the instrument or property which the instrument under calibration is compared with (dead weight manometer, calibrated weights etc.), and due to regression analysis to fit the calibration points to a linear calibration equation. The calculated uncertainty can be used as the total systematic uncertainty of the calibrated instrument with the given calibration equation.

CALIBRATION REPORT

CALIBRATION PROPERTIES

Calibrated by: Hvistendahl, Vefring og West

Type/Producer: Kulite XTL 190

SN: 8317-1-204

Range: 0-3.5 bar a kPa

Unit: kPa

CALIBRATION SOURCE PROPERTIES

Type/Producer: DW tester P3223-1

SN: 66256

Uncertainty [%]: 0,010000

POLY FIT EQUATION:

$Y = 35,009554 * X - 2,887937$

CALIBRATION SUMMARY:

Max Uncertainty : 0,271853 [%]

Max Uncertainty : 0,268338 [kPa]

RSQ : 0,999986

Calibration points : 28

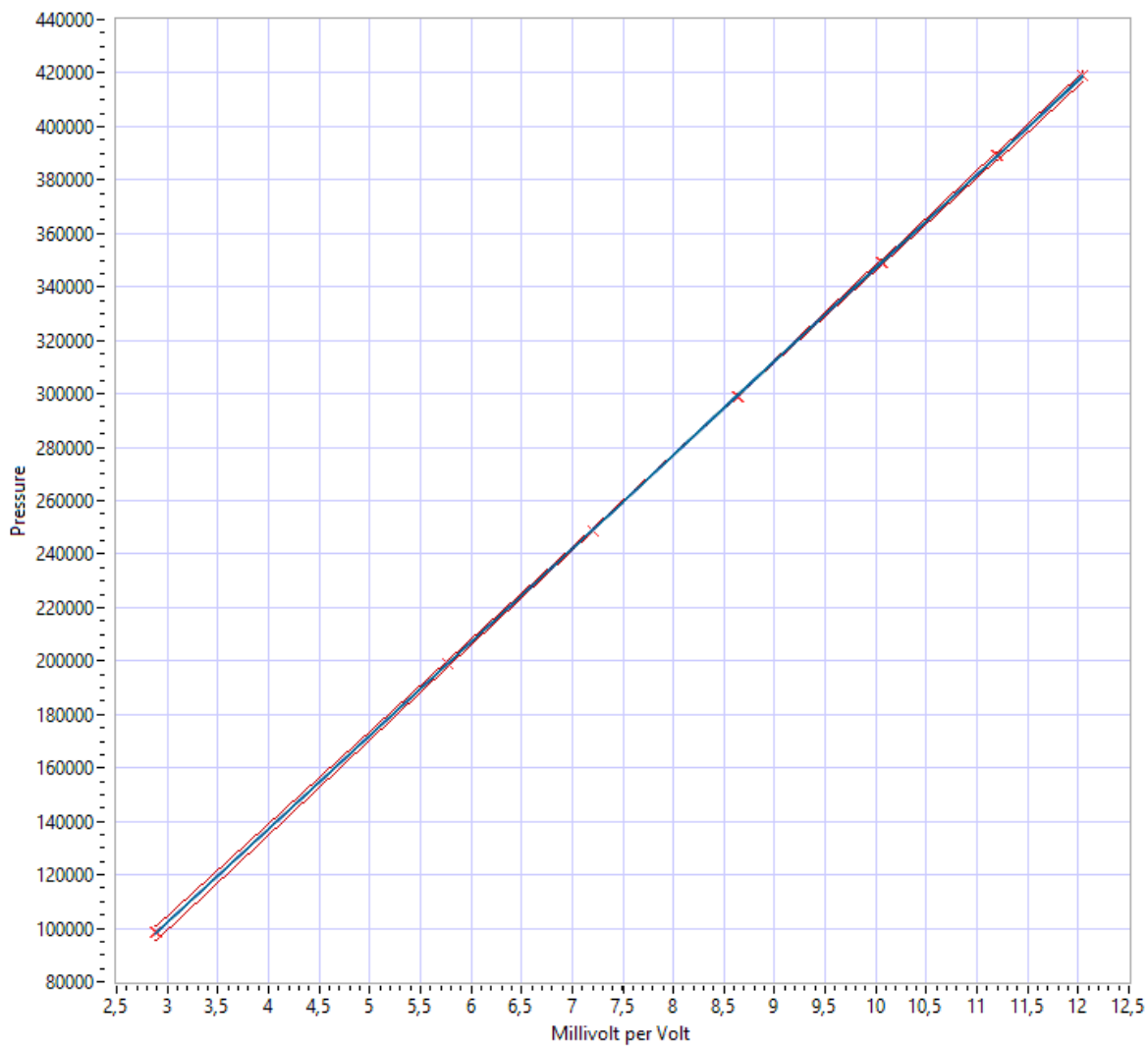


Figure 1 : Calibration chart (The uncertainty band is multiplied by 10)

CALIBRATION VALUES

<u>Value [kPa]</u>	<u>Voltage [V]</u>	<u>Best linear fit [kPa]</u>	<u>Deviation [kPa]</u>	<u>Total uncertainty [%]</u>	<u>Total uncertainty [kPa]</u>
<u>98,707122</u>	<u>2,886172</u>	<u>98,155646</u>	<u>0,551477</u>	<u>0,271690</u>	<u>0,268177</u>
<u>198,856177</u>	<u>5,772173</u>	<u>199,193253</u>	<u>-0,337076</u>	<u>0,063131</u>	<u>0,125540</u>
<u>248,930704</u>	<u>7,206895</u>	<u>249,422257</u>	<u>-0,491553</u>	<u>0,023288</u>	<u>0,057970</u>
<u>299,005231</u>	<u>8,635985</u>	<u>299,454037</u>	<u>-0,448806</u>	<u>0,011860</u>	<u>0,035462</u>
<u>349,079758</u>	<u>10,062243</u>	<u>349,386689</u>	<u>-0,306931</u>	<u>0,027708</u>	<u>0,096723</u>
<u>389,139380</u>	<u>11,196918</u>	<u>389,111179</u>	<u>0,028201</u>	<u>0,039035</u>	<u>0,151902</u>
<u>419,184096</u>	<u>12,044610</u>	<u>418,788494</u>	<u>0,395602</u>	<u>0,046216</u>	<u>0,193730</u>
<u>419,184096</u>	<u>12,044938</u>	<u>418,799957</u>	<u>0,384139</u>	<u>0,046221</u>	<u>0,193751</u>
<u>389,139380</u>	<u>11,197621</u>	<u>389,135783</u>	<u>0,003597</u>	<u>0,039045</u>	<u>0,151939</u>
<u>349,079758</u>	<u>10,064088</u>	<u>349,451289</u>	<u>-0,371531</u>	<u>0,027732</u>	<u>0,096807</u>
<u>299,005231</u>	<u>8,639597</u>	<u>299,580488</u>	<u>-0,575257</u>	<u>0,011890</u>	<u>0,035553</u>
<u>248,930704</u>	<u>7,209770</u>	<u>249,522886</u>	<u>-0,592182</u>	<u>0,023236</u>	<u>0,057843</u>
<u>98,707122</u>	<u>2,889481</u>	<u>98,271511</u>	<u>0,435611</u>	<u>0,271523</u>	<u>0,268012</u>
<u>98,707122</u>	<u>2,889352</u>	<u>98,266987</u>	<u>0,440135</u>	<u>0,271529</u>	<u>0,268019</u>
<u>198,856177</u>	<u>5,766733</u>	<u>199,002804</u>	<u>-0,146628</u>	<u>0,063264</u>	<u>0,125805</u>
<u>198,856177</u>	<u>5,766139</u>	<u>198,982004</u>	<u>-0,125827</u>	<u>0,063279</u>	<u>0,125834</u>
<u>248,930704</u>	<u>7,199958</u>	<u>249,179381</u>	<u>-0,248677</u>	<u>0,023415</u>	<u>0,058287</u>
<u>299,005231</u>	<u>8,629568</u>	<u>299,229381</u>	<u>-0,224150</u>	<u>0,011817</u>	<u>0,035334</u>
<u>349,079758</u>	<u>10,053730</u>	<u>349,088672</u>	<u>-0,008914</u>	<u>0,027593</u>	<u>0,096323</u>
<u>389,139380</u>	<u>11,189178</u>	<u>388,840213</u>	<u>0,299167</u>	<u>0,038940</u>	<u>0,151529</u>
<u>419,184096</u>	<u>12,038036</u>	<u>418,558334</u>	<u>0,625762</u>	<u>0,046140</u>	<u>0,193411</u>
<u>419,184096</u>	<u>12,038163</u>	<u>418,562785</u>	<u>0,621311</u>	<u>0,046140</u>	<u>0,193413</u>
<u>389,139380</u>	<u>11,189945</u>	<u>388,867036</u>	<u>0,272343</u>	<u>0,038948</u>	<u>0,151562</u>
<u>349,079758</u>	<u>10,055115</u>	<u>349,137140</u>	<u>-0,057382</u>	<u>0,027611</u>	<u>0,096386</u>
<u>299,005231</u>	<u>8,631227</u>	<u>299,287461</u>	<u>-0,282230</u>	<u>0,011819</u>	<u>0,035339</u>
<u>248,930704</u>	<u>7,201868</u>	<u>249,246256</u>	<u>-0,315553</u>	<u>0,023379</u>	<u>0,058196</u>
<u>198,856177</u>	<u>5,767945</u>	<u>199,045238</u>	<u>-0,189062</u>	<u>0,063235</u>	<u>0,125747</u>
<u>98,707122</u>	<u>2,882946</u>	<u>98,042707</u>	<u>0,664416</u>	<u>0,271853</u>	<u>0,268338</u>

COMMENTS:

Raw data was stored in the path C:\Users\logger6\Documents\Hvistendahl, Vefring og West calibration 2022-01-26 1353.tdms

Calibrated using the new and improved VKL calibration program made by J-Dawg

The uncertainty is calculated with 95% confidence. The uncertainty includes the randomness in the calibrated instrument during the calibration, systematic uncertainty in the instrument or property which the instrument under calibration is compared with (dead weight manometer, calibrated weights etc.), and due to regression analysis to fit the calibration points to a linear calibration equation. The calculated uncertainty can be used as the total systematic uncertainty of the calibrated instrument with the given calibration equation.

CALIBRATION REPORT

CALIBRATION PROPERTIES

Calibrated by: Vefring og West

Type/Producer: Unik5000

SN:

Range: kPa

Unit: kPa

CALIBRATION SOURCE PROPERTIES

Type/Producer: DW tester P3223-1

SN: 66256

Uncertainty [%]: 0,010000

POLY FIT EQUATION:

$Y = 62,556070 * X - 124,680889$

CALIBRATION SUMMARY:

Max Uncertainty : Inf [%]

Max Uncertainty : 0,102250 [kPa]

RSQ : 0,999998

Calibration points : 28

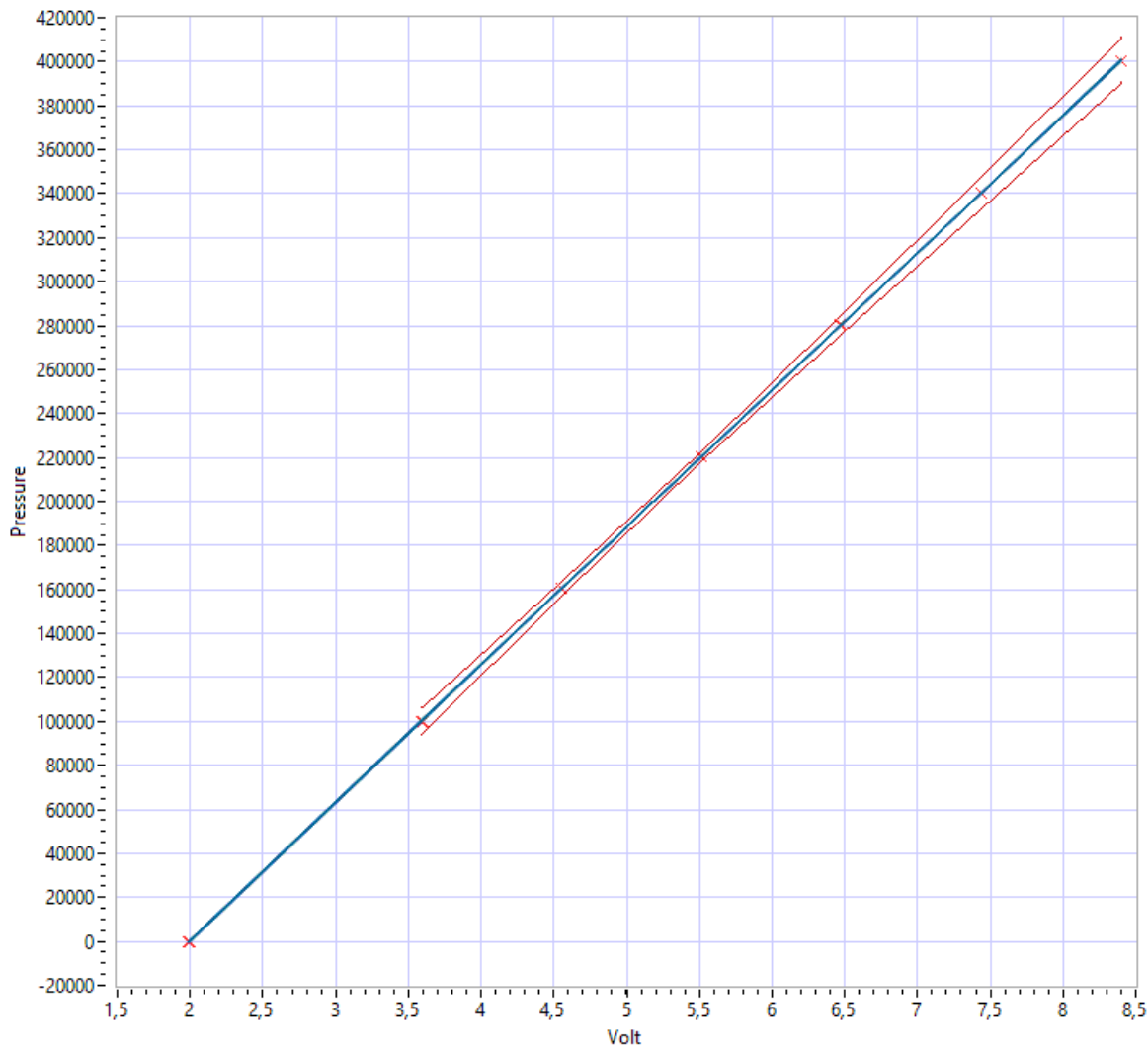


Figure 1 : Calibration chart (The uncertainty band is multiplied by 100)

CALIBRATION VALUES

<u>Value [kPa]</u>	<u>Voltage [V]</u>	<u>Best linear fit [kPa]</u>	<u>Deviation [kPa]</u>	<u>Total uncertainty [%]</u>	<u>Total uncertainty [kPa]</u>
<u>0,000000</u>	<u>1,992247</u>	<u>-0,053761</u>	<u>0,053761</u>	<u>Inf</u>	<u>NaN</u>
<u>100,152476</u>	<u>3,597325</u>	<u>100,353612</u>	<u>-0,201136</u>	<u>0,058555</u>	<u>0,058644</u>
<u>160,244282</u>	<u>4,556079</u>	<u>160,329505</u>	<u>-0,085223</u>	<u>0,019840</u>	<u>0,031793</u>
<u>220,335887</u>	<u>5,516040</u>	<u>220,380887</u>	<u>-0,044999</u>	<u>0,010092</u>	<u>0,022236</u>
<u>280,427493</u>	<u>6,463163</u>	<u>279,629204</u>	<u>0,798288</u>	<u>0,015518</u>	<u>0,043517</u>
<u>340,519098</u>	<u>7,436665</u>	<u>340,527616</u>	<u>-0,008517</u>	<u>0,021203</u>	<u>0,072200</u>
<u>400,610704</u>	<u>8,397056</u>	<u>400,605932</u>	<u>0,004772</u>	<u>0,025515</u>	<u>0,102217</u>
<u>400,610704</u>	<u>8,396946</u>	<u>400,599077</u>	<u>0,011627</u>	<u>0,025515</u>	<u>0,102214</u>
<u>340,519778</u>	<u>7,436579</u>	<u>340,522264</u>	<u>-0,002485</u>	<u>0,021202</u>	<u>0,072198</u>
<u>280,428053</u>	<u>6,476786</u>	<u>280,481385</u>	<u>-0,053333</u>	<u>0,015527</u>	<u>0,043542</u>
<u>220,336327</u>	<u>5,515640</u>	<u>220,355894</u>	<u>-0,019567</u>	<u>0,010091</u>	<u>0,022234</u>
<u>160,244602</u>	<u>4,555532</u>	<u>160,295318</u>	<u>-0,050717</u>	<u>0,019847</u>	<u>0,031803</u>
<u>100,152876</u>	<u>3,595457</u>	<u>100,236792</u>	<u>-0,083916</u>	<u>0,058607</u>	<u>0,058696</u>
<u>0,000000</u>	<u>1,990883</u>	<u>-0,139072</u>	<u>0,139072</u>	<u>Inf</u>	<u>NaN</u>
<u>0,000000</u>	<u>1,991254</u>	<u>-0,115895</u>	<u>0,115895</u>	<u>Inf</u>	<u>NaN</u>
<u>100,152876</u>	<u>3,596098</u>	<u>100,276896</u>	<u>-0,124020</u>	<u>0,058588</u>	<u>0,058678</u>
<u>160,244602</u>	<u>4,556186</u>	<u>160,336172</u>	<u>-0,091571</u>	<u>0,019838</u>	<u>0,031789</u>
<u>220,336327</u>	<u>5,516336</u>	<u>220,399389</u>	<u>-0,063062</u>	<u>0,010092</u>	<u>0,022237</u>
<u>280,428053</u>	<u>6,477247</u>	<u>280,510199</u>	<u>-0,082147</u>	<u>0,015531</u>	<u>0,043553</u>
<u>340,519778</u>	<u>7,436674</u>	<u>340,528237</u>	<u>-0,008458</u>	<u>0,021203</u>	<u>0,072200</u>
<u>400,611504</u>	<u>8,397771</u>	<u>400,650671</u>	<u>-0,039167</u>	<u>0,025521</u>	<u>0,102238</u>
<u>400,611504</u>	<u>8,398168</u>	<u>400,675468</u>	<u>-0,063964</u>	<u>0,025523</u>	<u>0,102250</u>
<u>340,520458</u>	<u>7,436665</u>	<u>340,527670</u>	<u>-0,007212</u>	<u>0,021203</u>	<u>0,072200</u>
<u>280,428613</u>	<u>6,476023</u>	<u>280,433640</u>	<u>-0,005027</u>	<u>0,015520</u>	<u>0,043524</u>
<u>220,336767</u>	<u>5,516407</u>	<u>220,403865</u>	<u>-0,067098</u>	<u>0,010092</u>	<u>0,022237</u>
<u>160,244922</u>	<u>4,555854</u>	<u>160,315428</u>	<u>-0,070507</u>	<u>0,019841</u>	<u>0,031794</u>
<u>100,153076</u>	<u>3,595427</u>	<u>100,234869</u>	<u>-0,081793</u>	<u>0,058607</u>	<u>0,058697</u>
<u>0,000000</u>	<u>1,991020</u>	<u>-0,130503</u>	<u>0,130503</u>	<u>Inf</u>	<u>NaN</u>

COMMENTS:

Raw data was stored in the path C:\Users\logger6\Documents\Calibration 2021-12-10 1221.tdms

Calibrated using the new and improved VKL calibration program made by J-Dawg

The uncertainty is calculated with 95% confidence. The uncertainty includes the randomness in the calibrated instrument during the calibration, systematic uncertainty in the instrument or property which the instrument under calibration is compared with (dead weight manometer, calibrated weights etc.), and due to regression analysis to fit the calibration points to a linear calibration equation. The calculated uncertainty can be used as the total systematic uncertainty of the calibrated instrument with the given calibration equation.

CALIBRATION REPORT

CALIBRATION PROPERTIES

Calibrated by: Vefring og West

Type/Producer: Fuji

SN:

Range: kPa

Unit: kPa

CALIBRATION SOURCE PROPERTIES

Type/Producer: DW tester P3223-1

SN: 66256

Uncertainty [%]: 0,010000

POLY FIT EQUATION:

$Y = 50,043148 * X - 99,602006$

CALIBRATION SUMMARY:

Max Uncertainty : Inf [%]

Max Uncertainty : 0,098972 [kPa]

RSQ : 0,999998

Calibration points : 28

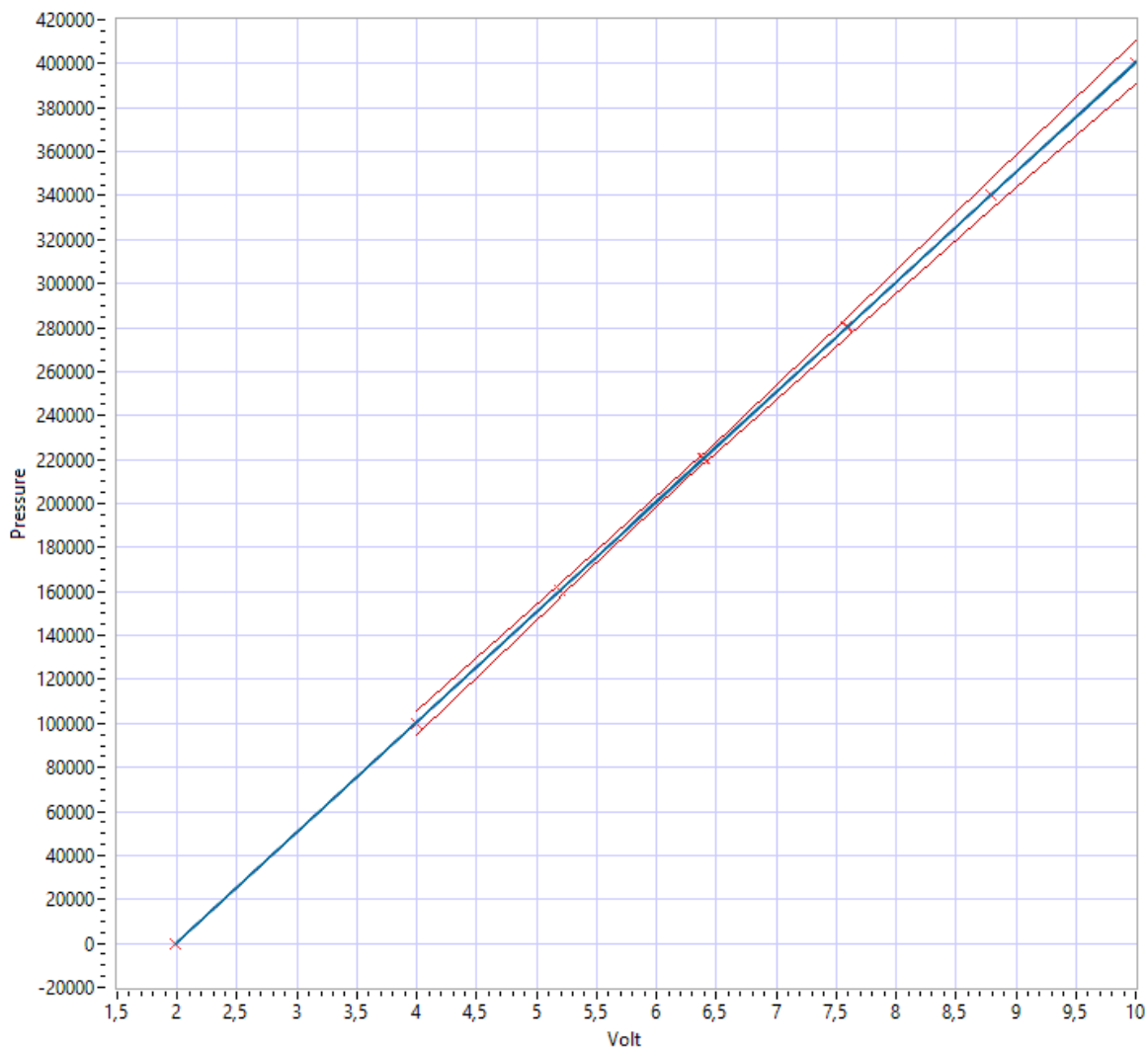


Figure 1 : Calibration chart (The uncertainty band is multiplied by 100)

CALIBRATION VALUES

<u>Value [kPa]</u>	<u>Voltage [V]</u>	<u>Best linear fit [kPa]</u>	<u>Deviation [kPa]</u>	<u>Total uncertainty [%]</u>	<u>Total uncertainty [kPa]</u>
<u>0,000000</u>	<u>1,987572</u>	<u>-0,137668</u>	<u>0,137668</u>	<u>Inf</u>	<u>NaN</u>
<u>100,152476</u>	<u>3,994442</u>	<u>100,292459</u>	<u>-0,139983</u>	<u>0,056436</u>	<u>0,056522</u>
<u>160,244282</u>	<u>5,194279</u>	<u>160,336072</u>	<u>-0,091790</u>	<u>0,019281</u>	<u>0,030897</u>
<u>220,335887</u>	<u>6,394097</u>	<u>220,378722</u>	<u>-0,042835</u>	<u>0,010085</u>	<u>0,022220</u>
<u>280,427493</u>	<u>7,578879</u>	<u>279,668947</u>	<u>0,758545</u>	<u>0,015195</u>	<u>0,042612</u>
<u>340,519098</u>	<u>8,794981</u>	<u>340,526548</u>	<u>-0,007450</u>	<u>0,020582</u>	<u>0,070086</u>
<u>400,610704</u>	<u>9,995880</u>	<u>400,623276</u>	<u>-0,012573</u>	<u>0,024703</u>	<u>0,098964</u>
<u>400,610704</u>	<u>9,995514</u>	<u>400,605001</u>	<u>0,005703</u>	<u>0,024701</u>	<u>0,098955</u>
<u>340,519778</u>	<u>8,794825</u>	<u>340,518709</u>	<u>0,001070</u>	<u>0,020581</u>	<u>0,070083</u>
<u>280,428053</u>	<u>7,595672</u>	<u>280,509306</u>	<u>-0,081253</u>	<u>0,015190</u>	<u>0,042596</u>
<u>220,336327</u>	<u>6,394296</u>	<u>220,388689</u>	<u>-0,052362</u>	<u>0,010085</u>	<u>0,022221</u>
<u>160,244602</u>	<u>5,194463</u>	<u>160,345273</u>	<u>-0,100672</u>	<u>0,019276</u>	<u>0,030889</u>
<u>100,152876</u>	<u>3,994034</u>	<u>100,272014</u>	<u>-0,119138</u>	<u>0,056440</u>	<u>0,056526</u>
<u>0,000000</u>	<u>1,988046</u>	<u>-0,113924</u>	<u>0,113924</u>	<u>Inf</u>	<u>NaN</u>
<u>0,000000</u>	<u>1,988032</u>	<u>-0,114636</u>	<u>0,114636</u>	<u>Inf</u>	<u>NaN</u>
<u>100,152876</u>	<u>3,993536</u>	<u>100,247117</u>	<u>-0,094241</u>	<u>0,056453</u>	<u>0,056539</u>
<u>160,244602</u>	<u>5,194019</u>	<u>160,323071</u>	<u>-0,078469</u>	<u>0,019284</u>	<u>0,030902</u>
<u>220,336327</u>	<u>6,394009</u>	<u>220,374334</u>	<u>-0,038007</u>	<u>0,010084</u>	<u>0,022220</u>
<u>280,428053</u>	<u>7,595339</u>	<u>280,492650</u>	<u>-0,064597</u>	<u>0,015188</u>	<u>0,042590</u>
<u>340,519778</u>	<u>8,794594</u>	<u>340,507161</u>	<u>0,012617</u>	<u>0,020580</u>	<u>0,070078</u>
<u>400,611504</u>	<u>9,995776</u>	<u>400,618108</u>	<u>-0,006604</u>	<u>0,024703</u>	<u>0,098961</u>
<u>400,611504</u>	<u>9,996254</u>	<u>400,642004</u>	<u>-0,030500</u>	<u>0,024705</u>	<u>0,098972</u>
<u>340,520458</u>	<u>8,794819</u>	<u>340,518420</u>	<u>0,002038</u>	<u>0,020581</u>	<u>0,070082</u>
<u>280,428613</u>	<u>7,594260</u>	<u>280,438677</u>	<u>-0,010064</u>	<u>0,015181</u>	<u>0,042570</u>
<u>220,336767</u>	<u>6,394806</u>	<u>220,414222</u>	<u>-0,077455</u>	<u>0,010086</u>	<u>0,022222</u>
<u>160,244922</u>	<u>5,194663</u>	<u>160,355262</u>	<u>-0,110341</u>	<u>0,019274</u>	<u>0,030885</u>
<u>100,153076</u>	<u>3,993761</u>	<u>100,258352</u>	<u>-0,105276</u>	<u>0,056445</u>	<u>0,056532</u>
<u>0,000000</u>	<u>1,987976</u>	<u>-0,117409</u>	<u>0,117409</u>	<u>Inf</u>	<u>NaN</u>

COMMENTS:

Raw data was stored in the path C:\Users\logger6\Documents\Calibration 2021-12-10 1221.tdms

Calibrated using the new and improved VKL calibration program made by J-Dawg

The uncertainty is calculated with 95% confidence. The uncertainty includes the randomness in the calibrated instrument during the calibration, systematic uncertainty in the instrument or property which the instrument under calibration is compared with (dead weight manometer, calibrated weights etc.), and due to regression analysis to fit the calibration points to a linear calibration equation. The calculated uncertainty can be used as the total systematic uncertainty of the calibrated instrument with the given calibration equation.

CALIBRATION REPORT

CALIBRATION PROPERTIES

Calibrated by: Vefring, Lunder og West

Type/Producer:

SN:

Range: kPa

Unit: kPa

CALIBRATION SOURCE PROPERTIES

Type/Producer: DW tester P3223-1

SN: 66256

Uncertainty [%]: 0,010000

POLY FIT EQUATION:

$Y = 22,447604 * X - 5,593137$

CALIBRATION SUMMARY:

Max Uncertainty : 0,027169 [%]

Max Uncertainty : 0,023936 [kPa]

RSQ : 1,000000

Calibration points : 29

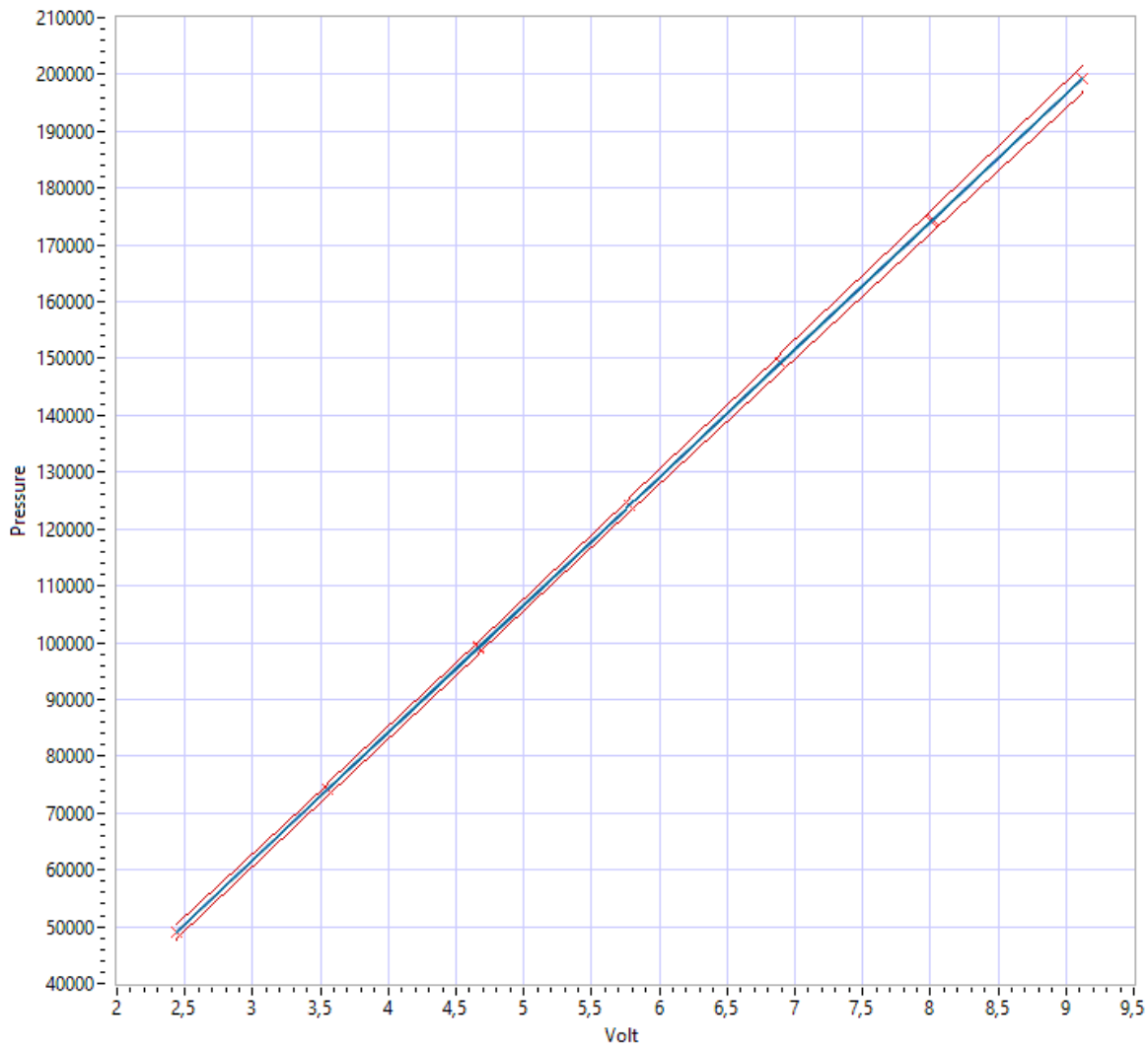


Figure 1 : Calibration chart (The uncertainty band is multiplied by 100)

CALIBRATION VALUES

<u>Value [kPa]</u>	<u>Voltage [V]</u>	<u>Best linear fit [kPa]</u>	<u>Deviation [kPa]</u>	<u>Total uncertainty [%]</u>	<u>Total uncertainty [kPa]</u>
<u>49,025164</u>	<u>2,434174</u>	<u>49,048242</u>	<u>-0,023078</u>	<u>0,027169</u>	<u>0,013320</u>
<u>74,062582</u>	<u>3,549205</u>	<u>74,078014</u>	<u>-0,015432</u>	<u>0,014830</u>	<u>0,010984</u>
<u>99,100000</u>	<u>4,664683</u>	<u>99,117810</u>	<u>-0,017810</u>	<u>0,010723</u>	<u>0,010627</u>
<u>124,137418</u>	<u>5,780654</u>	<u>124,168690</u>	<u>-0,031271</u>	<u>0,010007</u>	<u>0,012422</u>
<u>149,174836</u>	<u>6,896033</u>	<u>149,206279</u>	<u>-0,031443</u>	<u>0,010488</u>	<u>0,015646</u>
<u>174,212254</u>	<u>8,010442</u>	<u>174,222086</u>	<u>-0,009832</u>	<u>0,011253</u>	<u>0,019603</u>
<u>199,249673</u>	<u>9,123631</u>	<u>199,210514</u>	<u>0,039159</u>	<u>0,012011</u>	<u>0,023931</u>
<u>199,249673</u>	<u>9,123449</u>	<u>199,206437</u>	<u>0,043235</u>	<u>0,012010</u>	<u>0,023931</u>
<u>174,212254</u>	<u>8,010341</u>	<u>174,219822</u>	<u>-0,007567</u>	<u>0,011252</u>	<u>0,019603</u>
<u>149,170836</u>	<u>6,895833</u>	<u>149,201790</u>	<u>-0,030954</u>	<u>0,010488</u>	<u>0,015645</u>
<u>124,135418</u>	<u>5,780260</u>	<u>124,159848</u>	<u>-0,024430</u>	<u>0,010007</u>	<u>0,012422</u>
<u>99,100000</u>	<u>4,664152</u>	<u>99,105902</u>	<u>-0,005902</u>	<u>0,010724</u>	<u>0,010627</u>
<u>74,064732</u>	<u>3,547551</u>	<u>74,040892</u>	<u>0,023840</u>	<u>0,014837</u>	<u>0,010989</u>
<u>99,100000</u>	<u>4,663275</u>	<u>99,086220</u>	<u>0,013780</u>	<u>0,010725</u>	<u>0,010629</u>
<u>124,135268</u>	<u>5,779269</u>	<u>124,137604</u>	<u>-0,002335</u>	<u>0,010006</u>	<u>0,012422</u>
<u>149,170536</u>	<u>6,894523</u>	<u>149,172387</u>	<u>-0,001851</u>	<u>0,010487</u>	<u>0,015644</u>
<u>174,205804</u>	<u>8,009015</u>	<u>174,190057</u>	<u>0,015747</u>	<u>0,011251</u>	<u>0,019600</u>
<u>199,241073</u>	<u>9,122613</u>	<u>199,187671</u>	<u>0,053401</u>	<u>0,012010</u>	<u>0,023928</u>
<u>199,241073</u>	<u>9,126444</u>	<u>199,273667</u>	<u>-0,032594</u>	<u>0,012014</u>	<u>0,023936</u>
<u>149,270736</u>	<u>6,899280</u>	<u>149,279162</u>	<u>-0,008426</u>	<u>0,010490</u>	<u>0,015659</u>
<u>124,235368</u>	<u>5,784002</u>	<u>124,243851</u>	<u>-0,008482</u>	<u>0,010007</u>	<u>0,012432</u>
<u>99,200000</u>	<u>4,668318</u>	<u>99,199411</u>	<u>0,000589</u>	<u>0,010717</u>	<u>0,010631</u>
<u>49,129664</u>	<u>2,437138</u>	<u>49,114771</u>	<u>0,014892</u>	<u>0,027098</u>	<u>0,013313</u>
<u>49,129664</u>	<u>2,437260</u>	<u>49,117510</u>	<u>0,012154</u>	<u>0,027097</u>	<u>0,013313</u>
<u>49,129664</u>	<u>2,436936</u>	<u>49,110242</u>	<u>0,019422</u>	<u>0,027099</u>	<u>0,013314</u>
<u>49,129864</u>	<u>2,437284</u>	<u>49,118044</u>	<u>0,011819</u>	<u>0,027097</u>	<u>0,013313</u>
<u>74,164932</u>	<u>3,552226</u>	<u>74,145836</u>	<u>0,019096</u>	<u>0,014808</u>	<u>0,010982</u>
<u>74,164932</u>	<u>3,552515</u>	<u>74,152316</u>	<u>0,012616</u>	<u>0,014807</u>	<u>0,010982</u>
<u>174,304904</u>	<u>8,015394</u>	<u>174,333248</u>	<u>-0,028343</u>	<u>0,011256</u>	<u>0,019620</u>

COMMENTS:

Raw data was stored in the path C:\Users\logger6\Documents\Calibration 2021-10-15 0812.tdms

Calibrated using the new and improved VKL calibration program made by J-Dawg

The uncertainty is calculated with 95% confidence. The uncertainty includes the randomness in the calibrated instrument during the calibration, systematic uncertainty in the instrument or property which the instrument under calibration is compared with (dead weight manometer, calibrated weights etc.), and due to regression analysis to fit the calibration points to a linear calibration equation. The calculated uncertainty can be used as the total systematic uncertainty of the calibrated instrument with the given calibration equation.

CALIBRATION REPORT

CALIBRATION PROPERTIES

Calibrated by: Vefring, Lunder og West

Type/Producer:

SN:

Range: kPa

Unit: kPa

CALIBRATION SOURCE PROPERTIES

Type/Producer: DW tester P3223-1

SN: 66256

Uncertainty [%]: 0,010000

POLY FIT EQUATION:

$Y = 22,829246 * X - 7,043156$

CALIBRATION SUMMARY:

Max Uncertainty : 0,036023 [%]

Max Uncertainty : 0,026948 [kPa]

RSQ : 1,000000

Calibration points : 29

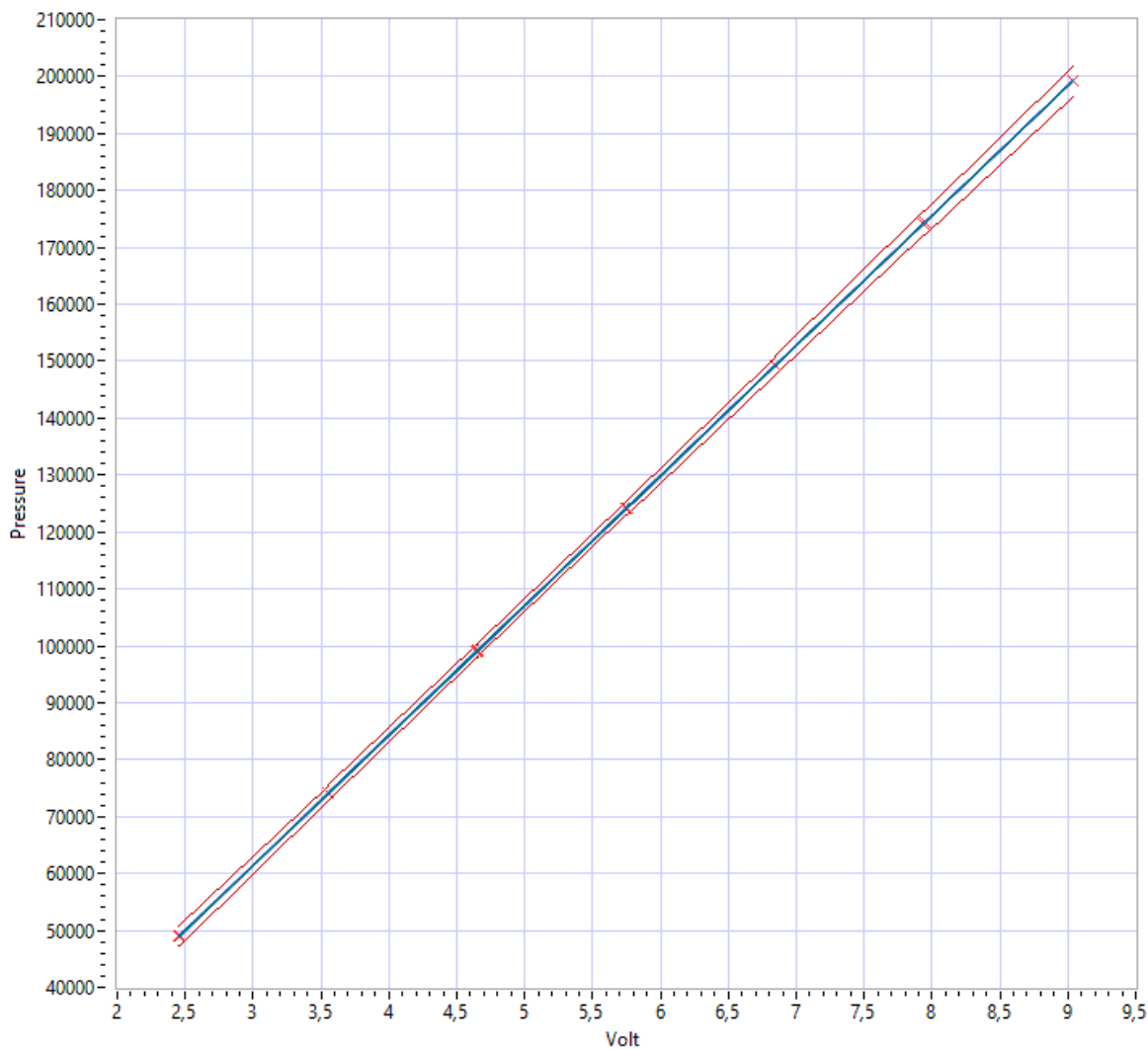


Figure 1 : Calibration chart (The uncertainty band is multiplied by 100)

CALIBRATION VALUES

<u>Value [kPa]</u>	<u>Voltage [V]</u>	<u>Best linear fit [kPa]</u>	<u>Deviation [kPa]</u>	<u>Total uncertainty [%]</u>	<u>Total uncertainty [kPa]</u>
<u>49,025164</u>	<u>2,453569</u>	<u>48,969978</u>	<u>0,055185</u>	<u>0,036023</u>	<u>0,017660</u>
<u>74,062582</u>	<u>3,550806</u>	<u>74,019078</u>	<u>0,043504</u>	<u>0,018033</u>	<u>0,013355</u>
<u>99,100000</u>	<u>4,648073</u>	<u>99,068842</u>	<u>0,031158</u>	<u>0,011322</u>	<u>0,011220</u>
<u>124,137418</u>	<u>5,746449</u>	<u>124,143935</u>	<u>-0,006517</u>	<u>0,010012</u>	<u>0,012429</u>
<u>149,174836</u>	<u>6,843555</u>	<u>149,190045</u>	<u>-0,015208</u>	<u>0,010895</u>	<u>0,016253</u>
<u>174,212254</u>	<u>7,939104</u>	<u>174,200608</u>	<u>0,011646</u>	<u>0,012240</u>	<u>0,021323</u>
<u>199,249673</u>	<u>9,033312</u>	<u>199,180555</u>	<u>0,069118</u>	<u>0,013521</u>	<u>0,026940</u>
<u>199,249673</u>	<u>9,033226</u>	<u>199,178572</u>	<u>0,071101</u>	<u>0,013521</u>	<u>0,026940</u>
<u>174,212254</u>	<u>7,939560</u>	<u>174,211007</u>	<u>0,001248</u>	<u>0,012241</u>	<u>0,021325</u>
<u>149,170836</u>	<u>6,844002</u>	<u>149,200258</u>	<u>-0,029422</u>	<u>0,010896</u>	<u>0,016254</u>
<u>124,135418</u>	<u>5,747333</u>	<u>124,164123</u>	<u>-0,028705</u>	<u>0,010012</u>	<u>0,012429</u>
<u>99,100000</u>	<u>4,649827</u>	<u>99,108898</u>	<u>-0,008898</u>	<u>0,011318</u>	<u>0,011216</u>
<u>74,064732</u>	<u>3,552713</u>	<u>74,062604</u>	<u>0,002128</u>	<u>0,018021</u>	<u>0,013347</u>
<u>99,100000</u>	<u>4,650078</u>	<u>99,114614</u>	<u>-0,014614</u>	<u>0,011317</u>	<u>0,011215</u>
<u>124,135268</u>	<u>5,747762</u>	<u>124,173925</u>	<u>-0,038657</u>	<u>0,010012</u>	<u>0,012429</u>
<u>149,170536</u>	<u>6,844560</u>	<u>149,212984</u>	<u>-0,042448</u>	<u>0,010897</u>	<u>0,016255</u>
<u>174,205804</u>	<u>7,940411</u>	<u>174,230434</u>	<u>-0,024629</u>	<u>0,012242</u>	<u>0,021327</u>
<u>199,241073</u>	<u>9,034806</u>	<u>199,214655</u>	<u>0,026418</u>	<u>0,013524</u>	<u>0,026945</u>
<u>199,241073</u>	<u>9,035677</u>	<u>199,234548</u>	<u>0,006525</u>	<u>0,013525</u>	<u>0,026948</u>
<u>149,270736</u>	<u>6,847429</u>	<u>149,278492</u>	<u>-0,007756</u>	<u>0,010900</u>	<u>0,016270</u>
<u>124,235368</u>	<u>5,751085</u>	<u>124,249781</u>	<u>-0,014413</u>	<u>0,010014</u>	<u>0,012441</u>
<u>99,200000</u>	<u>4,654015</u>	<u>99,204490</u>	<u>-0,004490</u>	<u>0,011305</u>	<u>0,011215</u>
<u>49,129664</u>	<u>2,459950</u>	<u>49,115655</u>	<u>0,014009</u>	<u>0,035887</u>	<u>0,017631</u>
<u>49,129664</u>	<u>2,460146</u>	<u>49,120112</u>	<u>0,009552</u>	<u>0,035885</u>	<u>0,017630</u>
<u>49,129664</u>	<u>2,460342</u>	<u>49,124592</u>	<u>0,005072</u>	<u>0,035883</u>	<u>0,017629</u>
<u>49,129864</u>	<u>2,460902</u>	<u>49,137381</u>	<u>-0,007517</u>	<u>0,035877</u>	<u>0,017626</u>
<u>74,164932</u>	<u>3,557763</u>	<u>74,177890</u>	<u>-0,012958</u>	<u>0,017975</u>	<u>0,013331</u>
<u>74,164932</u>	<u>3,558057</u>	<u>74,184595</u>	<u>-0,019663</u>	<u>0,017973</u>	<u>0,013330</u>
<u>174,304904</u>	<u>7,946773</u>	<u>174,375673</u>	<u>-0,070768</u>	<u>0,012251</u>	<u>0,021355</u>

COMMENTS:

Raw data was stored in the path C:\Users\logger6\Documents\Calibration 2021-10-15 0812.tdms

Calibrated using the new and improved VKL calibration program made by J-Dawg

The uncertainty is calculated with 95% confidence. The uncertainty includes the randomness in the calibrated instrument during the calibration, systematic uncertainty in the instrument or property which the instrument under calibration is compared with (dead weight manometer, calibrated weights etc.), and due to regression analysis to fit the calibration points to a linear calibration equation. The calculated uncertainty can be used as the total systematic uncertainty of the calibrated instrument with the given calibration equation.

CALIBRATION REPORT

CALIBRATION PROPERTIES

Calibrated by: Halvor West
Type/Producer: HBM something
SN: find later
Range: find later
Unit: Nm

CALIBRATION SOURCE PROPERTIES

Type/Producer: Calibrated Weights
SN: -
Uncertainty [%]: -

POLY FIT EQUATION:

$Y = +221.35370024E-3X^0 + 2.83554799E+0X^1$

CALIBRATION SUMMARY:

Max Uncertainty : Inf [%]
Max Uncertainty : 0.830400 [Nm]
RSQ : 0.986598
Calibration points : 28

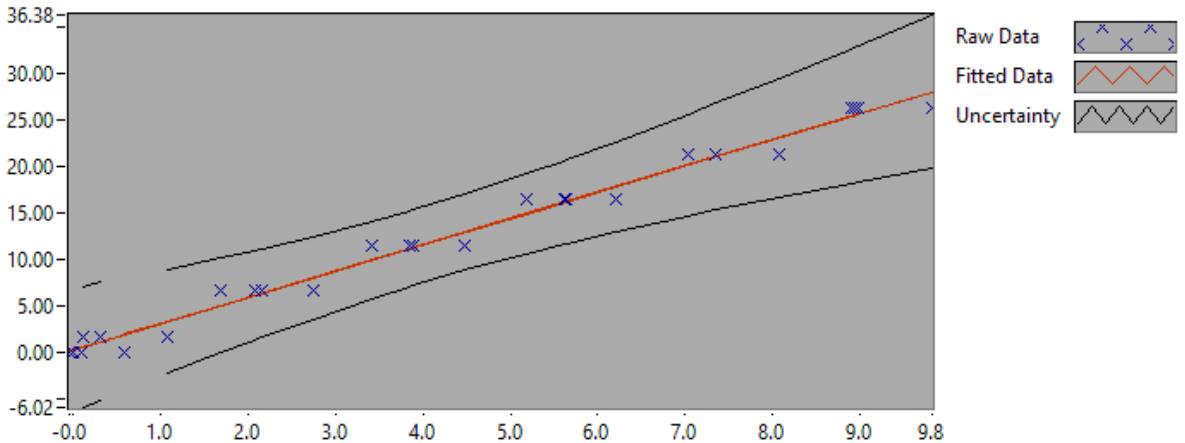


Figure 1 : Calibration chart (The uncertainty band is multiplied by 10)

Halvor West

CALIBRATION VALUES

<u>Value [Nm]</u>	<u>Voltage [V]</u>	<u>Best Poly. Fit [Nm]</u>	<u>Deviation [Nm]</u>	<u>Uncertainty [%]</u>	<u>Uncertainty [Nm]</u>
<u>-0.000000</u>	<u>0.596458</u>	<u>1.912639</u>	<u>-1.912639</u>	<u>Inf</u>	<u>NaN</u>
<u>1.609888</u>	<u>1.080201</u>	<u>3.284316</u>	<u>-1.674428</u>	<u>35.053798</u>	<u>0.564327</u>
<u>6.542180</u>	<u>2.741939</u>	<u>7.996254</u>	<u>-1.454074</u>	<u>6.820093</u>	<u>0.446183</u>
<u>11.475709</u>	<u>4.475777</u>	<u>12.912633</u>	<u>-1.436924</u>	<u>3.587875</u>	<u>0.411734</u>
<u>16.410474</u>	<u>6.212536</u>	<u>17.837297</u>	<u>-1.426823</u>	<u>2.967782</u>	<u>0.487027</u>
<u>21.345239</u>	<u>8.073062</u>	<u>23.112908</u>	<u>-1.767669</u>	<u>3.027823</u>	<u>0.646296</u>
<u>26.281241</u>	<u>9.823701</u>	<u>28.076930</u>	<u>-1.795689</u>	<u>3.159668</u>	<u>0.830400</u>
<u>26.281241</u>	<u>8.944350</u>	<u>25.583486</u>	<u>0.697755</u>	<u>2.797748</u>	<u>0.735283</u>
<u>21.345239</u>	<u>7.348140</u>	<u>21.057357</u>	<u>0.287882</u>	<u>2.707862</u>	<u>0.578000</u>
<u>16.410474</u>	<u>5.610774</u>	<u>16.130972</u>	<u>0.279502</u>	<u>2.743684</u>	<u>0.450251</u>
<u>11.475709</u>	<u>3.846609</u>	<u>11.128597</u>	<u>0.347112</u>	<u>3.582666</u>	<u>0.411136</u>
<u>6.542180</u>	<u>2.071750</u>	<u>6.095901</u>	<u>0.446280</u>	<u>7.433557</u>	<u>0.486317</u>
<u>-0.000000</u>	<u>-0.010128</u>	<u>0.192634</u>	<u>-0.192634</u>	<u>Inf</u>	<u>NaN</u>
<u>-0.000000</u>	<u>-0.041402</u>	<u>0.103956</u>	<u>-0.103956</u>	<u>Inf</u>	<u>NaN</u>
<u>1.609888</u>	<u>0.109644</u>	<u>0.532254</u>	<u>1.077634</u>	<u>40.704950</u>	<u>0.655304</u>
<u>6.542180</u>	<u>1.684757</u>	<u>4.998563</u>	<u>1.543617</u>	<u>7.864451</u>	<u>0.514507</u>
<u>11.475709</u>	<u>3.419651</u>	<u>9.917940</u>	<u>1.557770</u>	<u>3.655510</u>	<u>0.419496</u>
<u>16.410474</u>	<u>5.176287</u>	<u>14.898965</u>	<u>1.511510</u>	<u>2.621728</u>	<u>0.430238</u>
<u>21.345239</u>	<u>7.026019</u>	<u>20.143968</u>	<u>1.201272</u>	<u>2.576141</u>	<u>0.549883</u>
<u>26.278768</u>	<u>8.975427</u>	<u>25.671607</u>	<u>0.607161</u>	<u>2.810825</u>	<u>0.738650</u>
<u>26.278768</u>	<u>8.890799</u>	<u>25.431641</u>	<u>0.847127</u>	<u>2.776550</u>	<u>0.729643</u>
<u>21.345239</u>	<u>7.347484</u>	<u>21.055497</u>	<u>0.289742</u>	<u>2.707589</u>	<u>0.577941</u>
<u>16.410474</u>	<u>5.647190</u>	<u>16.234233</u>	<u>0.176241</u>	<u>2.755524</u>	<u>0.452195</u>
<u>11.475709</u>	<u>3.896088</u>	<u>11.268900</u>	<u>0.206810</u>	<u>3.578167</u>	<u>0.410620</u>
<u>6.542180</u>	<u>2.151560</u>	<u>6.322205</u>	<u>0.219975</u>	<u>7.351110</u>	<u>0.480923</u>
<u>1.609888</u>	<u>0.315086</u>	<u>1.114795</u>	<u>0.495093</u>	<u>39.452276</u>	<u>0.635137</u>
<u>1.609888</u>	<u>0.318775</u>	<u>1.125256</u>	<u>0.484632</u>	<u>39.430033</u>	<u>0.634779</u>
<u>0.000000</u>	<u>0.102599</u>	<u>0.512278</u>	<u>-0.512278</u>	<u>Inf</u>	<u>NaN</u>

COMMENTS:

The uncertainty is calculated with 95% confidence. The uncertainty includes the randomness in the calibrated instrument during the calibration, systematic uncertainty in the instrument or property which the instrument under calibration is compared with (dead weight manometer, calibrated weights etc.), and due to regression analysis to fit the calibration points to a linear calibration equation. The calculated uncertainty can be used as the total systematic uncertainty of the calibrated instrument with the given calibration equation.



WATERPOWER LABORATORY

Date: 13.01.2022

Operator:
Karl Escher
Håvor West
Johannes Kvemo

Calibration Sheet

Calibration of flow meter

Calibrator: Weighing tank system

Unit: Flowmeter, Francisrigg

Calibration constants for weighing tank correction	
a ₁	1,68E-23
a ₂	-2,63E-18
a ₃	2,58E-13
a ₄	-1,16E-08
a ₅	9,99E-01

nPoints	28
S _{yy}	0,00041

Corrected weight is calculated from formula where parameters a, b, c, d and e is achieved through substitution calibration.

$$W = a \cdot \frac{mW^5}{5} + b \cdot \frac{mW^4}{4} + c \cdot \frac{mW^3}{3} + d \cdot \frac{mW^2}{2} + e \cdot mW$$

Density of water is calculated from formula

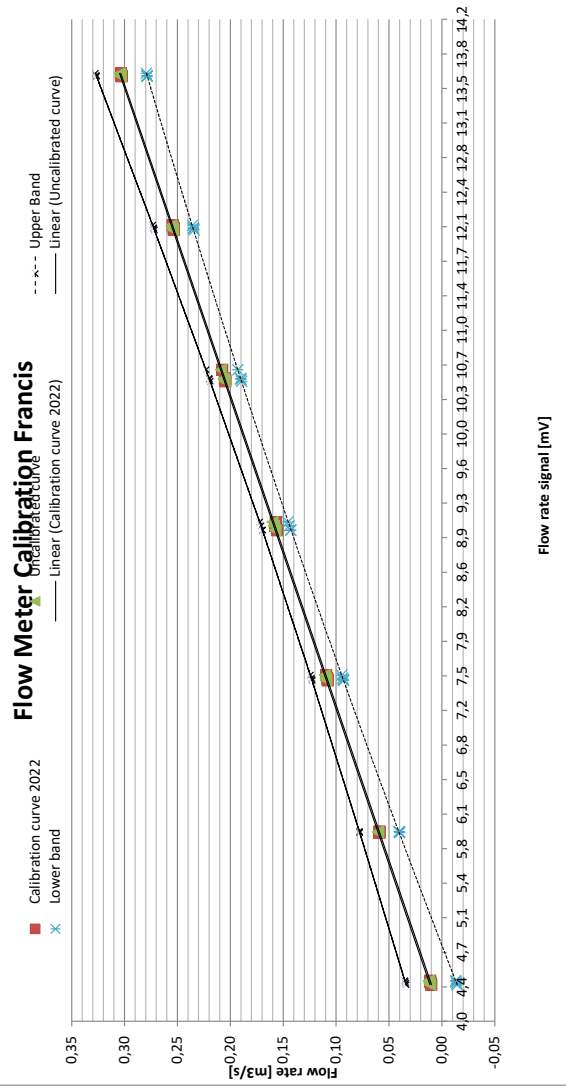
$$\rho_w = \frac{1000}{[-4,6897 \cdot 10^{-16} \cdot p_{abs}^4 + 8 \cdot 10^{-8} \cdot (-0,4721338913 \cdot 10^{-11} \cdot p_{abs}^3 - 6 \cdot 10^{-7} \cdot (-4,21338913 \cdot 10^{-11} \cdot p_{abs}^2)]}$$

Density of air is calculated from formula

$$\rho_a = \frac{(p_a - 3,4837 \cdot 10^3)}{(273,15 + \theta)}$$

Discharge is found from formula

$$Q = \frac{W_a - W_b}{\rho_a \cdot (1 - \frac{\rho_a}{\rho_w})}$$



Manual Observation before	Manual Observation after	Manual Current	Manual Observation Current	Equivalent Voltage	Time	Ambient pressure	Water temp	Air temp	Calculate d value before	Calculate d value after	Differential weight	Density of water	Density of air	Differential volume	Calculated Flow Rate	Estimate	Deviation	Outlier detection	Regression uncertainty	f
[kg]	[kg]	[A]	[A]	[V]	[s]	[kPa]	[°C]	[°C]	Weight [kg]	Weight [kg]	Weight [kg]	[kg/m ³]	[kg/m ³]	[m ³]	[m ³ /s]	[m ³ /s]	[%]	e _i	e/S _y	
4968.30	9666.92	0.004402	4.401833	2.200917	417.074	99.740	13.76	18.14	4963.2	9656.8	4693.6	999.3371	1.1937	4.70233	0.0112746	0.01090	-3.47749	0.00038	0.0002395	2.19938
9675.26	14658.82	0.005913	5.912844	2.956422	84.076	99.740	13.77	18.13	9685.2	14643.2	4978.1	999.3357	1.1937	4.98732	0.0593192	0.05896	-0.60430	0.00036	0.0001885	0.31970
14668.59	19819.68	0.007508	7.507713	3.753857	47.076	99.700	13.78	18.04	14653.0	19798.2	5145.3	999.3342	1.1936	5.15485	0.1095006	0.10970	0.17976	-0.00020	0.0001477	0.13465
19826.74	25027.18	0.009309	9.093804	4.529402	33.078	99.690	13.75	18.01	19805.3	24999.7	5194.5	999.3384	1.1936	5.20411	0.1573283	0.15779	0.08235	-0.00013	0.0001329	0.08359
25029.43	31203.28	0.010513	10.512751	5.256376	30.077	99.700	13.77	18.01	25002.0	31168.6	6166.7	999.3356	1.1937	6.17813	0.2054105	0.20529	-0.05777	0.00012	0.0001484	0.07229
31202.91	38824.99	0.012038	12.037873	6.018937	30.076	99.700	13.83	17.98	31168.3	38781.4	7613.1	999.3273	1.1939	7.62738	0.2536034	0.25381	0.08064	-0.00020	0.0001875	0.07387
38824.60	47938.81	0.013581	13.580865	6.790433	30.076	99.690	13.91	17.90	38781.0	47884.6	9103.6	999.3160	1.1941	9.12069	0.3032549	0.30289	-0.11960	0.00036	0.0002395	0.07907
47938.46	57040.38	0.013574	13.574253	6.787126	30.076	99.690	13.91	17.91	47884.2	56975.7	9091.5	999.3160	1.1940	9.10859	0.3028524	0.30268	-0.05620	0.00017	0.0002393	0.07905
57040.16	64659.56	0.012016	12.016307	6.008154	30.076	99.690	13.92	17.84	56975.5	64586.4	7610.9	999.3146	1.1943	7.62528	0.2535338	0.25312	-0.16270	0.00041	0.0001868	0.07381
64659.52	70813.75	0.010483	10.483478	5.241739	30.077	99.690	13.93	17.75	64586.4	70734.1	6147.7	999.3132	1.1947	6.15928	0.2047838	0.20436	-0.20703	0.00042	0.0001479	0.07235
70813.21	10213.75	0.009200	9.019512	4.509756	33.076	99.710	13.92	17.95	4986.1	10203.1	5205.0	999.3146	1.1941	5.21477	0.1576601	0.15779	0.08235	-0.00013	0.0001329	0.08424
10213.78	15302.12	0.007455	7.455002	3.725801	47.077	99.710	13.94	17.92	10203.1	15285.8	5082.7	999.3118	1.1942	5.09229	0.1081695	0.10802	-0.13749	0.00015	0.0001487	0.13768
15302.00	20274.93	0.005924	5.923560	2.961780	84.077	99.720	13.92	17.97	15285.7	20253.0	4967.3	999.3146	1.1941	4.97664	0.0591914	0.05930	0.18944	-0.00011	0.0001882	0.31730
20275.10	24689.77	0.004386	4.386189	2.193094	417.076	99.690	13.91	17.99	20253.1	24682.7	4409.6	999.3160	1.1937	4.41788	0.0105925	0.01040	-1.87062	0.00019	0.0002401	2.30904
24689.34	30598.73	0.004414	4.413521	2.206760	417.076	99.620	14.01	18.12	5867.3	10587.6	4720.3	999.3018	1.1923	4.72925	0.0113391	0.01127	-0.63549	0.00007	0.0002391	2.12210
30598.31	37059.90	0.005916	5.915576	2.957788	84.078	99.660	14.04	18.10	15575.6	20530.6	4955.0	999.2975	1.1929	4.96437	0.0590449	0.05905	0.00936	0.00000	0.0001884	0.31908
37059.72	43259.81	0.007462	7.462159	3.737079	47.079	99.670	13.98	18.14	20531.4	25611.7	5080.2	999.3061	1.1928	5.08982	0.1081170	0.10825	0.12158	-0.00013	0.0001486	0.13726
43259.41	50040.41	0.008978	8.978216	4.489708	33.079	99.660	13.96	18.14	25612.2	30766.2	6156.1	999.3089	1.1928	5.16381	0.1561053	0.15648	0.23712	-0.00037	0.0001329	0.08494
50040.35	56963.65	0.010503	10.503408	5.251704	30.078	99.670	13.97	18.18	30766.2	36922.2	6156.1	999.3075	1.1927	6.16770	0.2050569	0.20499	-0.03032	0.00006	0.0001482	0.07231
36963.52	44585.64	0.012032	12.031669	6.015835	30.078	99.700	13.98	18.14	36922.1	44535.3	7613.2	999.3061	1.1932	7.62758	0.2535932	0.25361	0.00689	-0.00002	0.0001873	0.07386
44585.60	53709.06	0.013604	13.603873	6.807936	30.079	99.690	14.01	18.05	44535.3	53648.2	9112.9	999.3018	1.1934	9.13018	0.3035400	0.30362	0.02783	-0.00008	0.0002403	0.07915
53708.97	62814.74	0.013575	13.575369	6.787684	30.079	99.680	14.00	18.06	53648.1	62743.6	9095.6	999.3032	1.1933	9.11278	0.3029816	0.30272	-0.08715	0.00026	0.0002393	0.07905
62814.80	70475.32	0.012065	12.065449	6.032725	30.077	99.690	14.04	17.97	62743.7	70396.0	7652.3	999.2976	1.1938	7.66686	0.2549079	0.25469	-0.08741	0.00022	0.0001883	0.07395
70475.21	27095.20	0.010602	10.601998	5.300999	30.077	99.680	14.06	18.22	20823.6	27085.4	6241.8	999.2947	1.1926	6.25364	0.2079209	0.20813	0.10092	-0.00021	0.0001502	0.07216
27095.42	32254.00	0.008975	8.975243	4.480692	33.076	99.700	14.07	18.13	27085.6	32218.1	5152.6	999.2933	1.1932	5.16237	0.1566079	0.15663	0.19561	-0.00031	0.0001329	0.08499
32253.88	37364.86	0.007478	7.477915	3.738957	47.079	99.710	14.08	18.16	32218.0	37323.9	5105.0	999.2918	1.1932	5.11471	0.1086409	0.10875	0.10011	-0.00011	0.0001483	0.13635
37364.78	42351.97	0.005922	5.921798	2.960699	84.080	99.650	14.08	18.15	37322.9	42304.2	4981.3	999.2918	1.1926	4.99082	0.0593580	0.05925	-0.18618	0.00011	0.0001882	0.31770
42351.99	46610.94	0.004371	4.371270	2.165635	417.076	99.650	14.11	18.21	42304.3	46558.2	4254.0	999.2875	1.1923	4.26209	0.0102190	0.00992	-2.97658	0.00030	0.0002406	2.42489

Calibration constants	Previous const.
C ₀	-0.129132384
C ₁	0.063363629

Sxx 262.442281
Syy 0.265585
Sxy 8.348630749
SEE 4.433E-06
s² 1.705E-07
L₁ value 1.703288446



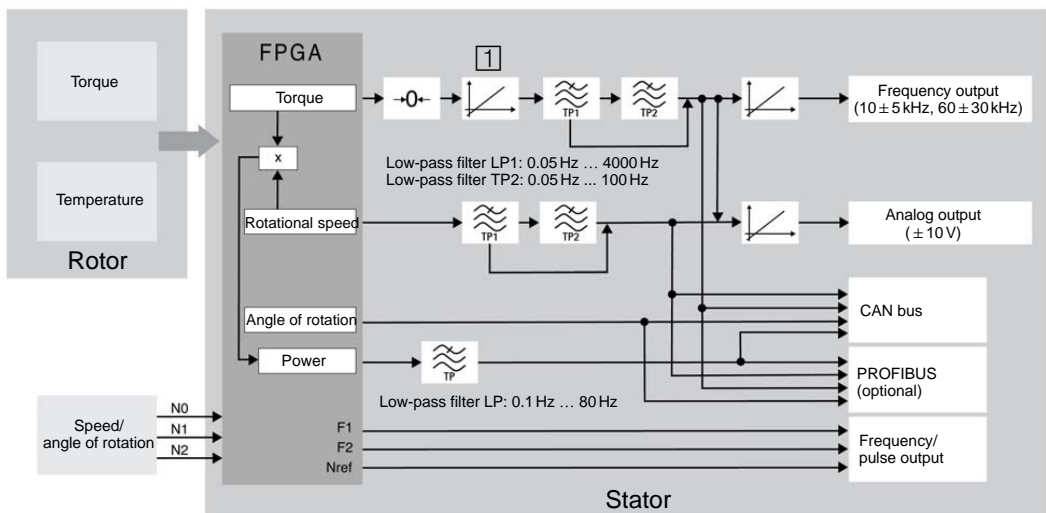
T12HP

Digital transducer

Special features

- Nominal (rated) torque 100 N·m, 200 N·m, 500 N·m, 1 kN·m, 2 kN·m, 3 kN·m, 5 kN·m and 10 kN·m
- Nominal (rated) rotational speeds of 10,000 rpm to 22,000 rpm
- Large measurement frequency range up to 6 kHz (-3 dB)
- Fast digital measurement signal transmission of 4800 measured values/s
- High resolution of 19 bits (integrative method)
- Monitoring functions
- Excellent temperature behavior with TC₀ of 0.005%/10K
- Minimal linearity deviation, including hysteresis of 0.007%
- Extensive options

Signal flow block diagram



Specifications

Type	T12HP									
Accuracy class	0.02									
Torque measuring system										
Nominal (rated) torque M_{nom}	N-m	100	200	500						
	kN-m				1	2	3	5	10	
Nominal (rated) rotational speed n_{nom} Option 4, code L ¹⁾ Option 4, code H ¹⁾ Option 4, code F ^{1), 8), 9)}	rpm	15,000		12,000			10,000			
	rpm	18,000		16,000			14,000 12,000			
	rpm	22,000		20,000		18,000		not available		
Linearity deviation including hysteresis, related to nominal sensitivity Fieldbuses, frequency output 10 kHz/60 kHz For a max. torque in range: between 0% of M_{nom} and 20% of M_{nom} > 20% of M_{nom} and 60% of M_{nom} > 60% of M_{nom} and 100% of M_{nom} Voltage output For a max. torque in range: between 0% of M_{nom} and 20% of M_{nom} > 20% of M_{nom} and 60% of M_{nom} > 60% of M_{nom} and 100% of M_{nom} Rel. standard deviation of repeatability per DIN 1319, related to the variation of the output signal Fieldbuses/frequency output Voltage output	%				< ± 0.005 (optional < ± 0.003)					
	%				< ± 0.010 (optional < ± 0.005)					
	%				< ± 0.015 (optional < ± 0.007)					
	%				< ± 0.015					
	%				< ± 0.035					
	%				< ± 0.05					
	%				± 0.005					
	%				± 0.03					
	Temperature effect per 10 K in the nominal (rated) temperature range on the output signal, related to the actual value of the signal span Fieldbuses/frequency output Voltage output on the zero signal, related to the nominal sensitivity Fieldbuses/frequency output Voltage output	%				± 0.02				
		%				± 0.05				
%					± 0.01 (optional ± 0.005)					
%					± 0.04					
Nominal sensitivity (spread between torque = zero and nominal (rated) torque) Frequency output 10 kHz/60 kHz Voltage output Sensitivity tolerance (deviation of the actual output quantity at M_{nom} from the nominal sensitivity) Frequency output Voltage output		kHz				5/30				
		V				10				
	%				± 0.05					
Output signal at torque = zero Frequency output 10 kHz/60 kHz Voltage output	kHz				10/60					
	V				0					
Nominal (rated) output signal Frequency output with positive nominal (rated) torque 10 kHz/60 kHz with negative nominal (rated) torque 10 kHz/60 kHz Voltage output at positive nominal (rated) torque at negative nominal (rated) torque	kHz				15/90 (5 V symmetrical ²⁾)					
	kHz				5/30 (5 V symmetrical ²⁾)					
	V				+10					
	V				-10					
	%				10 ... 1000 (of M_{nom})					
Resolution Frequency output 10 kHz/60 kHz Voltage output	Hz				0.03/0.25					
	mV				0.33					
Residual ripple Voltage output	mV				3					

1) See page 15.

2) RS-422 complementary signals, note termination resistance.

Specifications (continued)

Nominal (rated) torque M_{nom}	N·m	100	200	500						
	kN·m				1	2	3	5	10	
Maximum modulation range ³⁾										
Frequency output 10 kHz/60 kHz	kHz	4 ... 16/24 ... 96								
Voltage output	V	-10.2 ... +10.2								
Load resistance										
Frequency output	kΩ	≥ 2								
Voltage output	kΩ	≥ 10								
Long-term drift over 48 h										
Voltage output	mV	± 3								
Measurement frequency range										
Frequency output/voltage output -1 dB	Hz	0 ... 4000								
Frequency output/voltage output -3 dB	Hz	0 ... 6000								
Low-pass filter LP1	Hz	0.05 ... 4000 (fourth-order Bessel, -1 dB); factory setting 1000 Hz								
Low-pass filter LP2	Hz	0.05 ... 100 (fourth-order Bessel, -1 dB); factory setting 1 Hz								
Group delay (low pass LP1: 4 kHz)										
Frequency output 10 kHz/60 kHz	μs	320/250								
Voltage output	μs	500								
Energy supply										
Nominal (rated) supply voltage (DC) (safety extra-low voltage)	V	18 ... 30								
Current consumption in measuring mode	A	< 1 (typ. 0.5)								
Current consumption in startup mode	A	< 4								
Nominal (rated) power consumption	W	< 18								
Maximum cable length	m	50								
Shunt signal		50 % of M_{nom} or 10 % of M_{nom}								
Tolerance of the shunt signal, related to M_{nom}	%	± 0.05								
Speed/angle of rotation measuring system Optical, using infrared light and a metallic slotted disc										
Mechanical increments	Number	360							720	
Positional tolerance of the increments	mm	± 0.05								
Tolerance of the slot width	mm	± 0.05								
Pulses per revolution (adjustable)	Number	360; 180; 90; 60; 45; 30							720; 360; 180; 120; 90; 60	
Pulse frequency at nominal (rated) rotational speed										
n_{nom}										
Option 4, code L ⁴⁾	kHz	90	72				120			
Option 4, code H ⁴⁾	kHz	108	96				168			
Option 4, code F ⁴⁾	kHz	132	120	108		not available				
Minimum rotational speed for sufficient pulse stability	rpm	2								
Group delay	μs	< 5 (typ. 2.2)								
Hysteresis of direction of rotation reversal in the case of relative vibrations between rotor and stator										
Torsional vibration of the rotor	degrees	< approx. 2								
Radial vibrations of the stator	mm	< approx. 2								
Permitted degree of contamination , in the optical path of the sensor pickup (lenses, slotted disc)	%	< 50								
Effect of turbulence (slotted disk) on the zero point related to the nominal (rated) torque										
Option 4, code L ⁴⁾	%	< 0.05	< 0.03	< 0.03	< 0.02	< 0.01				
Option 4, code H ⁴⁾	%	< 0.08	< 0.04	< 0.03	< 0.02	< 0.01				
Option 4, code F ⁴⁾	%	< 0.12	< 0.06	< 0.05	< 0.03	not available				
Output signal for frequency/pulse output	V	5 ⁵⁾ symmetrical; 2 square-wave signals, approx. 90° out-of-phase								
Load resistance	kΩ	≥ 2								

³⁾ Output signal range in which there is a repeatable correlation between torque and output signal.

⁴⁾ See page 15.

⁵⁾ RS-422 complementary signals, note line terminations.

Specifications (continued)

Nominal (rated) torque M_{nom}	N·m	100	200	500						
	kN·m				1	2	3	5	10	
Rotational speed										
Fieldbuses										
Resolution	rpm	0.1								
System accuracy (with torsional vibrations of max. 3% of the current rotational speed at 2x rotational frequency)	ppm	150								
Max. rotational speed deviation at nominal (rated) rotational speed (100 Hz filter)	rpm	1.5								
Voltage output										
Measurement range	V	± 10								
Resolution	mV	0.33								
Scaling range	%	10 to 1000								
Overload limits	V	± 10.2								
Load resistance	kΩ	> 10								
Non-linearity	%	< 0.03								
Nominal (rated) power consumption	W	< 18								
Maximum cable length	m	50								
Temperature effect per 10 K in the nominal (rated) temperature range										
on the output signal, related to the actual value of the signal span	%	< 0.03								
on the zero signal	%	< 0.03								
Residual ripple	mV	< 3								
Angle of rotation										
Accuracy	degrees	1 (typ. 0.1)								
Resolution	degrees	0.01								
Correction of runtime deviation between torque LP1 and the angle of rotation for filter frequencies	Hz	4000; 2000; 1000; 500; 200; 100								
Measurement range	degrees	0 ... 360 (single-turn) to ± 1440 (multi-turn)								
Power										
Measurement frequency range	Hz	80 (-1 dB)								
Resolution	W	1								
Full scale value	W	$P_{max} = M_{nom} \cdot n_{nom} \cdot \frac{\pi}{30}$ <div style="display: flex; justify-content: space-between;"> $[M_{nom}]$ in N·m $[n_{nom}]$ in rpm </div>								
Temperature effect per 10 K in the nominal (rated) temperature range on the power signal, related to the full scale value	%	± 0.05 · n/n _{nom}								
Linearity deviation including hysteresis, related to the full scale value	%	± 0.02 · n/n _{nom}								
Sensitivity tolerance (deviation of the actual measurement signal span of the power signal related to the full scale value)	%	± 0.05								
Temperature signal of the rotor										
Accuracy	K	1								
Measurement frequency range	Hz	5 (-1 dB)								
Resolution	K	0.1								
Physical unit	-	°C								
Sample rate	Measured values/s	40								

Specifications (continued)

Fieldbuses		
CAN bus		
Protocol	-	CAN 2.0B, CAL/CANopen-compatible
Sample rate	Measured values/s	max. 4800 (PDO)
Hardware bus link		as per ISO 11898
Baud rate	kBit/s	1000 500 250 125 100
Maximum line length	m	25 100 250 500 600
Connection	-	5-pin, M12x1, A-coding per CANopen DR-303-1 V1.3, electrically isolated from power supply and measurement ground
PROFIBUS DP		
Protocol	-	PROFIBUS DP Slave, per DIN 19245-3
Baud rate	MBaud	max. 12
PROFIBUS Ident Number	-	096C (hex)
Input data, max.	bytes	152
Output data, max.	bytes	40
Diagnostic data	bytes	18 (2·4 byte module diagnosis)
Connection	-	5-pin, M12x1, B-coding, electrically isolated from power supply and measurement ground
Update rate ⁶⁾		
Configuration entries	≤ 2	4800
	≤ 4	2400
	≤ 8	1200
	≤ 12	600
	≤ 16	300
	> 16	150
	Measured values/s	
Limit value switches (on fieldbuses only)		
Number	-	4 for torque, 4 for rotational speed
Reference level	-	Torque low pass 1 or low pass 2 Rotational speed low pass 1 or low pass 2
Hysteresis	%	0 ... 100
Adjustment accuracy	digits	1
Response time (LP1 = 4000 Hz)	ms	typ. 3
TEDS (Transducer Electronic Data Sheet)		
Number	-	2
TEDS 1 (torque)	-	A choice of voltage sensor or frequency sensor
TEDS 2 (speed/angle of rotation)	-	Frequency/pulse sensor

⁶⁾ When CAN PDOs are activated simultaneously, the update rate on the PROFIBUS is reduced.

Specifications (continued)

Nominal (rated) torque M_{nom}	N·m	100	200	500						
	kN·m				1	2	3	5	10	
General information										
EMC										
Emission (EME) (per FCC 47, Part 15, Section C)										
Emission (per EN61326-1, Table 3)										
RFI voltage	-								Class A	
RFI power	-								Class A	
RFI field strength	-								Class A	
Immunity from interference (EN61326-1, Table A.1)										
Electromagnetic field (AM)	V/m								10	
Magnetic field	A/m								30	
Electrostatic discharge (ESD)										
Contact discharge	kV								4	
Air discharge	kV								8	
Fast transients (burst)	kV								1	
Impulse voltages (surge)	kV								1	
Conducted interference (AM)	V								3	
Degree of protection per EN 60 529									IP 54	
Reference temperature	°C								23	
Nominal (rated) temperature range	°C								+10...+70	
Operating temperature range	°C								-10...+70	
Storage temperature range	°C								-20...+75	
Mechanical shock and impact testing per EN 60068-2-27										
number	n								1000	
Duration	ms								3	
Acceleration (half sine)	m/s ²								650	
Vibration testing per EN 60068-2-6										
Frequency range	Hz								5 ... 2000	
Duration	h								2.5	
Acceleration (amplitude)	m/s ²								100	
Load limits ⁷⁾										
Limit torque, (static) ±	% of M_{nom}	200					160			
Breaking torque, (static) ±	% of M_{nom}	> 400					> 320			
Axial limit force (static) ±	kN	5	10	16	19	39	42	80	120	
Axial limit force (dynamic) amplitude	kN	2.5	5	8	8.5	19.5	21	40	60	
Lateral limit force (static) ±	kN	1	2	4	5	9	10	12	18	
Lateral limit force (dynamic) amplitude	kN	0.5	1	2	2.5	4.5	5	6	9	
Bending limit moment (static) ±	N·m	50	100	200	220	560	600	800	1200	
Bending limit moment (dynamic) amplitude	N·m	25	50	100	110	280	300	400	600	
Oscillation width per DIN 50100 (peak-to-peak) ⁹⁾	N·m	200	400	1000	2000	4000	4800	8000	16000	

⁷⁾ Each type of irregular stress (bending moment, lateral or axial force, exceeding nominal (rated) torque) can only be permitted up to its specified limit, provided none of the others can occur at the same time. If this condition is not met, the limit values must be reduced. If 30% of the bending limit moment and lateral limit force occur at the same time, only 40% of the axial limit force is permissible and the nominal (rated) torque must not be exceeded. The effects of 10% of the permissible bending moments, axial and lateral forces on the measurement result are $\leq \pm 0.02\%$ of the nominal (rated) torque.

⁸⁾ Limit loads / Option 4, Code F (high-speed version): Limit loads (bending moment, lateral, axial force and oscillation width (peak-to-peak)) are reduced by 20%.

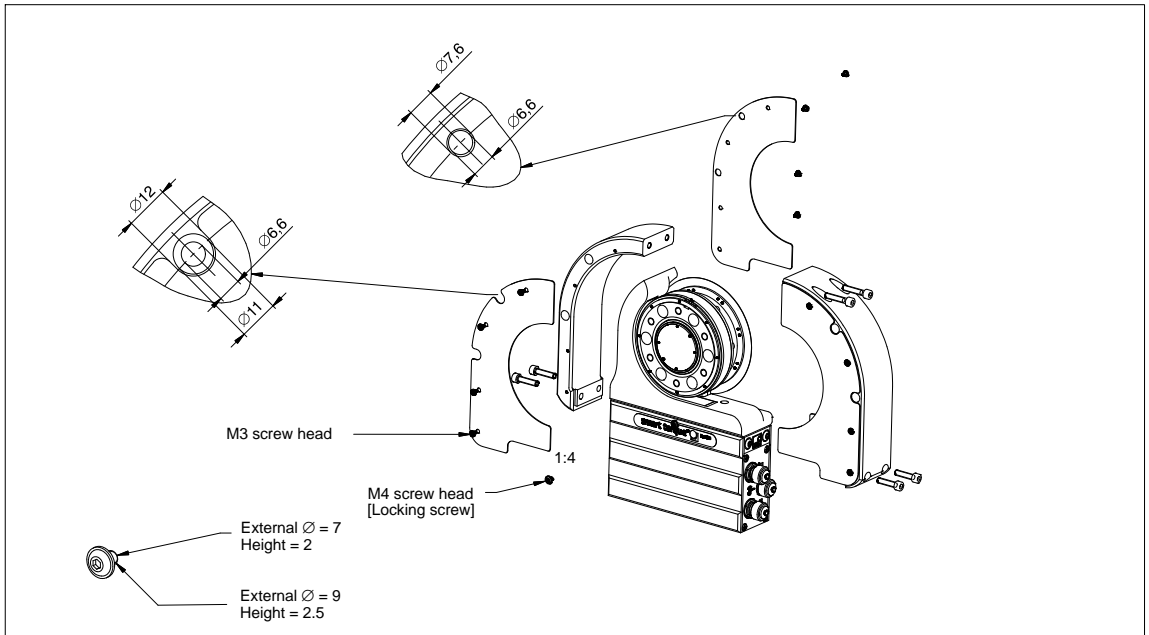
⁹⁾ The nominal (rated) torque must not be exceeded.

Specifications (continued)

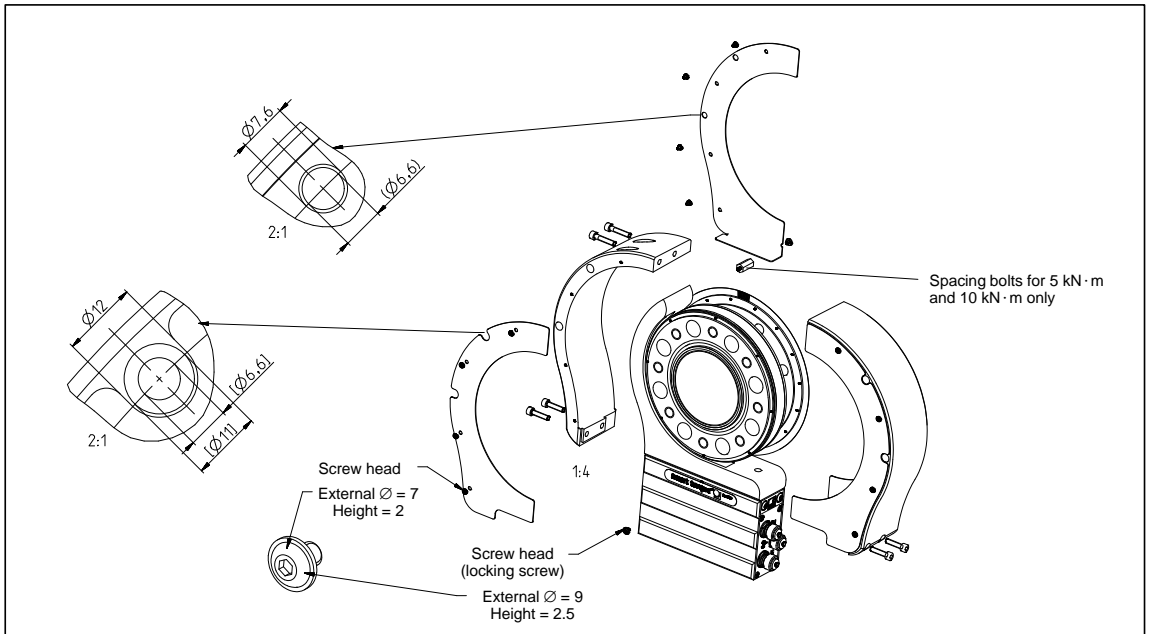
Nominal (rated) torque M_{nom}	N·m	100	200	500						
	kN·m				1	2	3	5	10	
Mechanical values										
Torsional stiffness c_T	kN·m/rad	230	270	540	900	2300	2600	4600	7900	
Torsion angle at M_{nom}	degrees	0.048	0.043	0.055	0.066	0.049	0.066	0.06	0.07	
Stiffness in the axial direction c_a	kN/mm	420	800	740	760	950	1000	950	1600	
Stiffness in the radial direction c_r	kN/mm	130	290	550	810	1300	1500	1650	2450	
Stiffness during the bending moment round a radial axis c_b	kN·m/deg.	3.8	7	11.5	12	21.7	22.4	43	74	
Maximum deflection at axial limit force	mm	< 0.02		< 0.03		< 0.05		< 0.1		
Additional max. radial deviation at lateral limit force	mm	< 0.02								
Additional deviation from plane parallelism at bending limit moment (at $\varnothing d_B$)	mm	< 0.03		< 0.05			< 0.07			
Balance quality level per DIN ISO 1940		G 2.5								
Max. limits for relative shaft vibration (peak-to-peak) ¹⁰⁾ Undulations in the connection flange area, based on ISO 7919-3	μm	Normal operation (continuous operation)					$s_{(p-p)} = \frac{9000}{\sqrt{n}}$			
		Start and stop operation/resonance ranges (temporary)					$s_{(p-p)} = \frac{13200}{\sqrt{n}}$			
(n in rpm)										
Mass moment of inertia of the rotor	I_y (around rotary axis)	kg·m ²	0.0023	0.0033	0.0059	0.0192	0.037	0.097		
	I_y with optical rotational speed measuring system	kg·m ²	0.0025	0.0035	0.0062	0.0196	0.038	0.0995		
Proportional mass moment of inertia for the transmitter side	without rotational speed measuring system	%	58	56	54	53				
	with optical rotational speed measuring system	%	56	54	53	52				
Max. permissible static eccentricity of the rotor (radially) to the center point of the stator	without rotational speed measuring system	mm	± 2							
	with rotational speed measuring system	mm	± 1							
Max. permissible axial displacement of the rotor to the stator	mm	± 2								
Weight, approx.	Rotor	kg	1.1	1.8	2.4	4.9	8.3	14.6		
	Stator	kg	2.3			2.4	2.5	2.6		

¹⁰⁾ The influence of radial deviations, impact, defects of form, notches, marks, local residual magnetism, structural inhomogeneity or material anomalies on the vibrational measurements needs to be taken into account and isolated from the actual undulation.

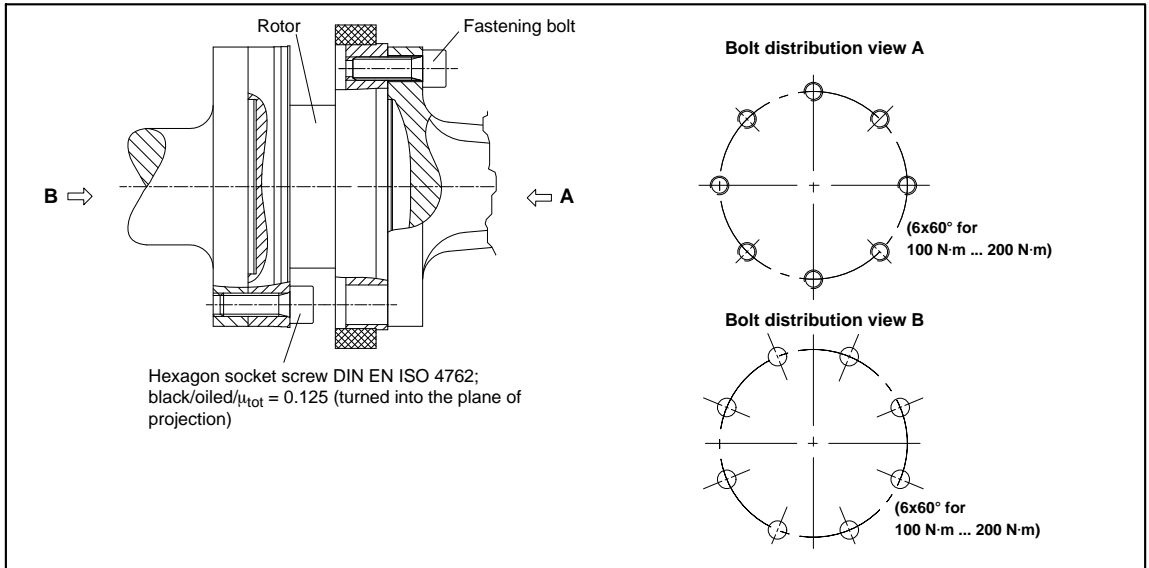
Plates for protection against contact 100 N·m ... 200 N·m (in mm)



Plates for protection against contact 500 N·m ... 10 kN·m (in mm)

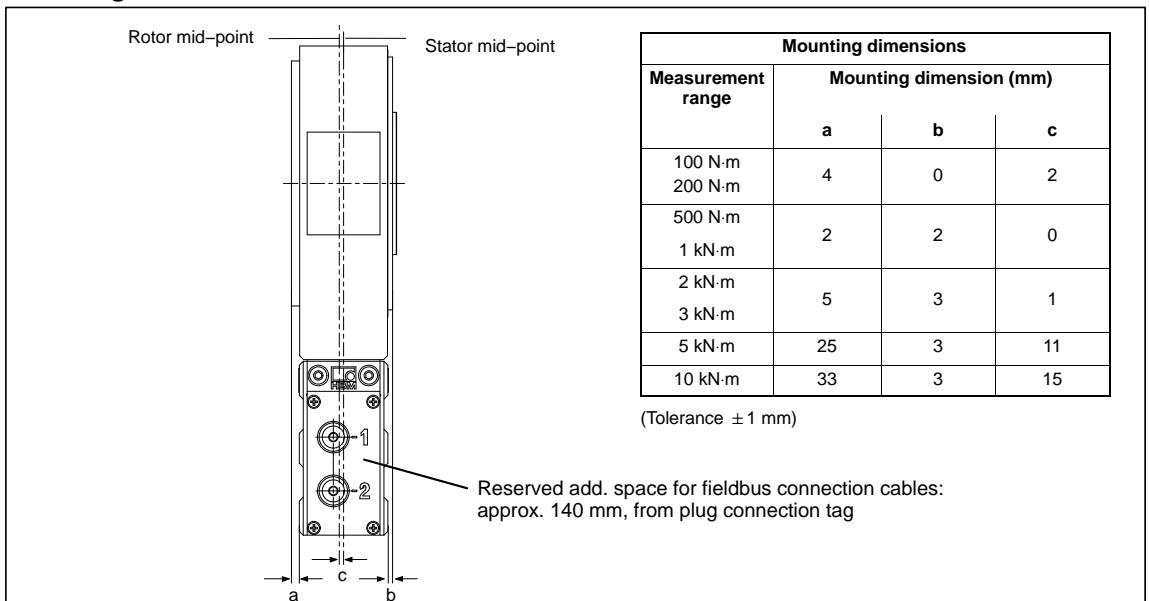


Bolted rotor connection

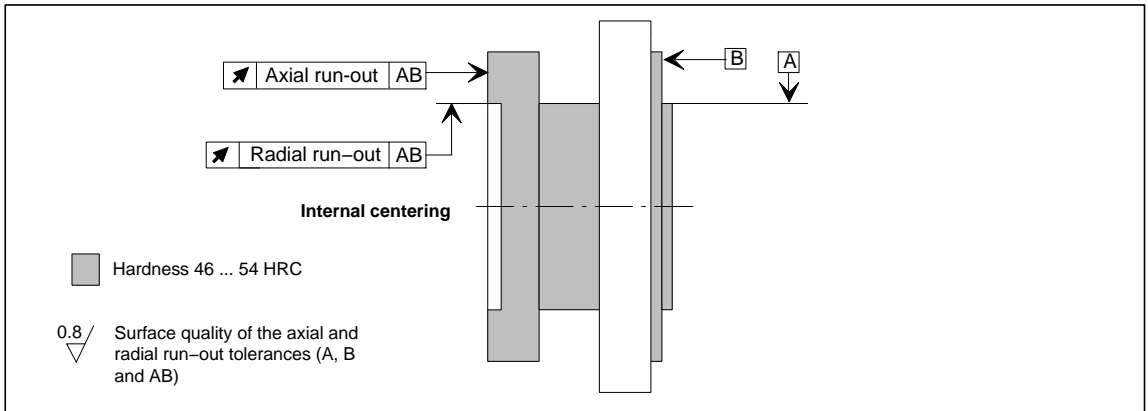


Nominal (rated) torque (N·m)	Fastening bolts	Fastening bolt property class	Prescribed tightening torque (N·m)
100	M8	10.9	34
200	M8		
500	M10		67
1k			
2k	M12	12.9	115
3k			135
5k		M14	220
10k	M16	340	

Mounting dimensions



Radial and axial run-out tolerances



Measurement range (N·m)	Axial run-out tolerance (mm)	Radial run-out tolerance (mm)
100	0.01	0.01
200	0.01	0.01
500	0.01	0.01
1 k	0.01	0.01
2 k	0.02	0.02
3 k	0.02	0.02
5 k	0.025	0.025
10 k	0.025	0.025

Ordering number

	Code	Measurement range
1	S100Q	100 Nm
	S200Q	200 Nm
	S500Q	500 Nm
	S001R	1 kNm
	S002R	2 kNm
	S003R	3 kNm
	S005R	5 kNm
	S010R	10 kNm

	Code	Components
2	MF	Complete
	RO	RO
	ST	ST

	Code	Accuracy
3	S	Lin. $\leq \pm 0.015\%$; TC0 $\leq \pm 0.010\%$ /10 K
	U	Lin. $\leq \pm 0.007\%$; TC0 $\leq \pm 0.005\%$ /10 K

	Code	Nominal (rated) rotational speed
4	L	10,000-15,000 rpm, rel. to meas. range
	H	12,000-18,000 rpm, rel. to meas. range
	F	18,000-22,000 rpm, rel. to meas. range (exclusively available for measuring ranges 100Nm to 3kNm)

	Code	Electrical configuration
5	DF1	Output 60 kHz ± 30 kHz
	DU2	Output 60 kHz ± 30 kHz and ± 10 V
	SF1	Output 10 kHz ± 5 kHz
	SU2	Output 10 kHz ± 5 kHz and ± 10 V

	Code	Bus connection
6	C	CANopen
	P	CANopen and Profibus DPV1

	Code	Rotational speed measuring system
7	N	No rotational speed measuring system
	1	Optical
	A	Optical and reference pulse

	Code	Protection against contact
8	N	No
	Y	Yes

	Code	Customized modification
9	U	None

K-T12HP - **S** - - - - - - - - - **U**
 1 **2** **3** **4** **5** **6** **7** **8** **9**

Accessories, to be ordered separately

Article	Ordering number
Connection cable, set	
Torque	
Torque connection cable, Binder 423 7-pin - D-Sub 15-pin, 6 m	1-KAB149-6
Torque connection cable, Binder 423 - free ends, 6 m	1-KAB153-6
Rotational speed	
Rotational speed connection cable, Binder 423 8-pin - D-Sub 15-pin, 6 m	1-KAB150-6
Rotational speed connection cable, Binder 423 8-pin, free ends, 6 m	1-KAB154-6
Rotational speed connection cable, reference pulse, Binder 423 8-pin - D-Sub 15-pin, 6 m	1-KAB163-6
Rotational speed connection cable, reference pulse, Binder 423 8-pin - free ends, 6 m	1-KAB164-6
CAN bus	
CAN bus M12 connection cable, A-coded - D-Sub 9-pin, switchable termination resistor, 6 m	1-KAB161-6
Plugs/sockets	
Torque	
423G-7S, 7-pin cable socket, straight cable entry, for torque output (plug 1, plug 3)	3-3101.0247
423W-7S, 7-pin cable socket, 90° cable entry, for torque output (plug 1, plug 3)	3-3312.0281
Rotational speed	
423G-8S, 8-pin cable socket, straight cable entry, for rotational speed output (plug 2)	3-3312.0120
423W-8S, 8-pin cable socket, 90° cable entry, for rotational speed output (plug 2)	3-3312.0282
CAN bus	
TERMINATOR M12/termination resistor, M12, A-coded, 5-pin, plug	1-CANHEAD-TERM
Termination resistor, CAN bus M12, A-coded, 5-pin, socket	1-CAN-AB-M12
T-SPLITTER M12/T-piece M12, A-coded, 5-pin	1-CANHEAD-M12-T
Cable plug/socket/CAN bus M12, cable socket 5-pin M12, A-coded, cable plug 5-pin M12, A-coded	1-CANHEAD-M12
PROFIBUS	
Connection cable, Y-splitter, M12 socket, B-coded; M12 plug, B-coded; M12 socket, B-coded, 2 m	1-KAB167-2
Cable plug/socket/PROFIBUS M12, cable socket 5-pin M12, B-coded, cable plug 5-pin M12, B-coded	1-PROFI-M12
Termination resistor PROFIBUS M12, B-coded, 5-pin	1-PROFI-AB-M12
T-piece PROFIBUS M12, B-coded, 5-pin	1-PROFI-VT-M12
Connection cable, by the meter	
Kab8/00-2/2/2	4-3301.0071
Kab8/00-2/2/2/1/1	4-3301.0183
DeviceNet cable	4-3301.0180
Other	
Setup toolkit for T12 (System-CD T12, PCAN-USB adapter, CAN bus connection cable, 6 m)	1-T12-SETUP-USB

Subject to modifications.
All product descriptions are for general information only. They are not to be understood as a guarantee of quality or durability.

Hottinger Baldwin Messtechnik GmbH
Im Tiefen See 45 · 64293 Darmstadt · Germany
Tel. +49 6151 803-0 · Fax +49 6151 803-9100
E-mail: info@hbm.com · www.hbm.com

measure and predict with confidence



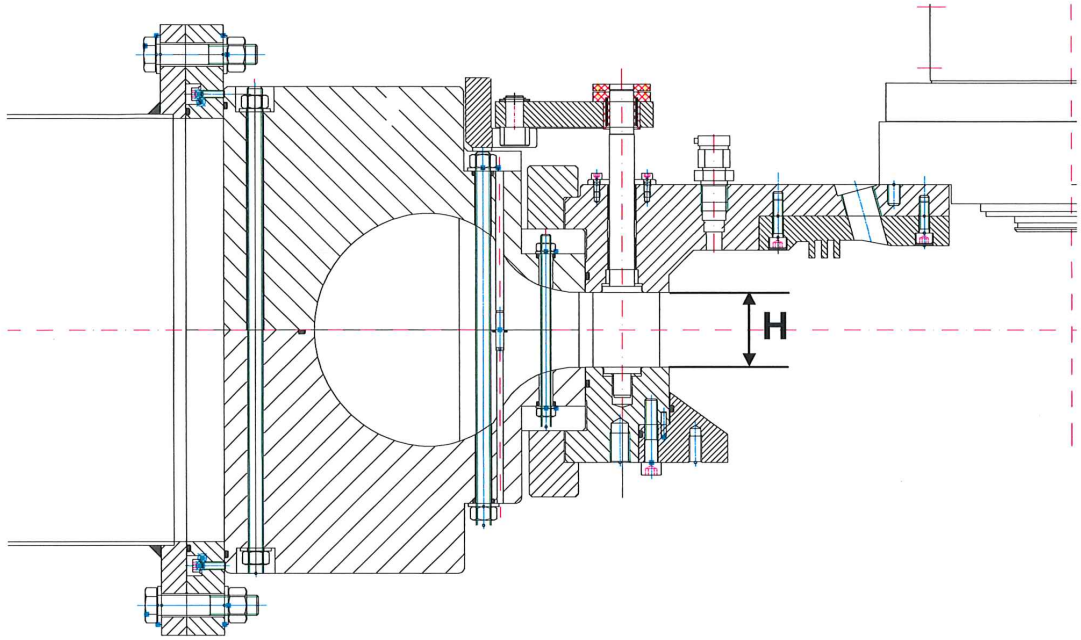
Appendices

Appendix B

Appendix B includes the measured height and distances after installation of the new guide vanes.



Project id: FRANCIS MODEL TURBINE			
Document: ASSEMBLY DIMENSIONS			Page 11 of 15
Model id: Tokke Power Plant	Assembly id:	Test No-test point no:	Reference drawing: VKL-2006-1000



	Measured height between head and bottom cover			
	East	West	North	South
	Between vane 14 and 15	Between vane 1 and 2	Between vane 7 and 8	Between vane 21 and 22
H [mm]	59,56	59,49	59,63	59,52

Comments

Thin metal sheets were placed between the covers and the spiral casing in order to have the correct height between the upper and lower cover.

On the upper cover the thickness of the metal sheet is 0,1 mm.

On the lower cover the thickness of the metal sheet is 0,15 and 0,2 mm.

The metal sheet with thickness 0,2 mm was placed between guide vane number 24 and 1.

The torque on the upper cover bolts is 50 Nm

The torque on the lower cover bolts is 50 Nm

Date/Sign 2/2-22

Approved



Project id: **FRANCIS MODEL TURBINE**

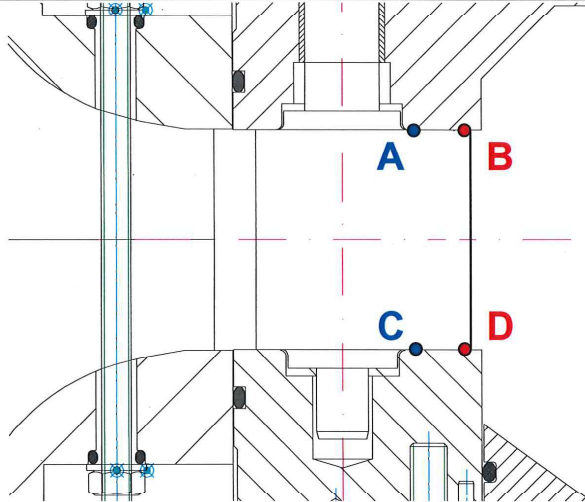
Document: **CLEARANCE DIMENSIONS BETWEEN GUIDE VANE AND COVER**

Page 15 of 15

Model id:
Tokke Power Plant

Test No-test point no:

Reference drawing:
VKL-2006-1000



Guide Vane #	A [mm]	B [mm]	C [mm]	D [mm]	Guide Vane #	A [mm]	B [mm]	C [mm]	D [mm]
1-2			0,1	0,1	15			0,15	
2					16			0,17	
3	Streckklapp		0,13		17			0,18	
4			0,13		18			0,15	
5			0,2		19			0,15	
6					20			0,13	
7					21			0,15	
8					22			0,08	
9-10			0,18		23			0,12	
10	59,62		0,15		24			0,12	
11			0,12		25			0,10	
12			0,08		26			0,08	
13	Streckklapp				27			0,08	
14			0,13		28			0,08	

Kann die
eher sein

Comments

The torque on the upper cover bolts is 50 Nm
The torque on the lower cover bolts is 50 Nm

Date/Sign

Approved



Project id: **FRANCIS MODEL TURBINE**

Document: **ASSEMBLY DIMENSIONS**

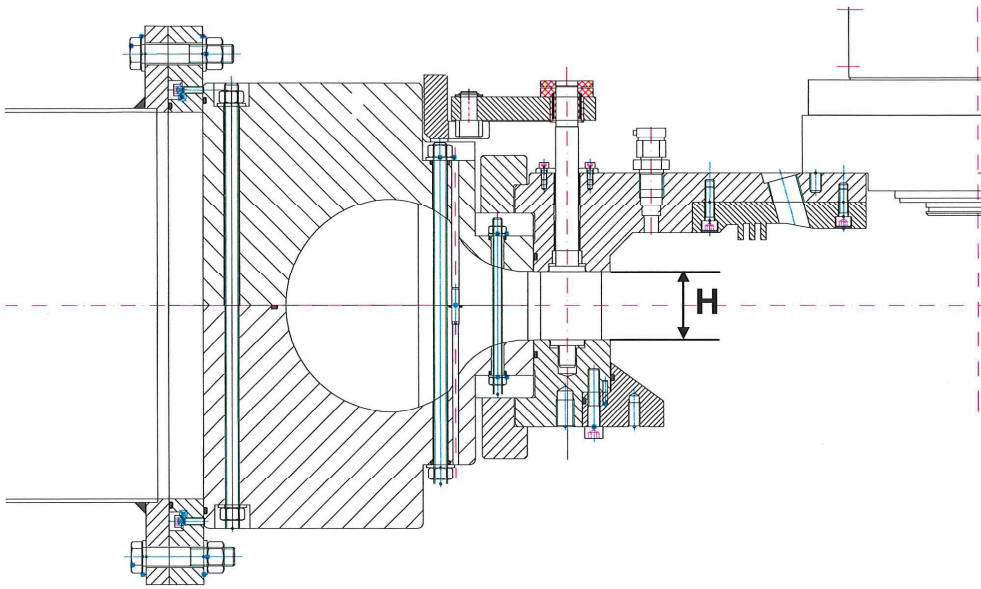
Page 11 of
15

Model id:
Tokke Power Plant

Assembly id:

Test No-test point no:

Reference drawing:
VKL-2006-1000



	Measured height between head and bottom cover			
	East	West	North	South
	Between vane 14 and 15	Between vane 1 and 2	Between vane 7 and 8	Between vane 21 and 22
H [mm]	59,56	59,49	59,63	59,52

Comments

Thin metal sheets were placed between the covers and the spiral casing in order to have the correct height between the upper and lower cover.

On the upper cover the thickness of the metal sheet is 0,1 mm.

On the lower cover the thickness of the metal sheet is 0,15 and 0,2 mm.

The metal sheet with thickness 0,2 mm was placed between guide vane number 24 and 1.

The torque on the upper cover bolts is 50 Nm

The torque on the lower cover bolts is 50 Nm

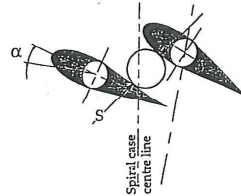
Date/Sign 2/2-22

Approved



Project id: FRANCIS MODEL TURBINE			
Document: GUIDE VANE OPENING DIMENSIONS			Page 5 of 15
Model id: Tokke Power Plant	Guide vane opening id:	Test No-test point no:	Reference drawing: VKL-2006-1021

Guide vane No	Guide vane opening, S [mm]				
	$\alpha = 0^\circ$	$\alpha = 10^\circ$	$\alpha = 20^\circ$	$\alpha = 0^\circ$	$\alpha =$
Theoretical	0	13,1	25,5		
1-2	0,10	13,05		0,20	
2-3	0	13,05		0,15	
3-4	0,05	13,05		0,10	
4-5	0	12,80		0	
5-6	0,10	12,90		0,10	
6-7	0	13,00		0,08	
7-8	0	13,05		0,15	
8-9	0,05	13,05		0,08	
9-10	0	13,05		0,08	
10-11	0,15	12,95		0,08	
11-12	0	12,80		0	
12-13	0,10	12,87		0	
13-14	0,05	12,90		0,05	
14-15	0,10	12,80		0	
15-16	0,10	12,85		0	
16-17	0,15	12,87		0,05	
17-18	0,10	12,92		0,15	
18-19	0,10	12,95		0,15	
19-20	0,10	12,97		0,10	
20-21	0	12,90		0,10	
21-22	0,10	13,00		0,15	
22-23	0,10	12,97		0,15	
23-24	0,08	13,02		0,15	
24-25	0,10	13,05		0,15	
25-26	0,15	13,00		0,20	
26-27	0,05	13,05		0,20	
27-28	0,10	13,05		0,20	
28-1	0	12,95		0,15	
Max.		13,05		0,20	
Min.		12,80		0,00	
Max.-Min		0,25			



α [°] expresses the guide vane opening from closed position. And S [mm] represents the guide vane opening in the most narrow area between the guide vanes.

Comments

Paul H. West

Date/Sign: *31/1 - 22 Pjette Opland* Approved

Appendices

Appendix C

C.1 Calibration report from Langleite[1]

Chapter IV

Calibration

■ Calibration has been a time-consuming part of the thesis, and detecting all the uncertainties is an essential aspect of having the model test accepted. This chapter goes through the calibration process for each of the sensors that require calibration. All the calibrated values have been controlled against the DKD-R 6-1 guideline regarding uncertainty to check that the values lie within limits given from the manufacturer.

4.1 Calibration of instrument

All the equipment regarding the calibration can be found in Appendix B. The procedures made during this thesis can be found in section D.2 and reflect what is provided in this chapter.

4.1.1 Weighing tank

The weighing tank system, is a system meant for calibration of flow meters and is the one in use at the Waterpower laboratory. The tank itself needs a substitution calibration, as the tank is resting on three load cells and indicates a secondary measurement method. The three load cells are connected to an amplifier, which further is connected to a computer. The water from and to the tank is guided through a pneumatically driven guiding system that can be controlled by the connected computer.

The calibration is conducted by using a number of weights calibrated by Justervesenet. By adding and remove weight several times with the use of the overhead crane and at the same time filling the tank with water, one can manage to find the slope

and calibration equation. The slope has to be found in the range of the tank capacity, which is approximately 86 metric tons, and according to the procedure, it is necessary to find a decent time of filling that gives around 5 tons per filling.

The load cell does not have a linear behaviour, and one therefore operate with a fifth order polynom function that is assumed to be able to record the behavior of the cells. The function is given as,

$$W = f(c) = a_0 \frac{c^5}{5} + a_1 \frac{c^4}{4} + a_2 \frac{c^3}{3} + a_3 + \frac{c^2}{2} + a_4 c \quad (4.1)$$

where $W = f(c)$ is the connection between amplifier reading and the applied weights on the load cells. The coefficients for the calibration is then found by integrating the function.

Calibration documents for the weights and the spreader can be found in appendix B.3 and B.3.

4.1.2 Discharge

A crucial point of calibration for the model test is the one regarding the flow meter. The flow meter is calibrated with the use of the weighing thank, as already mentioned. The pipe system for this calibration differs from the weighing thank, as one wants the flow through the flow meter that is located between the inlet of the turbine and the pressure tank. The flow meter is connected to an amplifier, and gives the output signal in voltage, which varies with the discharge. The calibration equation is therefore given as,

$$Q = a \cdot (mv) + b \quad (4.2)$$

where a and b are the coefficients to be found, and mv is the measured voltage. This applies to all calibration equations. To be able to solve this equation, the correct mass in the weighing tank has to be found. Therefore, the density of the water has to be calculated, and air density must be corrected. From this, the mean discharge can be calculated.

The formula for water density is given by the IEC60193,

$$\rho_w = \frac{10}{((1 - a \cdot p_{atm}) + b \cdot (\theta - 4.0 + c \cdot p_{atm})^2 - d \cdot (\theta - 4.0 - e \cdot p_{atm})^3)} \quad (4.3)$$

, where

$$\begin{aligned}
 a &= 4.6699 \cdot 10^{-10} \\
 b &= 8 \cdot 10^{-6} \\
 c &= 2.13189133 \cdot 10^{-7} \\
 d &= 6 \cdot 10^{-8} \\
 e &= 2.1318913 \cdot 10^{-7} \\
 \theta &= \text{measured temperature} \\
 p_{atm} &= \text{atmospheric pressure}
 \end{aligned}$$

The density of air is corrected by formula,

$$\rho_a = \frac{p_{abs} \cdot 3.4837 \cdot 10^3}{273.15 + \theta_a} \quad (4.4)$$

When knowing the density of the water and air, the corrected weights (coefficients) and filling time, the mean discharge can be found,

$$W = \frac{W_2 - W_1}{\rho_w t \left(1 - \frac{\rho_a}{\rho_w}\right)} \quad (4.5)$$

, and the coefficients a and b can then be determined using linear interpolation.

The calibration curve for the volume flow meter is shown in Figure 4.1.

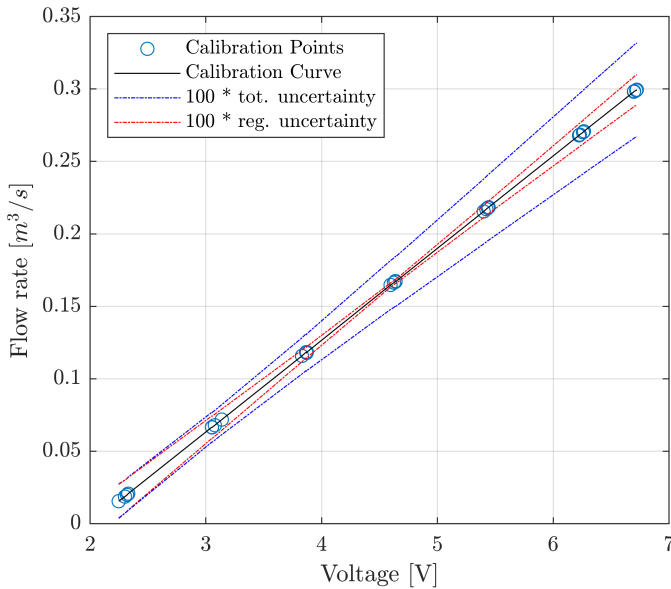


Figure 4.1: Total and regression uncertainty, multiplied by 100, in the flow meter calibration. This also includes the calibration of the weighing tank.

4.1.3 Water temperature

The water temperature probe consists of a PT100 element for measuring the temperature. The element has a linear behavior and gives a possibility to calibrate the sensor with two reference temperatures, ice water, and boiling water, where one assumes $0^{\circ}C$ and $100^{\circ}C$. Since there is an advantage to perform the calibration for the range where one assumes the temperature will lie in between, it is not necessary to calibrate from 0 - $100^{\circ}C$. An option is to use a reference to calibrate the sensor, as a SeaBird SBE 38. The SeaBird has an accuracy and stability of $0,001^{\circ}C$ and is a good option as the temperature calibration for a PT100 element normally gives a small percent uncertainty.

With this method, the calibration is performed from 0 - $32^{\circ}C$ or up to the highest temperature of the tap water. To make sure both probes measure the same temperature, something that can make the water rotate must be placed in the bucket together with the probes.

The logging program used for this check/calibration is one that combines the input

from both probes and saves a file with the output voltage, standard deviation, and the number of samples for both probes. This makes it possible to find the coefficients and calculate the uncertainty. The coefficients can be found using the least square method, and the equation is given as

$$\theta = a \cdot (mv) + b \quad (4.6)$$

The calibration curve for the PT100 element is shown in Figure 4.2, and the calibration documentation for the SeaBird sensor used can be found in appendix B.3.

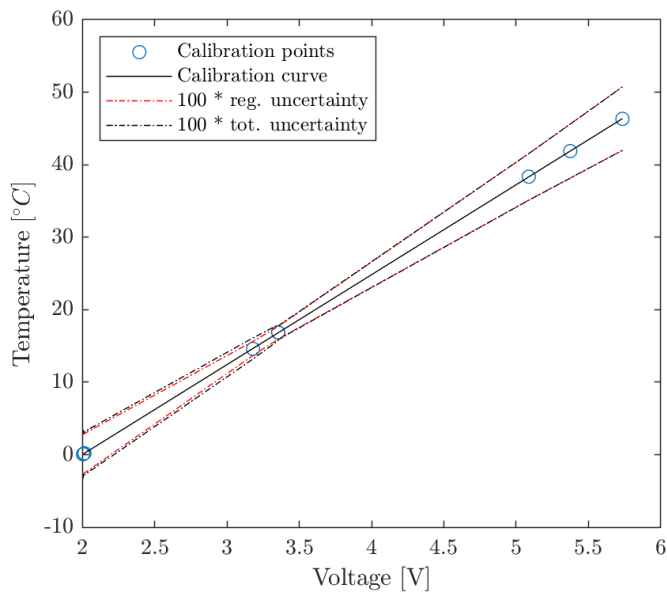


Figure 4.2: Total and regression uncertainty, multiplied by 100, in the water temperature calibration.

4.1.4 Dissolved oxygen

The probe that measures the dissolved oxygen typically needs no calibration. From old procedures, it says that it requires calibration, but from 2017 the sensor was replaced with a newer and more accurate one. This sensor only requires calibration or a check if the output data vary significantly from the normal.

The sensor must be taken out from the pipe during calibration, and the membrane must be cleaned and placed 2 cm above the water in a small bucket. An apparatus is connected to the probe and has a built-in calibration- and check program, and it is just to follow the steps given at the display to perform either calibration or a check of the sensor. After finishing the procedure, the display will show either a positive or negative result. No coefficients need to be found, as the DAQ-unit connected to the sensor will give exact numbers.

4.1.5 Pressure sensors

The pressure sensors are calibrated with the use of a dead weight manometer, as it is possible to calibrate several sensors with that instrument. The manometer used for this thesis has a range from 0-350 bar and is covering the range for all the sensors used for the model test. The working function is to simulate a known pressure input by placing known weights on a piston. When knowing the input weight and output voltage, a calibration curve can be determined using linear interpolation. It is crucial and important to make sure that both pipes to the sensors from the manometer are primed. The manometer itself also need to be primed, a separate procedure of how this is done is found in the data sheet for the manometer.

Seven points, from minimum to maximum pressure, and in total two series up and two series down must be performed for the calibration curve. The weights and the piston must be spinning with no friction during the logging.

The calibration equation is given as,

$$p = a \cdot (mv) + b \quad (4.7)$$

, and is yielding for all pressure sensors that are calibrated with a dead weight manometer. The only thing that may differ from one sensor to another is the coupling from the sensor to the DAQ-unit, and the logging program for this must be chosen based on this. If the unit requires a bridge-coupling, there is no need to change the default values set in the bridge logging program.

The calibration curve for the inlet pressure sensor is shown in Figure 4.3. The calibration curve for the differential pressure transducer is shown in Figure 4.4. Calibration documentation for the dead weight manometer can be found in appendix B.3.

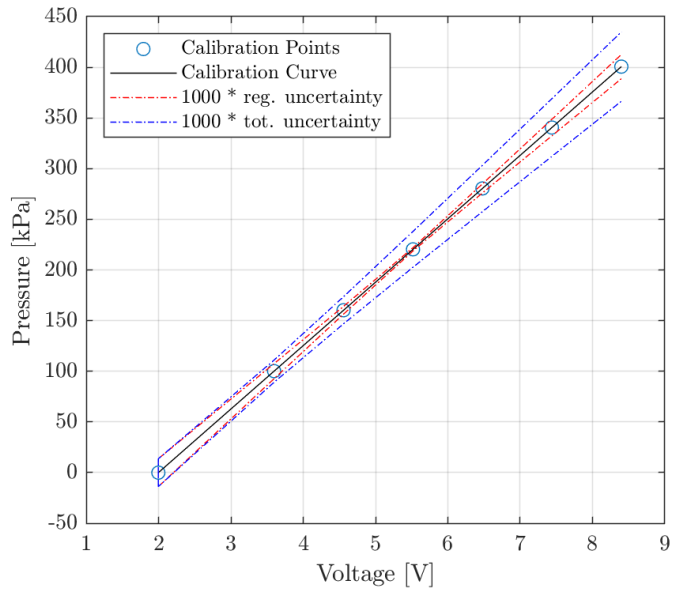


Figure 4.3: Total and regression uncertainty, multiplied by 1000, in the inlet pressure sensor calibration.

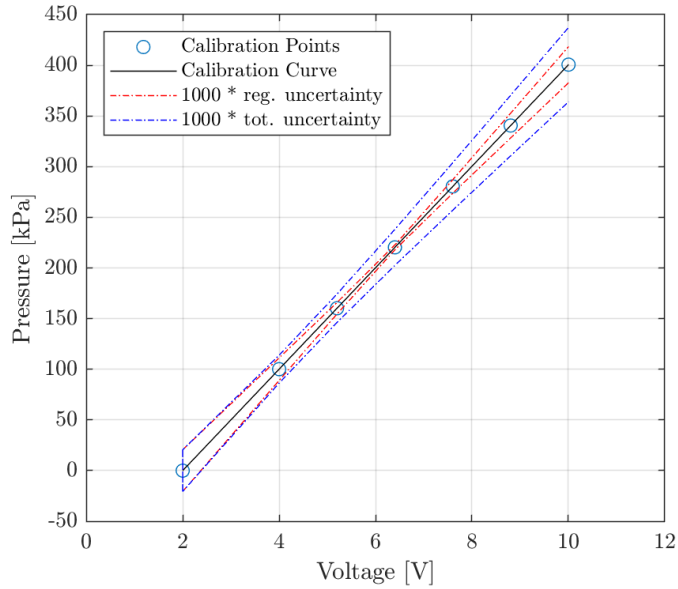


Figure 4.4: Total and regression uncertainty, multiplied by 1000, in the differential pressure sensor calibration.

4.1.6 Generator torque and arm length

The generator arm length is calibrated with the combination of measuring several lengths. With the use of a micrometer, the diameter of the generator shaft can be measured. The length of the shaft is measured with a calibrated rod. A slider can be used to measure the rest of the length of the metal band and the thickness of that band. The total length will be given as,

$$a_{gen} = \frac{a_{d,shaft}}{2} + a_{rod} + a_{slider} + \frac{a_{slider,band}}{2} \quad (4.8)$$

In this thesis, the arm length value gained from Pål-Tore's master's thesis is used. In Figure 4.5, the different lengths for the generator arm are illustrated.

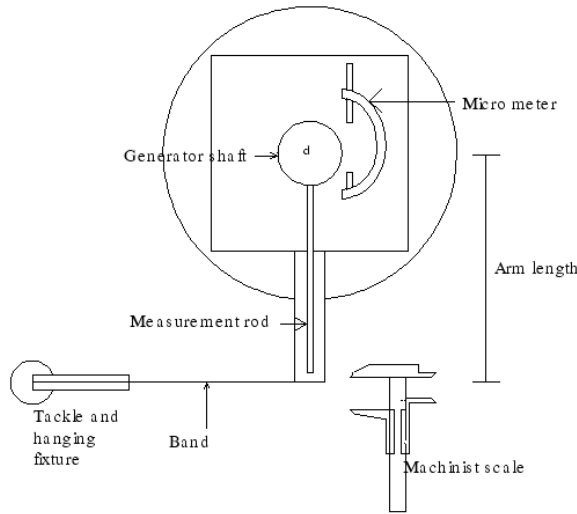


Figure 4.5: Measurement of generator arm length [11].

The load cell for the generator torque is calibrated with the use of calibrated weights at 5 kg. Since the generator is resting on a bed of pressurized oil, the oil temperature difference in the bearing must be canceled out before performing a calibration. This is done by turning the hydraulic pump on at least one hour in advance. To be able to calibrate for loads above 1000 Nm, the oil pressure for the rollers must be increased to 40 bar.

With the use of a laboratory-made hanging fixture that fits the calibrated weights, weights can be added and removed for creating the calibration curve. Seven points from minimum to maximum load, and two series up and two series down is preferable to use in the calibration. Since the load cell is very sensitive, the sensor needs help to understand if the load is increasing or decreasing, and the total weight applied to the sensor is either lifted and then set or the other way around to imply what the sensor will be exposed to.

The load cell will give an output signal in voltage that will vary linearly with applied weights, and the calibration equation is found by linear interpolation,

$$\tau_G = a \cdot (mv) + b \quad (4.9)$$

The calibration curve for the generator torque load cell is illustrated in Figure 4.6.

Calibration documentation for the weights can be found in appendix B.3. Sheet for substituted calibration of the weights can be found in appendix B.4

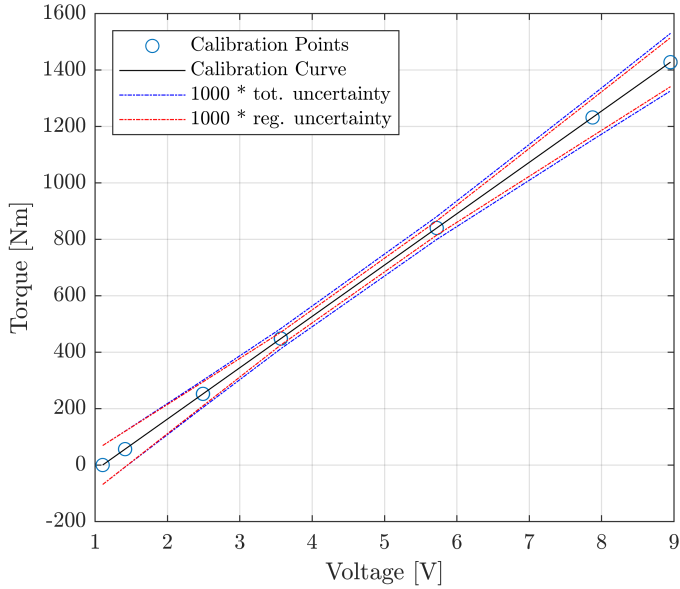


Figure 4.6: Total and regression uncertainty, multiplied by 1000, in the generator torque load cell calibration.

4.1.7 Friction torque

The friction torque load cell is calibrated with the similar system as the generator torque, but with 2 kg weights and a separate hanging fixture for those weights. The arm length, illustrated in Figure 4.7, is calibrated with the use of a slider, and the total length is given as,

$$a_{fric} = a_{tot,l} - \frac{a_{d,shaft}}{2} - \frac{a_{b,block}}{2} \quad (4.10)$$

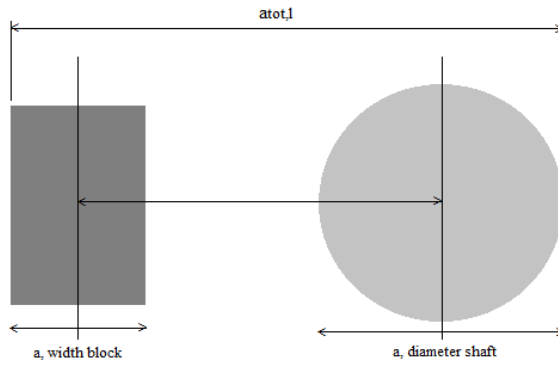


Figure 4.7: Measurement of friction arm length.

The load cell will give an output signal in voltage that will vary linearly with applied weights, and the calibration equation is found by linear interpolation.

$$\tau_F = a \cdot (mv) + b \quad (4.11)$$

The calibration curve for the friction torque load cell is illustrated in Figure 4.8. The same documentation for applied weights and substituted calibration applies for this sensor as for the generator load cell.

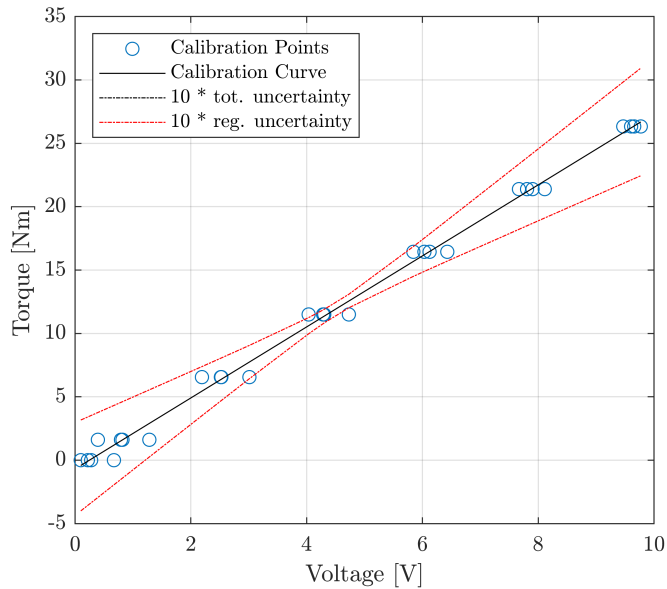


Figure 4.8: Total and regression uncertainty, multiplied by 10, in the friction torque load cell calibration.

Guide vane angle

The sensor measuring the angle of the guide vane is absolute, but in order to achieve the angle, the sensor must be calibrated against the one connected to the Francis logger. This means there exist two sensors that measure the guide vane angle, but the one connected to the Francis logger is difficult to connect to another logging computer. The calibration is easy to perform by only use the given angle from the Francis logger and the output voltage signal from the sensor. Two times series from minimum to maximum is preferred, with seven points each and a total of 28 calibration points.

The calibration equation will look like this,

$$\alpha = a \cdot (mv) + b \quad (4.12)$$

The calibration curve for the guide vane angle is illustrated in Figure 4.9.

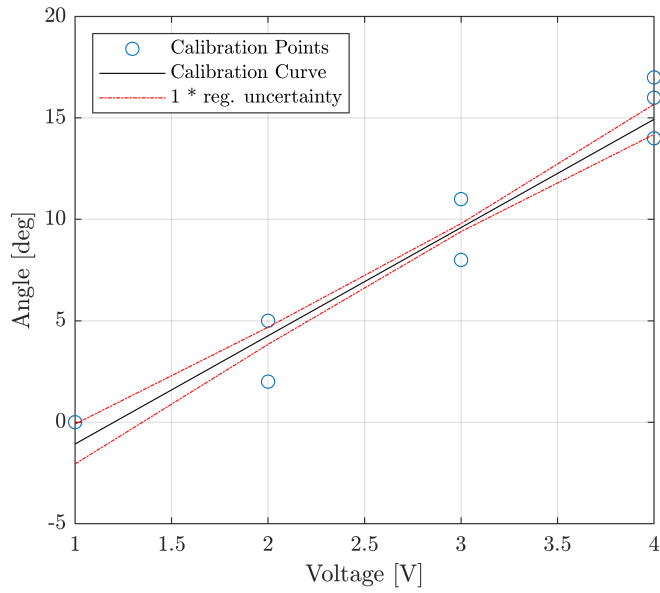


Figure 4.9: Total and regression uncertainty, multiplied by one, in the guide vane angle sensor calibration.

Appendix - A

Uncertainty analysis

A.1 Regression error

Several of the sensors used in this thesis have linear behavior, making them applicable for detecting errors by linear regression analysis methods. In the calibration curve, one assumes that all measurement points should be on the curve, but in reality, this is not true. If all points lie on the curve, the residual sum of squares or the sum of squares around the regression would be zero. An analysis of variance will detect the small variation in each of the points in axial directions and find the best relationship between the response Y and variable x. [33] The following equations are used in this thesis to find these small variations:

$$S_{XX} = \sum_{i=1}^N (x_i - \bar{X})^2 \quad (\text{A.1})$$

$$S_{YY} = \sum_{i=1}^N (y_i - \bar{Y})^2 \quad (\text{A.2})$$

$$S_{XY} = \sum_{i=1}^N (x_i - \bar{X})(y_i - \bar{Y}) \quad (\text{A.3})$$

S_{XX} and S_{YY} gives the variation along the x-axis and y-axis for the regression curve, and S_{XY} gives the combination of the variation in both x- and y-direction. S_{YY} and S_{XY} can be used in formula *SSE*, *Sum of squares error*, that gives the error/difference in the actual value and the predicted value. [33]

$$SSE = S_{YY} - bS_{XY} \quad (\text{A.4})$$

b is the slope of the line. The mean square of the SSE can be calculated with two degrees of freedom,

$$MSE = s^2 = \frac{SSE}{n-2} \quad (\text{A.5})$$

where n is the number of measurements. s^2 describes the random error/variation around the regression line. Two degrees of freedom are used based on numbers of independent pieces, as in a fitted line, two parameters are required. [33]

The interference between the slope and intercept are also of interest in linear regression. By assuming that the response is normally distributed with a 95 % confidence interval, the statistical bounds around the regression line can be found by,

$$\hat{Y}_0 - t_{\alpha/2} \cdot s \sqrt{\frac{1}{n} + \frac{(x_0 - \bar{X})^2}{S_{XX}}} \leq \mu_{Y|x_0} \leq \hat{Y}_0 + t_{\alpha/2} \cdot s \sqrt{\frac{1}{n} + \frac{(x_0 - \bar{X})^2}{S_{XX}}} \quad (\text{A.6})$$

where $t_{\alpha/2}$ is the value of the t-distribution with $n-2$ degrees of freedom. The formula can be simplified to,

$$f_{Y|x_0} = \pm t_{\alpha/2} \cdot s \sqrt{\frac{1}{n} + \frac{(x_0 - \bar{X})^2}{S_{XX}}} \quad (\text{A.7})$$

A.2 Propagation of uncertainties

If there exist a function Z that is a function of several variables x ,

$$Z = z(x_1, x_2, \dots, x_n) \quad (\text{A.8})$$

given that the variables x has their own uncertainty, this would lead to a change in Z ,

$$Z = Z \pm \Delta Z = z(x_1 \pm \Delta_{x_1}, x_2 \pm \Delta_{x_2}, \dots, x_n \pm \Delta_{x_n}) \quad (\text{A.9})$$

One therefore operates with the fact that the uncertainties in the variables propagate to the uncertainty of Z . By introducing the Taylor-theorem and use this to make a Taylor-series for the Z function to the right and neglect the ones with terms of higher order than one,

$$Z = Z \pm \Delta Z = z(x_1, \dots, x_n) + \frac{\delta z}{\delta x_1} \Delta x_1 + \dots + \frac{\delta z}{\delta x_n} \Delta x_n \quad (\text{A.10})$$

The maximum absolute error in Z can therefore be given as,

$$|\Delta Z| = \left| \frac{\delta z}{\delta x_1} \Delta x_1 \right| + \dots + \left| \frac{\delta z}{\delta x_n} \Delta x_n \right| \quad (\text{A.11})$$

If the change in each variables, Δx_i , can be treated as statistical bounds, the total change in Z due to individual changes in the variables can be expressed with the RSS-method to be,

$$\Delta Z = \pm \sqrt{\left(\frac{\delta z}{\delta x_1} \Delta x_1 \right)^2 + \dots + \left(\frac{\delta z}{\delta x_n} \Delta x_n \right)^2} \quad (\text{A.12})$$

[32], [34]

A.3 Uncertainties in the calibration

A.3.1 Flow meter

The systematic uncertainties for calibration of flow meter are:

- $f_{Q_{\Delta W}}$, uncertainty in the weight cells and their calibration. Found by Pål-Tore Storli, $\pm 0.05043\%$ [32].
- $f_{Q_{\Delta t}}$, uncertainty of time measurement, can be ignored due to its very small impact.
- $f_{Q_{divider}}$, uncertainty of the divider. $\pm 0.072611\%$ with a flow of 50 l/s, found by Pål-Tore Storli [32].
- $f_{Q_{\rho}}$, uncertainty in the calculation of water density. Can assume this to be 0.01% since the temperature is measured with a PT100 element that has low uncertainty [3].

With the use of the RSS-method, the systematic uncertainty for the calibration can be calculated,

$$f_{Q_a} = \sqrt{(f_{Q_{\Delta W}})^2 + (f_{Q_{\Delta t}})^2 + (f_{Q_{divider}})^2 + (f_{Q_{\rho}})^2} = \pm 0.08897\% \quad (\text{A.13})$$

The random uncertainties for the flow meter are given as,

- $(f_{Q_{\Delta W}})_r$, random uncertainty of the weight cells and their calibration. Found by Pål-Tore Storli, $\pm 0.00072\%$ [32].
- $(f_{Q_{divider}})_r$, random uncertainty for the divider. Found to be $\pm 0.050339\%$ for 50 l/s by Pål-Tore Storli [32].
- $(f_{Q_{\rho}})_r$, random uncertainty in the water density. Can be neglected as the value is assumed to be very small.

Combining these random uncertainties with the RSS-method gives,

$$f_{Q_b} = \sqrt{(f_{Q_{\Delta W}})_r^2 + (f_{Q_{divider}})_r^2} = \pm 0.0503\% \quad (\text{A.14})$$

A.3.2 Generator torque

The systematic uncertainties that is involved for the calibration of the generator torque are:

- $f_{\tau_{G_{arm}}} = \pm 0.000563\%$. Found by Pål-Tore Storli [32].
- $f_{\tau_{G_{wclamp}}}$, wire clamp at the top of rope to the attachment. Calculated to be $\pm 0.1075\%$.
- $f_{\tau_{G_{attachment}}}$, attachment for weights. Calculated to be $\pm 0.01087\%$.
- $f_{\tau_{G_{wclampv}}}$, wire clamp at bottom of rope to the attachment. Calculated to be $\pm 0.0732\%$
- $f_{\tau_{G_{weights}}}$, error in the applied weights. Calculated to be $\pm 0.097285\%$

With the fit function for BEP, the systematic error in the weight is $f_{\tau_{G_a}} = \pm 0.0043$ %.

The regression uncertainty for the BEP was found to be ± 0.00342 % by using the theory in section A.1 and the built-in fit function in Matlab.

The random uncertainties were not calculated and therefore neglected. It is assumed that this will be a meager percentage.

A.3.3 Friction torque

The systematic uncertainties that is involved in the calibration of the friction torque are:

- $f_{\tau_{F_{attachment}}}$, attachment for weights. Calculated to be ± 0.07675 %.
- $f_{\tau_{F_{arm}}}$, calculated to be ± 0.00488 %.
- $f_{\tau_{F_{weights}}}$, calculated to be ± 0.13 %.

With the fit function this gives a $f_{\tau_{F_a}} = \pm 0.029$ %

The regression uncertainty for the BEP was calculated to be ± 21.945 % by using the theory in section A.1 and the built-in fit function in Matlab.

The random uncertainties were not calculated and therefore neglected.

A.3.4 Inlet pressure sensor

The systematic uncertainties for calibration of the inlet pressure sensor are given as,

- $f_{P_{i_{dw}}}$, error in dead weight manometer. Given from manufacturer. Set to be ± 0.008 %.

Then this yields,

$$f_{P_{i_{\Delta W}}} = f_{P_{i_a}} = \pm 0.008\% \quad (\text{A.15})$$

The regression uncertainty for the BEP was found to be ± 0.00656 % by using the theory in section A.1 and the built-in fit function in Matlab.

The random uncertainties for the inlet pressure sensor are set to zero due to the coupling and logging during measurements leading to no known random uncertainties.

A.3.5 Differential pressure transducer

The systematic uncertainties for calibration of the differential pressure sensor is given as,

- $f_{Pd_{dw}}$, error in dead weight manometer. Given from manufacturer. Set to be $\pm 0.008\%$.

Then this yields,

$$f_{Pd_{\Delta W}} = f_{Pd_a} = \pm 0.008\% \quad (\text{A.16})$$

The regression uncertainty for the BEP was found to be $\pm 0.00656\%$ by using the theory in section A.1 and the built-in fit function in Matlab.

The random uncertainties for the differential pressure transducer are set to zero due to the coupling and logging during measurements leading to no known random uncertainties.

A.3.6 Temperature probe

The systematic uncertainties for calibration of the temperature probe are given as,

- $f_{PT_{sb}}$, systematic uncertainty in SeaBird probe, was found to be $\pm 0.004912\%$

Then this yields,

$$f_{PT_a} = f_{PT_{sb}} = \pm 0.004912\% \quad (\text{A.17})$$

The regression uncertainty for the BEP was found to be $\pm 0.04765\%$ by using the theory in section A.1 and the built-in fit function in Matlab.

The random uncertainties for the temperature probe are set to zero due to the coupling and logging during measurements leading to no known random uncertainties.

A.3.7 Guide vane angle

The guide vane angle is only calibrated against the values given by the other guide vane angle sensor with input to the Francis logger. Therefore, there only exist regression errors for that particular sensor.

$$f_{GV_a} = f_{GV_{reg}} = \pm 2.36\% \quad (\text{A.18})$$

A.4 Contributing uncertainties in the measurements

In the post-processing part of the measurements, uncertainty regarding physical properties must be taken into account in the computations. In the calculations, these uncertainties have been included for the inlet- and differential pressure.

- e_r , uncertainty regarding the radius of the pipe. Set to ± 0.1 [mm].
- e_{deltaZ} , uncertainty regarding the height difference. Found to be ± 0.436 [mm]. [32]
- e_{Z1} , uncertainty regarding the inlet height. Found to be ± 0.436 [mm].
- e_{Z2} , uncertainty regarding the outlet height. Found to be ± 0.436 [mm].
- e_{rho} , uncertainty in density, set to be ± 0.10001 [kg/m³].


The uncertainties are implemented in the uncertainty of the test by using the theory found in appendix A.2.

A.5 Table - Requirements from the standard

Table A.1: The requirements given by the standard.

Part	Primary/Sec. method	Limits
Arm length gen,s	Primary	$\pm 0,05 \%$ to $0,1 \%$
Gen. torque,s	Secondary	$\pm 0.15 \%$ to 0.25%
Fric. torque,s	Secondary	$\pm 0.02 \%$ to 0.05% of Tmax
Rotational speed,s	Primary	$\pm 0.01 \%$ to 0.05%
Discharge,s	Primary	$\pm 0.1 \%$ to 0.2%
Pressure sensors,s	Secondary	$\pm(1 \text{ to } 5) \cdot 10^{-3} p_{max}^2$

Water density,s	Secondary	$\pm 0.05 \%$
Regression,s	-	$\pm 0.05 \%$
Hydraulic efficiency,r	-	$\pm 0.1 \%$

NTNU	Risikovurdering				Utarbeidet av	Nummer	Dato
					HMS-avd.	HMSRV2603	22.03.2011
HMS					Godkjent av		Erstatter
				Rektor			01.12.2006



Sannsynlighet vurderes etter følgende kriterier:

Svært liten 1	Liten 2	Middels 3	Stor 4	Svært stor 5
1 gang pr 50 år eller sjeldnere	1 gang pr 10 år eller sjeldnere	1 gang pr år eller sjeldnere	1 gang pr måned eller sjeldnere	Skjer ukentlig

Konsekvens vurderes etter følgende kriterier:


Gradering	Menneske	Ytre miljø Vann, jord og luft	Øk/materiell	Omdømme
E Svært Alvorlig	Død	Svært langvarig og ikke reversibel skade	Drifts- eller aktivitetsstans >1 år.	Troverdighet og respekt betydelig og varig svekket
D Alvorlig	Alvorlig personskade. Mulig uførhet.	Langvarig skade. Lang resitusjonstid	Driftsstans > ½ år Aktivitetsstans i opp til 1 år	Troverdighet og respekt betydelig svekket
C Moderat	Alvorlig personskade.	Mindre skade og lang resitusjonstid	Drifts- eller aktivitetsstans < 1 mnd	Troverdighet og respekt svekket
B Liten	Skade som krever medisinsk behandling	Mindre skade og kort resitusjonstid	Drifts- eller aktivitetsstans < 1uke	Negativ påvirkning på troverdighet og respekt
A Svært liten	Skade som krever førstehjelp	Ubetydelig skade og kort resitusjonstid	Drifts- eller aktivitetsstans < 1dag	Liten påvirkning på troverdighet og respekt

Risikoverdi = Sannsynlighet x Konsekvens

Beregn risikoverdi for Menneske. Enheten vurderer selv om de i tillegg vil beregne risikoverdi for Ytre miljø, Økonomi/materiell og Omdømme. I så fall beregnes disse hver for seg.

Til kolonnen "Kommentarer/status, forslag til forebyggende og korrigerende tiltak":

Tiltak kan påvirke både sannsynlighet og konsekvens. Prioriter tiltak som kan forhindre at hendelsen inntreffer, dvs. sannsynlighetsreducerende tiltak foran skjerpet beredskap, dvs. konsekvensreducerende tiltak.

NTNU		Risikomatrixe		Dato	
				08.03.2010	
HMS/KS				Erstatter	
		utarbeidet av		Nummer	
		HMS-avd.		HMSRV2604	
		godkjent av			
		Rektor		09.02.2010	



MATRISSE FOR RISIKOVURDERINGER ved NTNU

		E1	E2	E3	E4	E5
Svært alvorlig						
Alvorlig		D1	D2	D3	D4	D5
Moderat		C1	C2	C3	C4	C5
Liten		B1	B2	B3	B4	B5
Svært liten		A1	A2	A3	A4	A5
		Svært liten	Liten	Middels	Stor	Svært stor
SANNSYNLIGHET						

KONSEKVENSENS

Prinsipp over akseptkriterium. Forklaring av fargene som er brukt i risikomatrixen.

Farge	Beskrivelse
Rød	Uakseptabel risiko. Tiltak skal gjennomføres for å redusere risikoen.
Gul	Vurderingsområde. Tiltak skal vurderes.
Grønn	Akseptabel risiko. Tiltak kan vurderes ut fra andre hensyn.

